A STUDY OF DEEP OCEAN CONVECTION AND THE SEA LEVEL VARIABILITY IN THE NORTH ATLANTIC

by

Feili Li

A dissertation submitted to the Faculty of the University of Delaware in partial fulfillment of the requirements for the degree of Doctor of Philosophy in Oceanography

Spring 2014

A STUDY OF DEEP OCEAN CONVECTION

AND THE SEA LEVEL VARIABILITY

IN THE NORTH ATLANTIC

by

Feili Li

Approved: ____
Mark A. Moline, Ph.D.
Director of the School of Marine Science and Policy

Approved: ____
Nancy M. Targett, Ph.D.
Dean of the College of Earth, Ocean, and Environment

Approved: ____
James G. Richards, Ph.D.
Vice Provost for Graduate and Professional Education

I certify that I have read this dissertation and that in my opinion it meets the academic and professional standard required by the University as a dissertation for the degree of Doctor of Philosophy.

Signed: ______________________________

Xiao-Hai Yan, Ph.D.
Professor in charge of dissertation

I certify that I have read this dissertation and that in my opinion it meets the academic and professional standard required by the University as a dissertation for the degree of Doctor of Philosophy.

Signed: ______________________________

Young-Heon Jo, Ph.D.
Member of dissertation committee

I certify that I have read this dissertation and that in my opinion it meets the academic and professional standard required by the University as a dissertation for the degree of Doctor of Philosophy.

Signed: ______________________________

Igor M. Belkin, Ph.D.
Member of dissertation committee

I certify that I have read this dissertation and that in my opinion it meets the academic and professional standard required by the University as a dissertation for the degree of Doctor of Philosophy.

Signed: ______________________________

Sirpa M. Häkkinen, Ph.D.
Member of dissertation committee

I certify that I have read this dissertation and that in my opinion it meets the academic and professional standard required by the University as a dissertation for the degree of Doctor of Philosophy.

Signed: ______________________________

Tobias Kukulka, Ph.D.
Member of dissertation committee

ACKNOWLEDGMENTS

First and foremost I would like to thank my adviser, Dr. Xiao-Hai Yan for his guidance, enthusiasm, and leading my research in the right direction. Things I have learned from him go far beyond what is required to be an oceanographer. I am very thankful for the many opportunities he has given me. I am very grateful to have worked with such a fine scientist and person. A big thanks goes to Dr. Young-Heon Jo for creative input, encouragement and guidance even when he is overwhelmed with lots of things as he just moves to his new position. I have thoroughly enjoyed working with him. I also thank my whole committee including Dr. Igor Belkin, Dr. Sirpa Häkkinen, and Dr. Tobias Kukulka for helpful input, suggestions and sharing their knowledge and time.

I have also received much help and advice from the group more or less working with Dr. Yan: Timothy Liu, Tony Lee, and Larry Breaker. It is much appreciated.

Thanks also goes to all the supporting staff in Robinson Hall on all floors and in Lewes who made the logistics of my studies possible.

I have been lucky to make many great friends in Robinson Hall and Lewes, and in particular my classmates and officemates deserve special recognition: Zhaoyun, Xiangbai, Weiwei, Jin, Autumn, Federico, Xinyou and Matt. I would also like to acknowledge soccer crowd that has provided important and much appreciated outlet during all seasons. It would have been very difficult, if at all possible, to go through the program without this community.

Last, but not least, I would like to thank my parents and brother for their continuous support and encouragement through all of these years.

Financial support for this work was provided by NASA Physical Oceanography Program, NASA EPSCoR Program, NASA Space Grant, and NOAA Sea Grant.

This work is dedicated to family and friends who are always there for me.

TABLE OF CONTENTS

LIST OF TABLES x
LIST OF FIGURES xi
ABSTRACT xvi

Chapter

1 INTRODUCTION 1

1.1 Background 1
1.2 Dissertation Outline 9

2 THERMAL VARIATIONS ASSOCIATED WITH DEEP CONVECTION IN THE CENTRAL LABRADOR SEA 15

2.1 Abstract 15
2.2 Introduction 16
2.3 Data Sources and Method 19

2.3.1 Data 19
2.3.2 Methods 21

2.4 The Variability of Deep Convection 22

2.4.1 Mixed Layer Depth 22
2.4.2 Buoyancy Frequency 23
2.4.3 Enhanced Deep Convection in the Winter of 2008 25

2.4.3.1 Observations from Argo Floats 25
2.4.3.2 Atmospheric Conditions 28

2.5 Thermal Changes in the Central Labrador Sea 29

2.5.1 Potential Temperature Variability 29
2.5.2 Heat Content Variability 34
2.5.3 NAO 35

2.6 Conclusions and Discussion 37

3 A DIPOLE PATTERN OF THE SEA SURFACE HEIGHT ANOMALY IN THE NORTH ATLANTIC: 1990S – 2000S 55

3.1 Abstract 55
3.2 Introduction 56
3.3 Data and Method 58
3.4 Sea Surface Height Anomaly 58
3.5 Geographic Differences in the SSHA 60
3.6 Dipole Pattern 64
3.7 Conclusions and Discussion 65

4 CHARACTERISTIC FEATURES OF THE SEA SURFACE HEIGHT ANOMALY IN THE NORTH ATLANTIC FROM ALTIMETER OBSERVATIONS 77

4.1 Abstract 77
4.2 Introduction 78
4.3 Data and Method 82
4.4 SSHA in the North Atlantic 83

4.4.1 Dipole Pattern 83
4.4.2 SSHA Variability 85
4.4.3 Characteristic Variations in the Subpolar Gyre 87

4.5 Possible Causes of the Variability in the SPG 91
4.6 Conclusions and Discussion 99

5 CONCLUSIONS AND DISCUSSION 116

5.1 External and Internal Forcing 117
5.2 Meridional Coherence of the Overturning Variations 119
5.3 Subpolar AMOC Variability 121

REFERENCES 125

Appendices

A HILBERT-HUANG TRANSFORM 139

A.1 Empirical Mode Decomposition 139
A.2 Statistical Significance Test 141
A.3 Hilbert-Huang Transforms 141

B CUMULATIVE NORTH ATLANTIC OSCILLATION INDEX 144

C SURFACE CHARACTERISTIC FEATURES RELATED TO DEEP CONVECTION 147

LIST OF TABLES

Table 1.1: All datasets used in this dissertation. 14

Table 3.1: The correlation coefficients between low-frequency SSHA in 'North' and 'South' with different indices. 70

LIST OF FIGURES

Figure 1.1: A simplified schematic of the AMOC showing both the overturning and gyre recirculation components. Warm water flows north in the upper ocean (red), gives up heat to the atmosphere (atmospheric flow gaining heat represented by the changing color of broad arrows), sinks, and returns as a deep cold flow (blue). (Courtesy of Srokosz et al., 2012)........ 12

Figure 1.2: Mixed layer depth climatology in the Labrador Sea. Blue area corresponds to convective site where sinking of surface waters have been mostly documented. Black lines indicate 1000m-, 2000m-, and 3000m-isobath, respectively........ 13

Figure 2.1: Weekly number of Argo profiles in the central Labrador Sea (56°W – 48°W, 56°N – 60°N)........ 42

Figure 2.2: Mixed Layer Depth in the Labrador Sea based on Argo data using density criteria........ 43

Figure 2.3: Total buoyancy change for each winter obtained from two density profiles. While the initial profile is the same (October and November averaged), the second density profiles are different for 1000m well mixed condition (blue line), 1500m well mixed condition (black line), and the observed mixing condition based on profiles whose MLDs are greater than 80% of the maximum MLDs during March of the next year (red line), respectively........ 44

Figure 2.4: The trajectories and corresponding buoyancy frequency of two floats that spent most of their lifetime in the central Labrador Sea. The position of each profile is labeled with solid dots in (a) and (c) with star indicating the initial release locations. Colored dots correspond to the winter of 2008 (see Figure 3 for profiles of specific dates). This period is also bounded by white dashed line in the depth-time plots of the squared buoyancy frequency in (b) and (d)........ 45

Figure 2.5: The evolution of potential temperature, salinity (from December 2007 to March 2008 with 10-day interval) of Float 4900494 (a)(b), Float 4900537 (c)(d) and Float 4900677 (e)(f). 46

Figure 2.6: The net heat flux of the (black) 1990 – 1995 winters average and of the winter of (a) 2008, and (b) the 2001 – 2007 averages. 47

Figure 2.7: The potential temperature at three depths of 500m, 1000m and 1500m, respectively, in the central Labrador Sea. 48

Figure 2.8: Progression of the EEMD results based on the potential temperature at the 500m depth averaged in the central Labrador Sea. Units are degree Celsius. 49

Figure 2.9: IMF significance test results for temperature variations at the 500m (a), 1000m (b), and 1500m (c) depths, respectively. The dashed and solid lines represent the 1th and the 5th percentiles determined from the probability distribution of the energy density of the white noise. The black dots correspond to the pairs of averaged mean normalized energy density (y-axis) and averaged mean period (x-axis) of the IMFs. 50

Figure 2.10: The Hilbert spectrum (left) and the marginal spectral density (right) for the IMFs obtained from temperature variations at the 500m (a), 1000m (b), and 1500m (c) depths respectively. 51

Figure 2.11: The Hilbert spectrum (a) and the marginal spectral density (b) of the IMF components from the EEMD of the heat content in the central Labrador Sea. 52

Figure 2.12: The IMF components (C5, C6, C7, all are significant at 99% confidence level) and the residual (R) used to reconstruct the low frequency heat content changes in the Labrador Sea interior. The original time-series (Input) is also shown for references. Units are $GJ\ m^{-2}$. 53

Figure 2.13: Time-series of the reconstructed low frequency heat content (black solid line) from the significant IMFs with periods > 1 year and the non-linear trend, the cumulative NAO index (red solid line; y-axis inverted), low frequency variations in the turbulent heat flux averaged over the Labrador Sea (blue solid line), and wintertime maximum MLD (yellow squares). Note that a 12-month running smoothing was applied to the cumulative NAO index. 54

Figure 3.1: Dipole pattern in the overall trend of the sea surface height anomaly of the northern North Atlantic from November 1992 to January 2011. Two blue boxes (labeled as 'North' and 'South') are the domains for averaging, corresponding to the subpolar region and the Gulf Stream region, respectively. 1000m-, 2000m- and 3000m-isobaths are shown in solid grey lines. 71

Figure 3.2: The intrinsic mode functions and the residuals decomposed from the spatially averaged sea surface height anomaly over regions 'North' (blue line) and 'South' (red line). Units are cm. The domain for averaging is shown in Figure 3.1 72

Figure 3.3: Significance test of the Intrinsic Mode Functions (IMFs) for the areas of 'North' and 'South' SSHA shown in Figure 3.1, respectively. 95% and 99% significant level were also displayed. 73

Figure 3.4: Low frequency SSHA oscillations and the long-term trends of the 'North' and 'South' regions, respectively (blue and red lines). The normal monthly NAO index (black dotted line) and the cumulative NAO index (black solid line) are also shown with reversed y-axis as references. A 9-month running smoothing was applied to both NAO indices. 74

Figure 3.5: Trends of the SSHA in the study domain for periods of (a) November 1992 to December 2001 and (b) January 2002 to January 2011, respectively. 1000m-, 2000m- and 3000m-isobaths are shown in solid grey lines. 75

Figure 3.6: Same as Figure 3.4 but with different division of 'South' region. 76

Figure 4.1: (a) The linear trend of the sea surface height anomaly in the study domain, and (b) the coefficient of determination which is a measure of the goodness of linear fit. The 1000m-, 2000m- and 3000m-isobaths are shown in solid grey lines. 105

Figure 4.2: The standard deviation of the sea surface height anomaly. 106

Figure 4.3: The temporal averages over the period of 1993 – 2010 of (a) original SSHA, (b) – (g) the IMFs at increasing timescales and (h) the residual (long-term trend). 107

Figure 4.4: The variations explained by the signals over different timescales corresponding to components in Figure 4.3b – 4.3h. 108

Figure 4.5: The IMFs and the residual decomposed from the spatially averaged sea surface height anomaly over the subpolar gyre. Units are cm. 109

Figure 4.6: The Hilbert transform of the IMFs (C1 – C8). (a) The instantaneous energy density level (IE) in cm^2, (b) the Hilbert spectrum and (c) marginal spectral density (MSD) of each frequency in cm. 110

Figure 4.7: Similar to Figure 4.6, but only applying the Hilbert transform to the selected IMFs (C5 – C8). (a) The instantaneous energy density level (IE) in cm^2, (b) the Hilbert spectrum and (c) marginal spectral density (MSD) of each frequency in cm. 111

Figure 4.8: The altimeter SSHA and steric height anomaly calculated from temperature and salinity observations in the SPG. 112

Figure 4.9: The IMFs and the residuals decomposed from the heat content anomalies estimated from surface heat flux (red line; right y-axis) and the SSHA (solid black line; left y-axis). The depth-integrated heat content anomaly (dashed black line; left y-axis) is also shown for comparison. Units are GJ m^{-2}. 113

Figure 4.10: Close relationships among the heat content of the central Labrador Sea (black solid line), the sea surface height anomaly of the central Labrador Sea (red solid line), the meridional overturning circulation transport at $26.5°N$ (green dash line) and the cumulative NAO index (blue line). The central Labrador Sea is defined by a box between $58°W - 48°W$ and $56°N - 61°N$. Unit and range of each index is labeled with y-axis of same color. Note that the y-axis of the CumNAO Index is reversed. 114

Figure 4.11: Domains of area 1, 2 and 3 used to spatially average the SSHA and examine the lagged correlation between each other. Arrows indicate possible propagation pathway of the AMOC variations. The 1000m-, 2000m- and 3000m-isobaths are shown in solid grey lines. 115

Figure B.1: Comparison of normal month NAO index (blue bar) and the cumulative NAO index (red line) calculated using Equation B.1. 145

Figure B.2: The cumulative NAO index integrated from 1992 Nov (blue) and from 1996 Jan (red), respectively. A 9-month running smoothing was performed to both lines. 146

Figure C.1: Land and sea surface temperatures of (a) Feb 6, 2007 and (b) Feb 9, 2008. Wind vectors are also displayed. There was a weak convection during the winter of 2007 but a strong convection during the winter of 2008 (see Chapter 2 for more details). The land surface temperature (LST) is measured by the MODIS/Terra and provided by NASA Goddard Space Flight Center, http://modis-land.gsfc.nasa.gov/temp.html). The AMSR-E sea surface temperature (SST) and QuikSCAT sea winds are obtained from the Remote Sensing Systems (http://www.remss.com). 149

Figure C.2: (a) Land/sea surface temperature composite for the winter of 2008 over the study area. Black boxes indicate locations for temperature average. (b) Sea surface temperature (SST) over box 3 minus land surface temperature (LST) over box1, box2 and box4, respectively. SST data is fusion of microwave and infrared measurements obtained from the Remote Sensing Systems (http://www.remss.com). 150

ABSTRACT

Aspects of convection in the Labrador Sea and the circulations from the mid- to high-latitude North Atlantic are investigated using a variety of in-situ, satellite, and atmospheric reanalysis data products.

Deep ocean convection in the Labrador Sea has transitioned from a period of intensification during the early 1990s into current stage of weakening with, however, higher variability in strength. Changes in hydrographic properties were used to investigate the evolution of deep convection at the monthly to interannual timescales. The atmospheric forcing characterized by the North Atlantic Oscillation (NAO) index has an important role in setting deep convection variability. On one hand, enhanced atmospheric forcing favors the extremely strong convective activity in the Labrador Sea as happened in the winter of 2008. On the other hand, over longer timescales, the cumulative NAO index is significantly correlated to the interannual variations in the heat content and mixed layer depths in the central Labrador Sea. Moreover, although ongoing warming in the intermediate layers tends to impede rigorous convection down to 1500m depth by steadily adding buoyancy, shallow convection will most likely remain active in the near future.

The linkages between the horizontal and the overturning circulations in the North Atlantic were investigated in terms of sea level changes based on altimeter

observations. A dipole pattern, centered between the Northern Atlantic subpolar region and the region near the Gulf Stream (GS), was observed in the linear trends of the sea surface height anomaly (SSHA). This dipole pattern is essentially associated with the interannual to decadal SSHA oscillations of the two regions. The low-frequency SSHA variability in the subpolar regions more effectively responds to the cumulative NAO forcing and leads that of the GS region by 29 months. Moreover, there is a remarkable reversal of the SSHA trends from the 1990s to the 2000s. This dipole pattern in sea level anomaly is a characteristic spatial pattern for the overturning circulation in the North Atlantic, whose changes closely relate to latitudinal coherence of different processes involved.

Besides the dipole pattern in the sea level anomaly, the SSHA was used to investigate various processes at annual and longer timescales. The sea level variations in the subpolar gyre (SPG) are dominated by the annual cycle and the long-term increasing trend. In comparison, the SSHA along the GS is dominated by variability at intra-seasonal and annual timescales. The sea level rise in the SPG developed at a reduced rate in the 2000s compared to rates in the 1990s, which was accompanied by an increase in spectral energy starting from around 2002 after a period of energy loss in the system. These changes in both apparent trend and low-frequency SSHA oscillations reveal the importance of low-frequency variability in the SPG. To identify the possible contributing factors for these changes, the heat content balance (equivalent variations in the sea level) in the subpolar region was examined. The results indicate that horizontal circulations may primarily contribute to the interannual to decadal variations, while the air-sea heat flux is important at annual timescale. Furthermore, the low-frequency variability in the SPG might be related to the propagation of the Atlantic meridional overturning circulation (AMOC) variations from the deep-water formation region to mid-latitudes in the North Atlantic.

Chapter 1

INTRODUCTION

1.1 Background

As part of the global thermohaline circulation, the meridional overturning circulation in the North Atlantic (AMOC) transports large amount of heat and freshwater between high latitudes and tropics and plays an important role in moderating Earth temperature and thus preventing the Earth from any regional extreme weather conditions (Figure 1.1). As the oceanic heat is advected poleward by the upper limb of the AMOC, there is a strong transfer of heat from the ocean to the atmosphere at midlatitudes, contributing to the temperate climate of northwest Europe (Srokosz et al., 2012). Intermediate and deep-water masses, as the sources of the lower limb of the AMOC, is either produced locally or transported through the subpolar gyre (SPG) and further southward. Paleoclimate proxy records have shown the significance of the AMOC variations in relation to abrupt climate changes (Clark et al., 2002; McManus et al., 2004; Lynch-Stieglitz et al., 2007; Lynch-Stieglitz et al., 2011), which were also observed by numerical studies that simulated the climate changes during and just after the last glacial period (Ganopolski and Rahmstorf, 2001). Into the 21st century, the AMOC intensity was projected to be in a mode of weakening (Latif et al., 2006; Lohmann et al., 2008; Cunningham and Marsh, 2010), which has raised a variety of interests for understanding its probable influences on the climate in the near future. However, the way of predicting the future climate from the past has been called into question (e.g., Ganopolski and Robinson, 2011), revealing an incomplete understanding of the role of the AMOC.

Strong linkages between the SPG circulation and the AMOC intensity have been well suggested by model simulations (e.g., Bentsen et al., 2004; Böning et al., 2006; Xu et al., 2013). The linkage is resulted from not only the involvement of strong horizontal advections at both surface and depth, but also the important convective processes that contribute to the formation of the intermediate and deep water masses constituting part of the deep western boundary current (DWBC). In fact, among other factors contributing to the AMOC variations, deep-water formation at high latitudes is believed to play a critical role, especially in setting the strength and variability of the AMOC (see Kuhlbrodt et al., 2007). A host of model simulations have established the response of the mid- to low-latitude AMOC to variations in subarctic deep-water formation (Häkkinen, 1999; Gulev et al., 2003; Bentsen et al., 2004; Bailey et al., 2005; Biastoch et al., 2008; Xu et al., 2013). The observed strength variability of the SPG circulation (e.g., Belkin, 2004; Häkkinen and Rhines, 2004; Rhein et al., 2011) was linked to variations in deep-water formation rates in the Labrador Sea given their close relationship with each other, as well as with the AMOC (Böning et al., 2006; Bersch et al., 2007; Rhein et al., 2011). Therefore, deep-water formation, the AMOC variability and the SPG variability are not independent phenomena, but are instead interacting with each other at different scales. They are linked to energy propagation and increased through atmospheric and oceanic circulation occurring at different spatial and temporal scales.

There are only a few regions in the World Ocean where the dense and intermediate waters are formed. One of these places is the Labrador Sea. The Labrador Sea is a part of the SPG that is located in the northwestern corner of the North Atlantic Ocean between Greenland and the Labrador coast of Canada (Figure 1.2). The circulation of the Labrador Sea consists of the weakly-stratified convective interior, the cyclonically flowing boundary current system and the various types of eddies that populate the Labrador Sea and connect the boundary current region with the interior. Deep convection occurs in the interior of the basin during the winter. It is primarily driven by the large wintertime heat loss (Dickson et al., 2002) and tends to be confined to the western part of the central Labrador Sea (Lazier et al., 2002; The Lab Sea Group, 1998; Pickart et al., 2002). After being formed in the interior, the product of convection, Labrador Sea Water (LSW), spreads at intermediate depths southward and eastward and is found in the North Atlantic to the north of $40°N$ and along its western boundary to $18°N$ (Talley and McCartney, 1982). In order for the convection to occur, the water must be weakly stratified, and the strong surface fluxes must act for prolonged times to extract enough buoyancy. All the conditions are satisfied in the Labrador Sea. The dry and cold air blows over the relatively warm waters of the sea (~ $2°C$) resulting in mean heat losses of the order of 300 W m^{-2} (The Lab Sea Group, 1998; Marshall and Schott, 1999) resulting in LSW production rates of 4.5-10.8 Sv (Yashayaev, 2007). After convection ceases, the second phase, called the restratification, begins to play a leading role in the water mass transformation (Straneo, 2006). Restratification is characterized by the removal of newly formed dense water away from the interior and the replacement by the warm and salty waters from the boundary current system that is achieved by means of the numerous eddies (Marshall and Schott, 1999).

Geographic remoteness, small size, and temporal irregularity of deep convection make the study of this very important process difficult and challenging. Wust (1935) first noted a minimum salinity intermediate water mass in his very limited data and conjectured its source regions as the Labrador Sea. Nielsen (1928) and Smith et al. (1937) suggested that deep water mass formed in the Labrador Sea as well as in the area south of Greenland by vertical convection. However, due to the harsh wintertime conditions companied this phenomenon, and also due to the fact that the lateral scales of the convective plumes are very small (Paluszkilewicz et al., 1994; Marshall and Schott, 1999), the direct observation of the occurrence of deep convection was not made until the 1970s in the Labrador Sea using a shipboard conductivity-temperature-depth (CTD) profiler (Clarke et al., 1983). Data collected during the World Ocean Circulation Experiment in the mid-1980s and the 1990s, the Labrador Sea Deep Convection Experiment in the 1990s (The Lab Sea Group, 1998), and the recent development of the Argo program, together with repeat ocean surface measurements from various oceanic satellites since the 1970s, have provided more and more new insights on important variables associated with deep convection at the annual to interannual timescales. Nevertheless, a few researches used remote sensing to study open ocean deep convection process since the spatial and temporal scales of the major stages of deep convection potentially limit the usefulness of satellite data. The possibility to detect subsurface water mass changes from altimeter data was already suggested by Stammer et al. (1991) and Yan et al. (2006), who showed the detectability of Mediterranean outflow eddies from altimeter data. A pilot remote sensing investigation of deep convection was conducted by Hermann et al. (2009), suggesting a correlation between deep convection and sea level variations based on altimetry and model output. Based on theory and in-situ measurements of the mixed layer depth (MLD), Gelderloos et al. (2013) suggested the possibility of using altimetry to detect deep convection in the Labrador Sea away from the annual hydrographic repeat section. However, the authors noted 'false' detection of deep convection using their method, which might reflect anomalous wind forcing other than convective activity.

Dramatic changes of physical and dynamical origins have undergone in the mid- to high-latitude North Atlantic significantly during past decades. Belkin (2004) found accelerated gyre circulation in the 1980s and 1990s compared to circulation in the 1970s by estimating advection rates of the three 'Great Salinity Anomaly' (GSA) in the subpolar North Atlantic. The author also pointed out a much greater intensification of the upper ocean circulation in the Labrador-Irminger Gyre. Using altimeter and hydrographic data, Häkkinen and Rhines (2004) derived a large reduction of the SPG strength after mid-1990s along with reduced heat fluxes, which is attributed to decline of deep ocean convection in the Labrador Sea (see also Böning et al., 2006; Bersch et al., 2007; Häkkinen et al., 2009). Changes in the ocean surface circulation accompany the variations in the northern North Atlantic water properties. It is noted that the weakening of the SPG coincides with a warming and salinification trend in the northern North Atlantic since mid-1990s (Hátún et al., 2005; Holliday et al., 2008; Sarafanov et al., 2008; Häkkinen et al., 2011). This trend ended a period of freshening and cooling that had lasted for decades (Curry et al., 2003; Curry and Mauritzen, 2005). Such a reversal of trends in the temperature and salinity, especially in the intermediate layer, may be influenced by both the SPG strength and the deep convection intensity in the Labrador Sea (Sarafanov, 2009). Studies have shown that it is the westward contraction of the SPG associated with its weakening that enables more salty and warm waters to reach further north and thus enter the Nordic seas (e.g., Hátún et al., 2005). Meanwhile, decline of deep convective activities in the Labrador Sea has been observed since the late 1990s (Lazier et al., 2002; Kieke et al., 2007; Yashayaev, 2007). The decline contributed to the decay of the doming isopycnals in the SPG interior, which was suggested to be linked to the weakening of the SPG surface circulation (Böning et al., 2006; Bersch et al., 2007; Yeager and Jochum, 2009). The resultant weakened SPG creates a broad pathway in the eastern North Atlantic for advancement of the subtropical gyre, which, in turn, could probably further temper the strength of the SPG by transporting more salty and warm waters of tropical origin towards high latitudes.

Resulted warming of the northern North Atlantic could have great impacts on mass loss due to melting ice sheets and glaciers at high latitudes. Using a three-year record of Gravity Recovery and Climate Experiment (GRACE) measurements, Chen et al. (2006) derived a contribution of approximately $0.54\ \mathrm{mm} \cdot \mathrm{yr}^{-1}$ to the global sea level rise from Greenland ice loss. Khan et al. (2010) revealed some ongoing acceleration of the Greenland ice sheet melting since 2005 that spreads from a known southeastern location to regions along the northwest coast. These estimates were based on GRACE and Global Positioning System (GPS) data. Warming subsurface ocean waters were considered as a major contributor for the accelerated glacier melting (Bindschadler, 2006; Holland et al., 2008). This implies a potential relationship between the SPG intensity, which determines the amount of heat transported along Greenland coast, and the melting ice mass along the margin of the SPG. An abnormal warming condition was not only observed in the SPG, but also in the regions north toward the Labrador Sea across the Baffin Bay (Ribergaard et al., 2008; Ribergaard, 2009; Ribergaard, 2010) and the Canadian Arctic Archipelago (Gardner et al., 2011). Furthermore, significant changes in the sea ice extent in the Arctic Sea (Stroeve et al., 2008; Kwok et al., 2009; Stroeve et al., 2012) and transport in the Nares Strait (Kwok et al., 2010) can potentially freshen the SPG and change its intensity.

A major source of low-frequency variability in the atmospheric conditions in mid- to high-latitudes in the North Atlantic is the North Atlantic Oscillation (NAO), which strongly influences climate variability from the Arctic to the subtropical Atlantic, especially during boreal winters (Hurrell, 1995; Marshall et al., 2001). The NAO index varies annually, but also exhibits a tendency to remain in one phase for intervals lasting several years. For example, there were several consecutive winters with positive NAO index in the first half of the 1990s. During a positive NAO, conditions are colder and drier than average over the northwestern North Atlantic and Mediterranean regions, whereas conditions are warmer and wetter than average in northern Europe, the eastern United States, and parts of Scandinavia (Visbeck et al., 2001). The winter NAO is thought to have a close correlation with the intensity and variability of gyre scale transport (Bersch, 2002; Sarafanov, 2009) and with the interannual to inter-decadal variability in the North Atlantic (Curry and McCartney, 2001). More specifically, Esselborn and Eden (2001) found coincident sign changes between the dipole pattern in sea level anomalies between the subtropical and subpolar North Atlantic, and the NAO during 1995 and 1996. Lohmann et al. (2009a, 2009b) pointed out that changes in the SPG circulation could not only be due to a sign change of the NAO (from positive to negative) but also to its initial state, with the persisting positive NAO eventually leading to weakened SPG. Cromwell (2006), however, found no significant correlation between the NAO index and the amplitudes of the first four principal components of interannual sea surface height variability in the North Atlantic.

To summarize: The subpolar North Atlantic is a critical component of the global climate system. Deep ocean convection in the SPG releases heat from the ocean to the atmosphere, and is crucial to the climate of northwestern Europe (e.g., Vellinga and Wood, 2002). Atmospheric variability, primarily NAO-related, strongly affects convective activity as well as the circulation and extent of the SPG. The density anomaly generated at the high latitudes propagates from the Labrador Sea to the mid-latitudes along either basin boundaries (e.g., Köhl and Stammer, 2007) or the interior pathway (e.g., Bower et al., 2009). The meridional coherence of the AMOC variations has been suggested by model simulations at a wide range of timescales (Getzlaff et al., 2005; Biastoch et al., 2008; Msadek et al., 2010; Zhang, 2010; Xu et al., 2013), but it may depend on model resolution (Getzlaff et al., 2005) and the results are conflicting (e.g., Bingham et al., 2007). In addition, low frequency signals can be masked by high frequency fluctuations due to local wind forcing and eddy activities (Biastoch et al., 2008; Lorbacher et al., 2010). Direct observations of key components of the AMOC at the mid- to high-latitude North Atlantic and their meridional coherences are rare and are far from enough and evident. For example, crucial arrays to obtain time-series of the meridional volume and heat transport in the subpolar North Atlantic are still missing (Rhein et al., 2011).

Based on key oceanic variables obtained from satellite and in-situ measurements, this study provides observation and analysis of the important deep convective process in the Labrador Sea and its associated characteristic features and dominant timescales. In addition, the meridional covariability of the AMOC variations is isolated using newly developed multi-variant time-series analysis (Ensemble Empirical Mode Decomposition (EEMD)/Hilbert-Huang Transform (HHT)).

1.2 Dissertation Outline

The focus of this dissertation is on convection and circulation variability in the mid- to high-latitude North Atlantic, with a special emphasis on the latitudinal coherence of the overturning changes from an observational perspective.

In Chapter 2 the recent observation of temperature and heat content variations in the Labrador Sea is documented primarily based on Argo measurements. Using the EEMD and the Hilbert spectral analysis, signals are separated based on their characteristic timescales, ranging from a couple of weeks to a few decades. The changes associated with deep convection activity, at the interannual timescales, can therefore be separated and analyzed with details.

In Chapter 3, the dipole pattern in the sea surface height anomaly (SSHA) is presented and its relationship to the overturning circulation is investigated. The EEMD method is employed to elucidate the low-frequency changes in the sea level over the subpolar region and the Gulf Stream region, respectively.

The main objectives of Chapter 4 are to identify the dominant modes of sea level variability in the North Atlantic and to examine the corresponding contributing factors, e.g., changes related to surface heating or advective processes over the interannual and longer timescales.

Collectively the dissertation chapters are intended to add to our body of knowledge regarding the variability of deep convective activity, the structure and variability of the circulation in the subpolar region, and the latitudinal connectivity of the overturning circulation across the North Atlantic. The purpose is to contribute to a basis from which we can better interpret existing observations and improve models, so that we can ultimately understand more thoroughly how Earth's climate system works.

The dissertation is structured as three self-contained articles. Chapter 2 is an article under review in Deep-Sea Research, Part I (Li, F., Y.-H. Jo, X.-H. Yan, and W.

T. Liu, 2013: Thermal variations associated with deep convection in the central Labrador Sea). Chapter 3 has been published as an article in the Geophysical Research Letters (Li, F., Y.-H. Jo, X.-H. Yan, and W. T. Liu, 2012: A dipole pattern of the sea surface height anomaly in the North Atlantic: 1990s – 2000s). Chapter 4 is a journal article forthcoming in the Journal of Climate (Li, F., Y.-H. Jo, and X.-H. Yan, 2013: Characteristic features of the sea surface height anomaly in the North Atlantic from altimeter observations). The word ‘we’ in all chapters refers of all authors.

Figure 1.1: A simplified schematic of the AMOC showing both the overturning and gyre recirculation components. Warm water flows north in the upper ocean (red), gives up heat to the atmosphere (atmospheric flow gaining heat represented by the changing color of broad arrows), sinks, and returns as a deep cold flow (blue). (Courtesy of Srokosz et al., 2012)

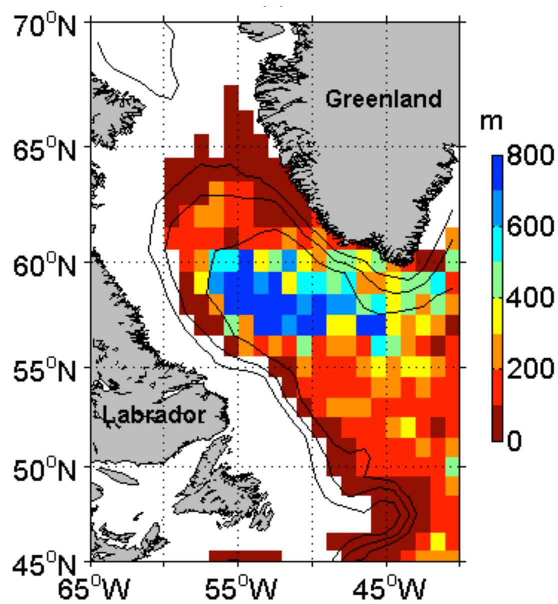

Figure 1.2: Mixed layer depth climatology in the Labrador Sea. Blue area corresponds to convective site where sinking of surface waters have been mostly documented. Black lines indicate 1000m-, 2000m-, and 3000m-isobath, respectively.

Table 1.1: All datasets used in this dissertation.

Data	Period	Resolution	Website
Argo (T, S)	2002 – 2013	Profiles; ~10 day	http://www.nodc.org
Turbulent Flux	2002 – 2013	1º gridded; monthly	http://oaflux.whoi.edu
Surface Flux	1993 – 2010	~1.9º gridded; monthly	http://www.esrl.noaa.gov/psd/
Sea Level Anomaly	1992 – 2011	1/3º gridded; monthly	http://aviso.oceanobs.com
EN3 (T, S)	1992 – 2010	1º gridded; monthly	http://hadobs.metoffice.com/en3/

Chapter 2

THERMAL VARIATIONS ASSOCIATED WITH DEEP CONVECTION IN THE CENTRAL LABRADOR SEA

2.1 Abstract

The dominant modes of variability in the temperature and ocean heat content (OHC) of the central Labrador Sea were investigated using the Hilbert-Huang Transform (HHT) based on collected Argo profiles. Warming trends of approximately $0.03\ ^{\circ}\mathrm{C\ yr^{-1}}$ were observed in the entire water columns during the period of 2003 – 2012. A strong annual cycle exists and dominates at the 500 m depth, while signals at the interannual timescales can explain most of the variability at the 1000 m and 1500 m depths. Further analysis on the timescales of interannual variability indicates longer periods of signals at deeper layers. These interannual signals are closely correlated to the variability of deep convection in the Labrador Sea, which has a typical mixed layer depth (MLD) of 1000 m with an intermittent enhancement of MLD > 1500 m. The Hilbert spectrum from heat content (0 – 1000 m) in the Labrador Sea interior reveals two important components at frequencies of $0.8-1.2\ \mathrm{cycle\ yr^{-1}}$ and $0.2-0.3\ \mathrm{cycle\ yr^{-1}}$, respectively, superimposed on the overall warming trends. The former corresponds to the dominant seasonal cycle due to surface heating, while the

latter is concomitant with the timing of the reoccurrence of strong convection events. The cumulative North Atlantic Oscillation (NAO) index is significantly correlated to the low frequency variations in the heat content reconstructed from the Ensemble Empirical Mode Decomposition (EEMD) results. Therefore, the interannual signals in the Labrador Sea at especially the intermediate layers are attributed to changes in the deep convective processes and atmospheric conditions. Moreover, over longer timescales, underlying warming trends from a 9-year record might be part of multi-decadal variations that reflect the Atlantic Multi-decadal Variability (AMV).

2.2 Introduction

The semi-enclosed Labrador Basin is known to host open ocean convection, a key yet localized process bridging the intermediate ocean waters and the atmosphere. Deep convection has impacts on the variability of the SPG circulation (Langehaug et al., 2012; Medhaug et al., 2012), and the transport of the newly produced intermediate water masses has been linked to dynamical changes at lower latitudes (Bower et al., 2009; Li et al., 2012; Msadek et al., 2010; Rhein et al., 2011; Xu et al., 2013; Zhang, 2010). Paleoclimatic records have also indicated a close relationship between the changes in deep convection and an abrupt climate change in the North Atlantic due to its impacts on the AMOC (Lynch-Stieglitz et al., 2007; McManus et al., 2004). Therefore, the Labrador Sea may serve as a source region of low frequency AMOC variations (i.e., set the shape and strength of the variability therein; Kuhlbrodt et al., 2007). It is of great importance, then, to understand the variability of deep convection through its associated changes in key parameters, especially at the interannual and longer timescales.

Decline of deep convection has been observed in the Labrador Sea after a period of consecutive strong events during the 1980s and the early 1990s (Lazier et al., 2002; Kieke et al., 2007; Yashayaev, 2007; van Aken et al., 2011). This decline contributes to the decay of the doming isopycnals in the SPG interior, which is linked to the weakening of the SPG surface circulation (Böning et al., 2006; Bersch et al., 2007; Yeager and Jochum, 2009). Interannual variations in the Labrador Sea have close correlation to the local atmospheric forcing through active air-sea interactions during especially harsh winters (The Lab Sea Group, 1998; Luo et al., 2012). However, the North Atlantic Oscillation (NAO) index, which characterizes most of the atmospheric variability at interannual timescales, shows no one-to-one correspondence with deep convection in the Labrador Sea (Yashayaev, 2007). In addition, recent warming events embedded in the northern North Atlantic import buoyancy into the surface and subsurface layers, and therefore tend to prevent the water columns from convecting.

Meanwhile, hydrographic and satellite observations have shown significant changes in the North Atlantic SPG at the interannual and decadal timescales. Belkin (2004) found accelerated gyre circulation in the 1980s and 1990s compared to circulation in the 1970s by estimating advection rates of the three 'Great Salinity Anomaly' in the subpolar North Atlantic. Using altimeter and hydrographic data, Häkkinen and Rhines (2004) derived a large reduction of the SPG strength after the mid-1990s along with reduced heat fluxes, which is attributed to a decline in the deep ocean convection activities in the Labrador Sea (see also Bersch et al.; 2007; Böning et al., 2006). Changes in upper ocean circulation effectively contribute to variations in water properties in the northern North Atlantic. The weakening of the SPG has also coincided with a warming and salinification trend in the northern North Atlantic beginning in the mid-1990s (Häkkinen et al., 2011; Hátún et al., 2005; Holliday et al., 2008; Sarafanov et al., 2008). This, therefore, altered a period of freshening and cooling that had lasted for decades (Curry et al., 2003; Curry and Mauritzen, 2005). Such a reversal of temperature and salinity trends, especially at the intermediate layers, may have been influenced both by the strength of the SPG and the intensity of deep convection (Sarafanov, 2009). For example, the westward contraction of the SPG associated with its weakening enables more salty and warm waters to reach further north and thus enter the northern North Atlantic (e.g., Hátún et al., 2005; Häkkinen et al., 2011).

Nevertheless, the 1990s' deceleration of the SPG's surface circulation, which was accompanied by a decreased surface layer transport in the boundary currents as observed from repeat hydrographic sections, is followed by a partial rebound in the early 2000s (Han et al., 2010; Daniault et al., 2011). Meanwhile, the deep-water transport strengthened in subpolar regions, in direct opposition to its surface layer counterpart in the 1990s (Dengler et al., 2006; Sarafanov et al., 2010). These changes, together with the appearance of recent rigorous deep convection events (for example, in the winter of 2008, Våge et al., 2009; Yashayaev and Loder, 2009), have cast questions on the further decline of deep convection as well as the SPG circulation.

This study presents observational analysis of recent changes in the Labrador Sea as pertaining to deep convection, focusing on the dominant modes of variability in the potential temperature and the heat content. Using the Ensemble Empirical Mode Decomposition (EEMD) and the Hilbert-Huang Transform (HHT), signals at different timescales were separated and investigated in the central Labrador Sea. We also explore the relationship especially between low frequency oceanic signals and the atmospheric forcing. Data sources and methods are first described in Section 2.3. Section 2.4 discusses the recent variability in deep convection in terms of the mixed layer depth (MLD). Section 2.5 focuses on the dominant modes of variability in the temperature and heat content with emphasis on the low-frequency signals. The final section includes a discussion of the results and concluding remarks.

2.3 Data Sources and Method

2.3.1 Data

Temperature and salinity were sampled by profiling floats as part of the Argo program (http://www.argo.ucsd.edu). Argo data was gathered from the National Oceanographic Data Center (NODC). For this analysis, a combination of real-time and delayed-mode data with quality flag of 1 or 2 (1-good; 2-probably good) were used. In addition to the quality flags, the grey list of Argo floats (http://www.nodc.noaa.gov/argo/grey_floats.htm) was used to reject all problematic data. All profiles were then checked for their listed variables, and profiles having no salinity records were also rejected. Altogether, 3064 profiles were collected in the central Labrador Sea from 2002 to 2013 (Figure 2.1). The central Labrador Sea is defined as $(56°\mathrm{W} - 48°\mathrm{W}, 56°\mathrm{N} - 60°\mathrm{N})$. All selected profiles were linearly interpolated on to 26 vertical levels that transition from 10 m vertical spacing at the surface to 250 m at depth. These individual profiles were directly used for determine MLD. Furthermore, spatial averaging was applied to all selected profiles within the central Labrador Sea for each week during the period of 2003 – 2012. Although the convective process occurs at rather smaller spatial scales $(O \sim 1\ \mathrm{km})$, its impacts on water properties can spread throughout the entire region. This suggests that the spatially averaged estimates can be representative of the Labrador Sea interior (Lazier et al., 2002). We also tested the results with further selection of profiles by adding a 3000m-isobath constraint (e.g., Yashayaev and Loder, 2009), and found no discernable differences.

Monthly turbulent flux data was obtained from WHOI OAFlux project with spatial resolution of 1 degree by 1 degree (http://oaflux.whoi.edu). The OAFlux project applies objective analysis approach to take into account data errors in the development of enhanced global flux fields. The OAFlux products are calculated by using the best-possible estimates of flux-related surface meteorology and the sate-of-the-art bulk flux parameterizations (Yu et al., 2008). The latent and sensible heat flux estimates are computed from the objectively analyzed surface meteorological variables by using the COARE bulk flux algorithm 3.0 (Fairall et al., 2003).

2.3.2 Methods

In the present study we adopted the HHT, a combination of EMD and Hilbert spectral analysis (Huang et al., 1998). The EMD method can decompose any complicated data set into a finite number of IMFs. The instantaneous frequency defined by the Hilbert transform denotes the physical meaning of the local phase change better for IMFs than for any other non-IMF time series. The EMD method is adaptive and therefore highly efficient. The combination of the Hilbert spectral analysis and the EMD is designed specifically for analyzing non-linear and non-stationary data (Huang et al., 1998; Huang and Wu, 2008). This method, to a large extent, overcomes the difficulties of the more commonly used spectral analysis that include leakage problem. The Hilbert transform is a useful tool to estimate amplitude and frequency of a signal over time, allowing localization of specific events in time-frequency space. Extensive details about the HHT and the significance test can be found in Appendix A. For more details on the applications of the HHT to geophysical research, please refer to Huang and Wu (2008).

2.4 The Variability of Deep Convection

2.4.1 Mixed Layer Depth

Argo floats drifting in the central Labrador Sea during the convective seasons were collected as direct records of deep convection activity. We calculated the MLD as the depth where the change in potential density becomes larger than 0.01 kg m^{-3} compared to the density at 10 m depth. The selection of 10 m depth as the reference level aims to avoid high frequency and large density variations in surface layer (e.g., due to diurnal heating; de Boyer Montégut et al., 2004). Figure 2.2 shows MLDs obtained from all individual density profiles collected in the central Labrador Sea during the period of 2003 – 2012. The convection in the winter of 2008 was quite enormous with the maximum MLD reaching 1638m in March. The evolution of this return to vigorous convective activity has been well documented by previous studies (e.g., Våge et al., 2009; Yashayaev and Loder, 2009). The MLD then retreated back and maintained an average depth of 1000m or so for the winters of 2009 – 2011. The maximum MLD was 911m during the winter of 2010, which was the shallowest in all recent winters. However, an intensification of convection returned for the winter of 2012 with maximum MLD of 1507 m.

The maximum MLD in the recent winters is shallower than it was in the early 1990s (~2000m) while the mean MLD is somewhat deeper than that of the late 1990s. This complex blend of generally weak convection and intermittent strong events might suggest a change in the dominant modes of variability in deep convection. We therefore consider deep convection as a non-linear, non-stationary process responding to a combination of factors either locally or remotely. For example, the causes of the strong degree of variability might reflect a switch from a primary oceanic response to atmospheric forcing to a response that includes both atmospheric forcing and internal changes in the water column, such as warming of the column itself. Note that extrema of the MLD over the years correspond well to positive and negative winter NAO index. This is, however, not enough to support the notion of an oversimplified 'linear' NAO-driven convective system in the Labrador Sea (Dickson et al. 1996; Pickart et al., 2002; Yashayaev, 2007). The lack of one-to-one correspondence implies a role of other factors, such as remote input of heat from the subtropics and weak stratification due to previous convective seasons, in causing deep convections in the 2000s. More discussion about the influences of the NAO forcing in the Labrador Sea will be presented in Section 2.5.3.

2.4.2 Buoyancy Frequency

Heat content variations of the first order affect the water column's density structure by changing its total buoyancy. The more buoyant the upper layers are, the more difficult it is for the convection to develop and strengthen. We first generated domain-averaged density profiles over the central Labrador Sea based on all profiles collected during October and November. This was done in order to best represent oceanic conditions prior to the initiation of deep convection. Using two profiles of density, the buoyancy flux can be approximated by integrating the difference between the densities:

$$b = -\frac{g}{\rho_0} \frac{\int_{1500}^{0} \left[\rho_{t_i}(z) - \rho_{t_{i+1}}(z)\right] dz}{t_{i+1} - t_i} \quad (\mathrm{m}^2 \cdot \mathrm{s}^{-3}), \tag{2.1}$$

where, ρ_{t_i} is the mean density profile based on all profiles collected during October and November and $\rho_{t_{i+1}}$ corresponds to the mean density profile of March of the next year. A major change in buoyancy can be found in the upper layers, and the choice of 1500m depth from which to start the integral is capable of capturing the buoyancy flux variability. The buoyancy flux was calculated for 3 cases: convection down to 1000m depth; convection down to 1500 m depth; and observed convection by March of the next year (Figure 2.3). Several points can be made here in terms of changes in total buoyancy flux and its relationship to deep convection in the Labrador Sea. First of all, it requires more and more buoyancy to remove in order to yield deep convection in the Labrador Sea. This is especially the case for convection as deep as 1500m, and indicates a rather constant increase of buoyancy at the lower layers. A slight increase in the discrepancy between the 1000 m and the 1500 m conditions may, in addition, reveal a continuous stratification for the past years. Furthermore, the assumption of well-mixed conditions at the depth of 1000 m yields buoyancy anomalies close to those found in observations, corresponding to shallow convection during the time period of this study. Finally, the observed conditions involve stronger interannual variability compared to the assumed well-mixed conditions. Note that the latter corresponds to the pre-convection conditions in October and November. Therefore, the stronger interannual variability in the observed buoyancy anomaly can only be attributed to winter conditions, i.e. changes in wintertime atmospheric forcing.

2.4.3 Enhanced Deep Convection in the Winter of 2008

2.4.3.1 Observations from Argo Floats

The deep convection that occurred in the winter of 2008 was exceptional given a general warming Labrador Sea in the 2000s. It is of great interest to understand the interactions between the development of this strong deep convection and its associated conditions. Argo floats that drifted in the Labrador Sea during the convective events provide the most direct observations of the deep convection progress. Two floats, Float 4900494 and Float 4900537, were used, which drifted in the central Labrador Sea for most of their life spans, including during the winter of 2008. Float 4900494 was released on June 4, 2004 and its last measurement was received on July 23, 2008. Float 4900537 has nearly the same total life span – from June 11, 2005 to Mar 2, 2009, although it moved eastward out of the Labrador Basin after the winter of 2008 following the recirculation path. Both of these records, being nearly 4-year in length, show strong mixing as deep as 1600 m in February and March of 2008 – the buoyancy frequency at this time was on the order of $10^{-4}\,\text{sec}^{-1}$ corresponding to a period longer than 1 hour (Figure 2.4b and 2.4d, white dashed boxes). For the earlier winters of 2005, 2006 and 2007, the convection events typically only reached 1000 m depth at the most. There were no convection signals from Float 4900494 for the winters of 2006 and 2007 because, during that time, the float was drifting around $56°N$, $50°W$ and was therefore too close to the warm and buoyant North Atlantic Current. By comparison, Float 4900537 for the two winters drifted in the southwestern basin, near $58°N$, $54°W$, where the well-known deep convection site lies (e.g., The Lab Sea Group, 1998). Strong mixing signals were also observed in the southeastern basin from Float 4900494 during the winter of 2005, as well as from Float 4900537 during the winter of 2008. However, the mechanism for deep convection in this region has not been fully understood. Furthermore, it was noted that the layer of 1000 m – 1500 m was occupied by a well-mixed water mass, which represents the LSW formed in the winter of 2000 (e.g., Yashayaev and Loder, 2009). The convection in the winter of 2008 was able to change water properties in the intermediate and deep layers, which, therefore, enabled the classic Labrador Sea Water produced during the early 1990s to come in contact with the surface layer for the first time since their formation (Yashayaev, 2007; Rhein et al., 2011).

Time-series of potential temperature and salinity profiles presented a time frame for the deepening of the strong mixing in the winter of 2008 (Figure 2.5), which finally lead to uniform water columns with an average potential temperature of $3.3°C$ and a salinity of 34.85 (LSW_{2008}, Yashayaev and Loder, 2009). Caution must be taken when analyzing Argo profiles because changes in water properties may be due to the changing locations of the floats while submerged. Since both Float 4900494 and Float 4900537 came in contact with the well-stratified west boundary currents in early winter, measurements from Float 4900677 were added for comparison in order to avoid any bias in the analysis (Figure 2.5e and 2.5f). Float 4900677 sampled the water properties of the convective site during the winter of 2008 (trajectory of this float not shown). Enhanced surface cooling initiated deep convection, which gradually cooled the surface layer (0 – 500 m) by $1.5°C$ within the first 4 – 6 weeks (e.g., Figure 2.5e). The sudden deepening of the mixing in late January has cooled the layer below to about 1000 m depth within 10 days. During the next several weeks, the mid- to deep layer (800 – 1400 m) was continuously cooled. By the end of February, the temperature profiles became constant from the surface all the way to depths greater than 1500 m, which lasted for at least the entire month of March. The fresh and cold surface waters seen on Mar 30, 2008 (Figure 2.5e and 2.5f) are from the Labrador Current as the float entered and started following the boundary current. Because of its close position to the west coast of Greenland for the first few weeks, Float 4900537 sampled water properties of both cold, fresh West Greenland Current and warm, saline Irminger Water. Erosion of the stratification took about 4 weeks and the strong mixing lasted for at least 5 weeks. Float 4900494 drifted westward and then southward during the course of deep convection. Hence, in the first 3 weeks, the characteristic Irminger Water can be seen from Argo profiles at depths between 200 m to 1000 m. West of about $50°W$, the water was continuously mixed in the upper 400 m as of the beginning of January, followed by a progressive deepening of the mixing down to 1600 m depth by the beginning of March.

2.4.3.2 Atmospheric Conditions

Figure 2.6a shows the wintertime surface heat flux of 2008 vs. the average extent of the 1990 – 1995 winters. The condition of the 1990 to 1995 winters was used as a baseline for comparison in order to put all discussion in the context of the deep convection variability. The deep convection events switched from a period of intense occurrence in the early 1990s to a period of weak and limited appearance afterwards, and the upper layer of the Labrador Sea experienced a transition from cooling to warming. It was noted that the sea ice coverage in the winter of 2008 was similar to that of the early 1990s, yet with even more southeastward extension of the sea ice edge – especially in the region between 55°N and 66°N (not shown here). The central Labrador Sea was subjected to a maximum heat loss ($Q_{net} <$ -350 W m^{-2}) in the winter of 2008, overlapping well with an area of the greatest heat loss during the early 1990s. Because of the extended sea ice edge, strong northwesterlies could maintain much of their intensity until reaching the central Labrador Sea, where they would pick up heat from the ocean surface layer and initiate vertical mixing in the water column. In contrast, for the period from 2001 – 2007, atmospheric and oceanic conditions were quite different from those of the early 1990s (Figure 2.6b). The sea ice edge retreated northwestward and over the central Labrador Sea the heat flux is smaller with $Q_{net} >$ -200 W m^{-2}. Therefore, the winter of 2008 was the only winter in the 2000s that matched the atmospheric conditions with the winters of the early 1990s. Although there has been a warming trend in the water column, the return of a strong deep convection event may highlight the more important role of the atmospheric forcing in setting the variability of deep convection despite an increasingly buoyant surface layer.

The correlation between atmospheric forcing and the development of deep convection shown in Figure 2.5 can be observed at finer temporal scales. The Q_{net} was on an average -400 W m^{-2} from early Dec 2007 to early Jan 2008, corresponding to gradual deepening of vertical mixing in the upper 500 m of the water column. Around Jan 20th, 2008, however, an enormous heat loss ($Q_{net} =$ -600 W m^{-2}) was suddenly introduced, in accordance with the sudden drop of the mixed layer depth down to 1000 m in the following 10 days (from Jan 20 to Jan 30, Figure 2.5e). For the next one and half months (Feb to mid-Mar), the net heat flux (average of -300 W m^{-2}) was large enough to maintain the vertical mixing through the end of March. The timing also indicates a time lead of a few days of the atmospheric forcing to oceanic responses.

2.5 Thermal Changes in the Central Labrador Sea

2.5.1 Potential Temperature Variability

The Labrador Sea interior has experienced a substantial warming during the time period of study. Increasing values of potential temperature were observed at depths of 500 m, 1000 m and 1500 m with linear trends of 0.031 °C yr^{-1}, 0.038 °C yr^{-1}, 0.028 °C yr^{-1}, respectively (Figure 2.7). Furthermore, temperatures have different dominant modes of variability at different depths. Lower frequency variations become more important with depth.

At the 500 m depth, the temperature was found to have strong annual cycle whose amplitude varied from year to year. In 2008, the maximum temperature difference at this depth was $0.7\ °C$, while dropping to $0.3\ °C$ for 2010. The winters of 2010 and 2011 were the warmest winters for the past two decades on record. By comparison, temperature variations at the middle and lower layers provide more information concerning changes at the interannual and longer timescales. The intermittent cooling periods of 2003, 2008 – 2009, and 2012 were embedded into the warming trend at the 1000 m depth. Only the 2008 winter cooling event was observed at the 1500 m depth (about 0.2 °C drop for that winter), suggesting an abnormally strong cooling condition in the entire water column. Therefore, interannual variations declined and lower frequency signals became more important at the lower depths. In addition, water temperatures at all depths, particularly those above 1000m, were relatively uniform for the winters of 2003, 2005, 2008, 2009, and 2012. These coincidences correspond to the development of convective processes that are intense enough to break stratification in the water column down to at least 1000 m. Note that the winter of 2009 had different situations compared to the other ones, given that the water temperatures for 1000 m and 1500 m had been nearly same for the entire preceding year.

As discussed above, there are different dominant modes of temperature variability at different depths. It is interesting, then, to quantitatively differentiate the dominant timescales of temperature variability at the upper, middle and lower layers. First, we separate original temperature variations into the components with varying frequencies using the EEMD. Figure 2.8 shows the progression of the obtained IMFs with high to low frequencies decomposed from temperature records at the 500 m depth. Large amount information is obtained through this decomposition, specifically regarding properties within the data's frequency domain. The IMF components C1, C2, and C3 can be interpreted as high-frequency temperature changes with periods less than one year, i.e., those that are associated with eddies in the Labrador Sea. C4 has a mean period of one year, corresponding to annual temperature changes in the Labrador Sea. This seasonal cycle has the largest amplitudes compared to all the other IMFs, indicating its primary contribution to the overall temperature variations at the 500 m depth. IMFs C5 to C8 correspond to signals at interannual timescales. The last component is the residual left out after extracting all periodic or quasi-periodic components. Since the residual contains monotonic changes in the original signal, it can be regarded as a long-term trend, or variation with very low frequency that cannot be resolved by the length of record used. This non-linear trend has the advantage over a simple linear trend obtained by a linear regression that it contains time-varying features, and therefore permits detection of non-linear and non-stationary processes, such as the acceleration or deceleration of temperature rises. The same EEMD procedure was applied to the temperature variations at all three depths.

Once the decomposition was completed, a significance test of the obtained IMFs was performed, comparing the spectral energy of each decomposed mode to that of white noise. Figure 2.9 shows the significance test of all three EEMD results. All IMFs are significant above the 95% confidence level, and can be interpreted with physical meanings. It is not surprising that the annual cycle of temperature (C4) at the 500m depth has the largest energy. Strong seasonality in surface layer water temperature reflects its close relationship to either local surface heating or current boundary currents whose temperature is known to have strong seasonal cycles. By comparison, interannual variability dominates at lower layers in the water columns. Note that intermittent cooling events can also be found at the 500 m depth in mode C5. The component C6 has the largest energy level at the 1000 m depth, corresponding to changes with a period of approximately 5 years (cooling events). At the 1500 m depth, it is the mode C7 that has the largest energy (mean period is approximately 7 – 8 years). However, its amplitude is not only small but also not much different from its companions. This means that temperature variations become weak and lack fluctuations as depth increases.

We then checked the time-frequency-dependent details of the modes of variability given the presumably non-stationary nature of the original data. We applied the Hilbert Transform to the significant IMFs for each depth. The HHT method generates unique frequency-time-amplitude (energy) plots as shown in Figure 2.10. Figure 2.10a displays the Hilbert spectrum and the MSD for temperature variations at the depth of 500 m. Two broad MSD peaks are located at $0.8-1.2\ \text{cycle yr}^{-1}$ and $0.2-0.3\ \text{cycle yr}^{-1}$, respectively. The former corresponds to a quasi-annual signal, which becomes more representative after 2008. The latter corresponds to a signal repeating approximately every 4 – 5 years, corresponding to the cooling events as shown in Figure 2.7. A broad peak in the MSD around the frequency of 1 cycle yr^{-1} corresponds to the annual cycle of temperature but with fluctuations with time. This takes advantage of the HHT and cannot be obtained from other spectral analysis methods with predefined periodic basis. Although spectrum amplitudes are generally small at high frequencies, they appear to be even smaller during years with strong convection events (see the blank periods in Figure 2.10a prior to 2005, 2008 and 2012 for frequencies of $1.4-2$ cycle yr^{-1}). This may reflect the tendency of high frequency signals (mean period of several months, such as eddies in the Labrador Sea) to have lower occurrence prior to years of strong convection.

At the 1000 m depth, the Hilbert spectrum presents no seasonal cycles and shows an increased energy over the time in the low-frequency bands of $0.1-0.4$ cycle yr^{-1} (Figure 2.10b). Moreover, there is a shift of localization of energy from 0.1 cycle yr^{-1} in the early 2000s to a combination of signals at frequencies of $0.1-0.3$ cycles yr^{-1} around 2008 and of $0.2-0.6$ cycle yr^{-1} around 2012. This indicates that water temperature at the 1000 m depth has become more variable than it was in the early 2000s. Signals with shorter periods of 2 – 5 years have become more dominant for the recent years. In contrast, there are fewer variations in the temperature at the 1500 m depth throughout the study period, which are dominated by a quasidecadal signal at the frequency slightly greater than 0.1 cycle yr^{-1} (Figure 2.10c). At this depth, the total spectral energy has no significant change over time, with only a slight increase in 2008.

2.5.2 Heat Content Variability

We first used the domain-averaged temperature measurements from Argo profiles to calculate heat content using

$$\mathrm{OHC} = C_P \cdot \int_{1000}^{0} \rho(z) \cdot \theta(z)\, dz\,, \tag{2.2}$$

where C_P is the heat capacity of seawater ($4000\ \mathrm{J\ kg^{-1}\ {}^{\circ}C^{-1}}$), ρ and θ are density and potential temperature respectively. Most of the annual and interannual temperature variability is observed at the 500m and 1000m depths. In the meantime, changes at the 1500 m depth rather represent low frequency variability that is not well resolved by the Argo record length. Therefore, the heat content integration is performed from the sea surface to a depth of 1000 m. Figure 2.11 displays the Hilbert spectrum of all significant IMFs after applying the EEMD to the obtained heat content components. There are two MSD peaks appearing around $0.8-1.2$ cycle yr^{-1} and $0.2-0.35$ cycle yr^{-1}, respectively. Such presence of maximum energy corresponds to two dominant timescales in heat content variations with characteristic periods of approximately 1 year and 3 – 5 years, respectively. Therefore, it is a blend of these different modes of variability that makes the most contribution to the total heat content variation in the central Labrador Sea. Furthermore, there was increased energy at the low frequency components that become significant after 2008 (dark red in Figure 2.11a).

We are concerned with changes over the longer timescales that could be related to deep convection and lateral advection, i.e., changes at the interannual timescales. We therefore focused on the cyclic motions with periods longer than 1 year. Three periodic components and the residual were filtered out as signals at the interannual and longer timescales as well as the long-term trend, which are later used to reconstruct the low frequency heat content variations (Figure 2.12). The instantaneous energy of the Hilbert spectrum applied to the selected low frequency IMFs shows a low energy level around 2005 – 2006, followed by a high energy level around 2010 (not shown here). Abrupt change (increase) in the heat content during 2009 – 2010 was also observed in the IMF components C5 and C6. The heat content reached a local maximum after its preceding minimum in 2009. Moreover, the residual ('R' in Figure 2.12) from the EEMD implies a trend of 1.36×10^{8} J m^{-2} year^{-1} in the heat content of the Labrador Sea interior. The long-term trend is similar to a linear trend, suggesting a scenario of persistent accumulation of heat in the Labrador Sea. In fact, the residual over the 9-year timescale might be part of a periodic variation over interdecadal to multi-decadal timescales as suggested from model results (e.g., Zhang, 2008).

2.5.3 NAO

Interannual variability in atmospheric forcing in the subpolar North Atlantic is characterized by the NAO index. The NAO index is associated with basin-wide changes in the wind patterns and large-scale modulations of the normal patterns of heat and moisture transport (Hurrell, 1995). Since the mid-1990s, the NAO index has become weak yet with increased fluctuation corresponding to generally mild winter conditions as compared to the previous harsh winters which had intensified westerlies and colder than normal air temperature. The high correlation between NAO-forcing and extreme deep convection discussed in Section 2.4 represents the effective oceanic response to the atmospheric variability. However, the NAO index itself is not an adequate indicator of deep convection occurrence given that even for winters with positive NAO index could have only a relatively small amount of heat extraction from the surface layer (e.g., due to changes in wind direction, Våge et al. 2009). Instead of the monthly NAO index, we considered the cumulative NAO index by accumulating monthly NAO index with time (https://climatedataguide.ucar.edu/climate-data/hurrell-north-atlantic-oscillation-nao-index-station-based), which better reflects the cumulative response of the oceanic signals to the overlying atmospheric conditions. Periods with a persistent positive (negative) NAO index correspond to increasing (decreasing) slopes in the cumulative NAO index, while sign changes yield local maxima and minima in the cumulative index. The NAO index used in this study is station-based and therefore has more consistency in time.

Figure 2.13 displays a direct comparison between the cumulative NAO index and the low-frequency heat content variations in the central Labrador Sea. The cumulative NAO index decreases (increases) when the ocean heat content increases (decreases). The low-frequency heat content variations are significantly negatively correlated with the cumulative NAO index with correlation coefficient of -0.73. In contrast, the correlation coefficient drops to -0.2 between the heat content and the monthly NAO index. Therefore, the cumulative NAO index more accurately accounts for the low-frequency variability in the upper ocean heat content. Maximum MLD during each winter based on Argo profiles is also displayed in Figure 2.13 (yellow squares). The occurrence of large MLD (for example, during 2005, 2008, 2012) is concomitant with enhanced heat flux, implying the impact of air-sea interaction on the convective process. Furthermore, the low-frequency turbulent heat flux variations lead the low-frequency changes in the heat content by a couple of months, and the latter is more reflected by the cumulative NAO index as stated above. Over longer timescales, there is a lagged (cumulative) response of heat content variations to the atmospheric forcing, reflecting the significant role of ocean's 'memory' (i.e., through deep convection and advection). This may suggest low-frequency rectification in ocean circulations, and associated heat transport, under impact of the NAO forcing.

2.6 Conclusions and Discussion

Using Argo data and the HHT method, we have presented an analysis on the temperature and heat content variability in the central Labrador Sea over the most recent decade in the context of deep convection variability. Although it has become generally weak and shallow, convection in the Labrador Sea experienced significant fluctuations during recent winters. Changes in the MLD closely relate to the temperature variations in the water column, which have different dominant modes of variability at different depths. We therefore investigated the dominant timescales of temperature variations by using the EEMD to decompose the original time-series into components with varying frequencies. While strong annual cycles exist at the 500m-depth level, signals at the interannual and longer timescales dominate the temperature variations in the middle (1000 m) and lower layers (1500 m). The Hilbert spectrum further indicates that most of the maximum amplitudes (energy) have been associated with a small band of frequencies, namely those between $0.1 - 0.3$ cycle yr^{-1}. Such changes were more evident at the depths of 500m and 1000m, corresponding to in-phase variations in temperature at the upper and intermediate layers beyond the observed warming trends. This may relate to the variability of the convective processes, which has the ability to change the overall temperature in the upper water columns.

In order to fully understand the role of convection in regulating the interannual signals in the upper layers (0 – 1000 m), we also examined the heat content variations in the central Labrador Sea. The use of heat content as a key variable also takes into account the influences of air-sea interaction. The HHT method revealed that low frequency signals at frequencies of $0.2 - 0.3$ cycle yr^{-1} are very important besides the strong seasonal cycles. Furthermore, the degree of the low frequency variations ($0.05 - 0.5$ cycle yr^{-1}) became stronger from the lows in the early 2000s to the high around 2010. Changes in the heat content of the deeper layer (1000 m – 1500 m) were also examined for comparison. The temporal pattern is like that of the temperature variations at the 1000 m depths (blue line, Figure 2.7) – an overall increase of heat content interrupted with two cooling events in the winters of 2008 and 2012 respectively. Their similar patterns reflect much less variation in the temperature field at the deeper layers. In terms of the decadal trends, the upper layer heat content (0 – 1000 m, 0.135 GJ m^{-2} yr^{-1}) increased faster than that of the deeper layers (1000 – 1500 m, 0.096 GJ m^{-2} yr^{-1}).

The atmospheric forcing works to effectively set the interannual variability in the heat content in the Labrador Sea. Based on a primitive heat balance model, van Aken et al. (2011) showed that 4-year averaged turbulent heat flux has strong correlation to the low frequency variations in the heat content at the intermediate layers in the Labrador Sea. Moreover, over the interannual and longer timescales, strong correlations between the cumulative NAO index and the upper ocean heat content ($r=-0.73$) also suggest the importance of ocean internal changes. Fast warming since the mid-1990s to the 2000s should be due to the increased advective heating caused by ventilation of large volumes of the Labrador Sea Water (Yashayaev et al., 2007) and by the compensation by the warmer incoming current system (Myers et al., 2007; Luo et al., 2012). However, note that the accumulated oceanic conditions may, in turn, contribute to the variability of deep convections, i.e., by changing the size of the accessible heat reservoir (e.g., Zhu and Demirov, 2011; Gelderloos et al., 2012).

The ongoing warming in the subpolar North Atlantic has raised more concerns of the further decline of deep convection in the Labrador Sea. However, the total buoyancy changes during the winters reveal that weak convection limited to 1000m depth most likely continue into the near future. The stronger degree of the interannual variability observed for the most recent winters might be local fluctuations embedded in the overall low frequency change at high latitudes. In fact, the residual (long-term trend) over the 9-year timescale may be part of a periodic variation over timescales of interdecadal to multi-decadal timescales. Häkkinen et al. (2013) presented a strong relationship between the subpolar heat content and the Atlantic Multi-decadal Variability (AMV). Zhang (2008), based on 1000-year coupled ocean-atmosphere model simulation, revealed that subsurface temperature variations in the subpolar gyre are part of the distinct dipole pattern in the North Atlantic. This dipole pattern relates to AMV and represents changes in the AMOC. We adopted an extended heat content record in the Labrador Sea interior based on Ishii's OHC dataset (1945 – 2010). Here, the low frequency heat content was used by combining the IMF component that has the second largest energy (the first one corresponds to the annual cycle) and the residual from the EEMD results. Since the residual in heat content contains information on the long-term trend, we chose to use the AMV index also containing the warming trend. There is a strong correlation between the low frequency heat content and the AMV with correlation coefficient of 0.77. In addition, the maximum cross correlation is 0.79 in which the AMV leads 2 years, suggesting that the source of low frequency signals in the Labrador Sea may come from low to mid-latitudes. If we removed the warming trend from the AMV index as well as the residual from the low frequency heat content, the correlation coefficient then drops to 0.53. This indicates the important contribution of warming in the Labrador Sea over the past decades. Heat content variations in the

Labrador Sea interior dominate the low frequency changes in the entire subpolar gyre in response to the century-timescale AMV. In addition, abrupt changes in heat content were observed in low frequency components during 2009 – 2010, which is concomitant with changes in the entire subpolar gyre. The Labrador Sea interior, therefore, hosts most of the low frequency variability in the subpolar North Atlantic and serves as the indicative region in the high latitudes of climate change and climate variability.

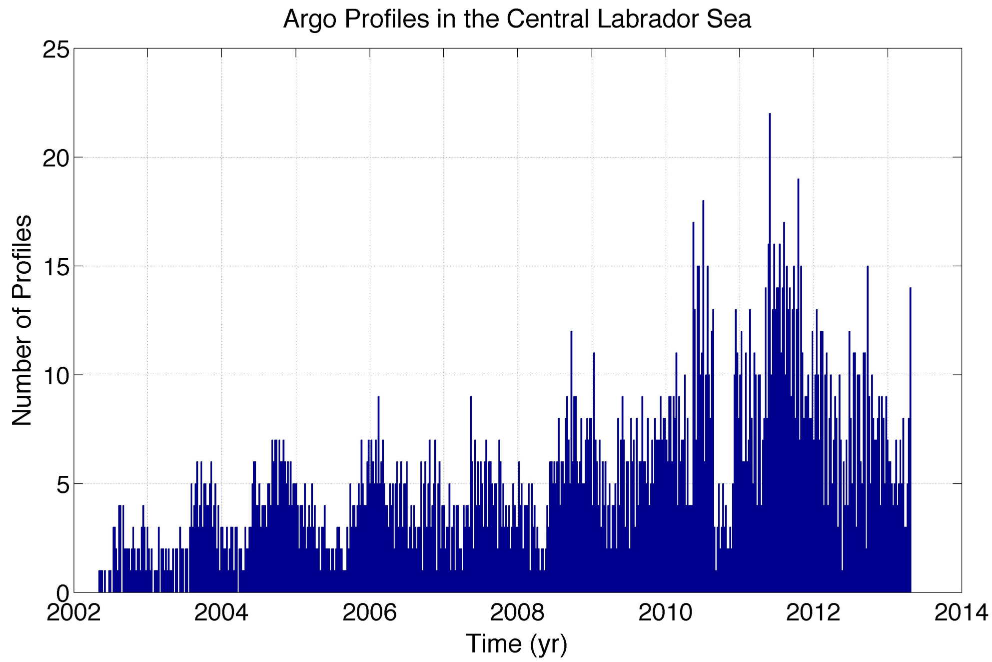

Figure 2.1: Weekly number of Argo profiles in the central Labrador Sea ($56°W-48°W$, $56°N-60°N$).

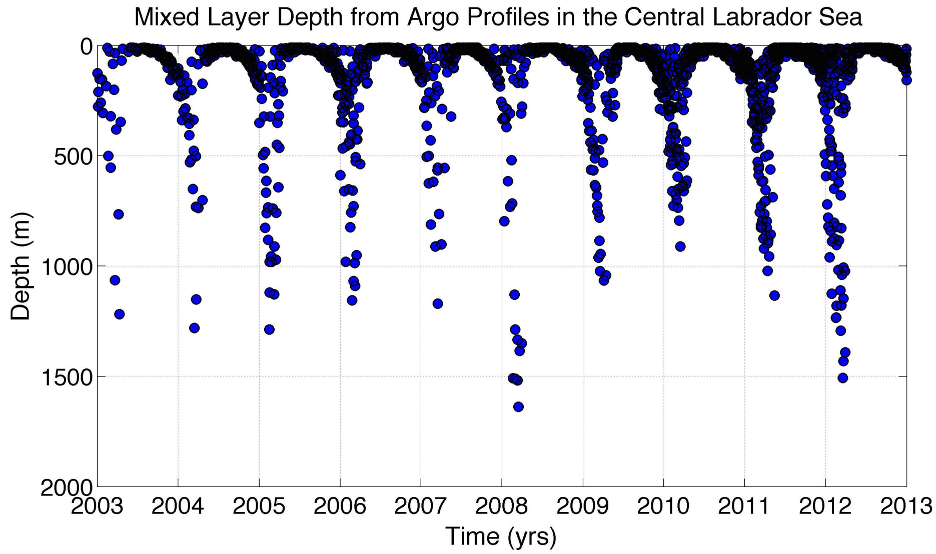

Figure 2.2: Mixed Layer Depth in the Labrador Sea based on Argo data using density criteria.

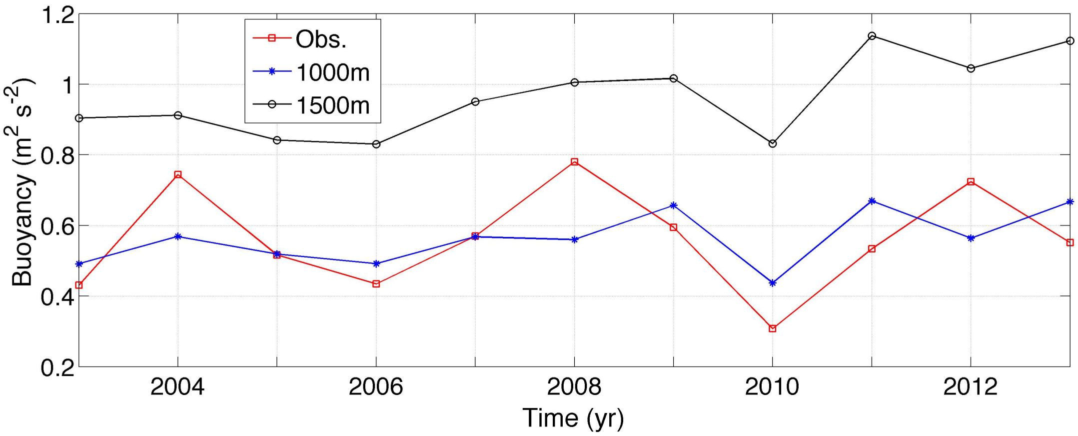

Figure 2.3: Total buoyancy change for each winter obtained from two density profiles. While the initial profile is the same (October and November averaged), the second density profiles are different for 1000m well mixed condition (blue line), 1500m well mixed condition (black line), and the observed mixing condition based on profiles whose MLDs are greater than 80% of the maximum MLDs during March of the next year (red line), respectively.

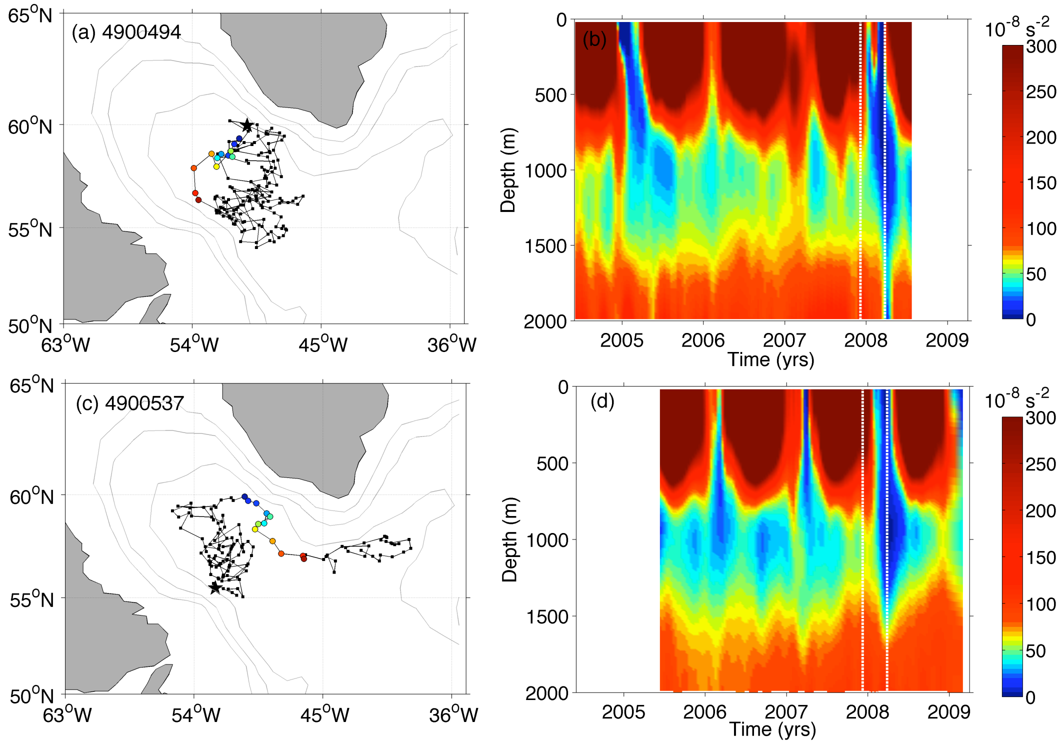

Figure 2.4: The trajectories and corresponding buoyancy frequency of two floats that spent most of their lifetime in the central Labrador Sea. The position of each profile is labeled with solid dots in (a) and (c) with star indicating the initial release locations. Colored dots correspond to the winter of 2008 (see Figure 3 for profiles of specific dates). This period is also bounded by white dashed line in the depth-time plots of the squared buoyancy frequency in (b) and (d).

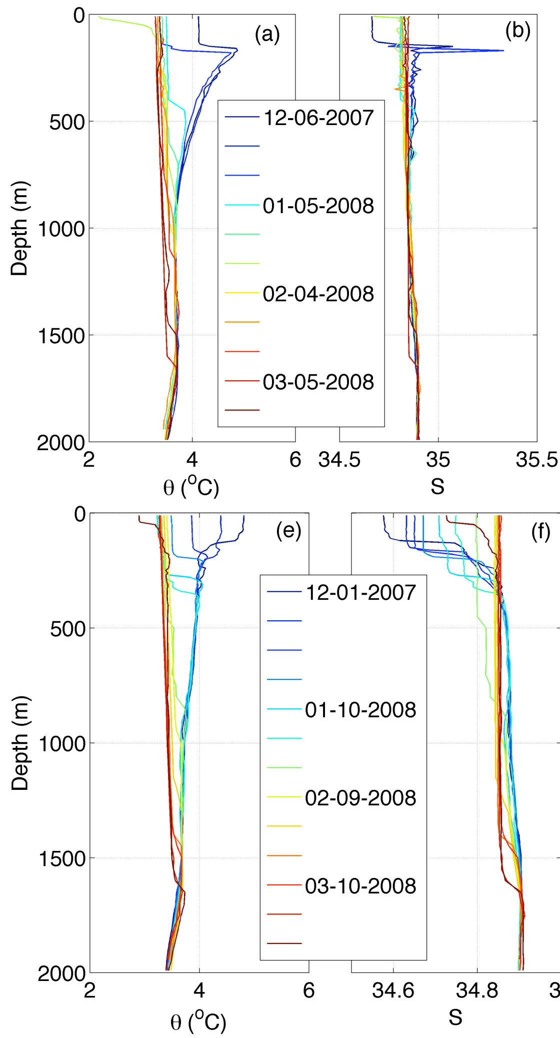

Figure 2.5: The evolution of potential temperature, salinity (from December 2007 to March 2008 with 10-day interval) of Float 4900494 (a)(b), Float 4900537 (c)(d) and Float 4900677 (e)(f).

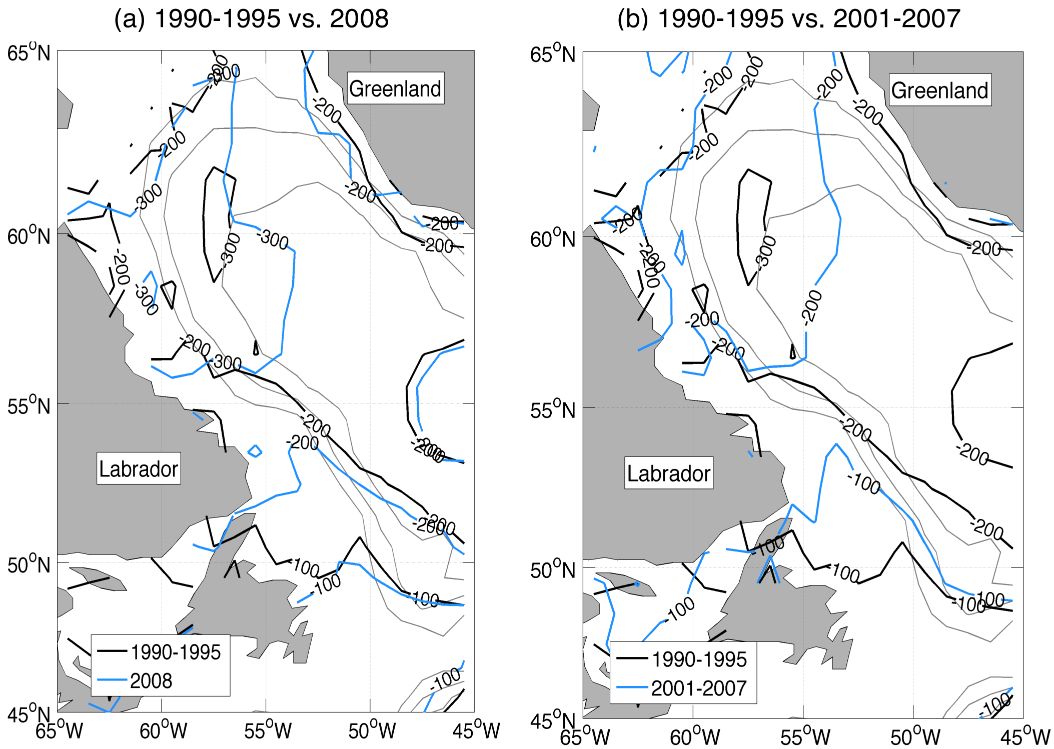

Figure 2.6: The net heat flux of the (black) 1990 – 1995 winters average and of the winter of (a) 2008, and (b) the 2001 – 2007 averages.

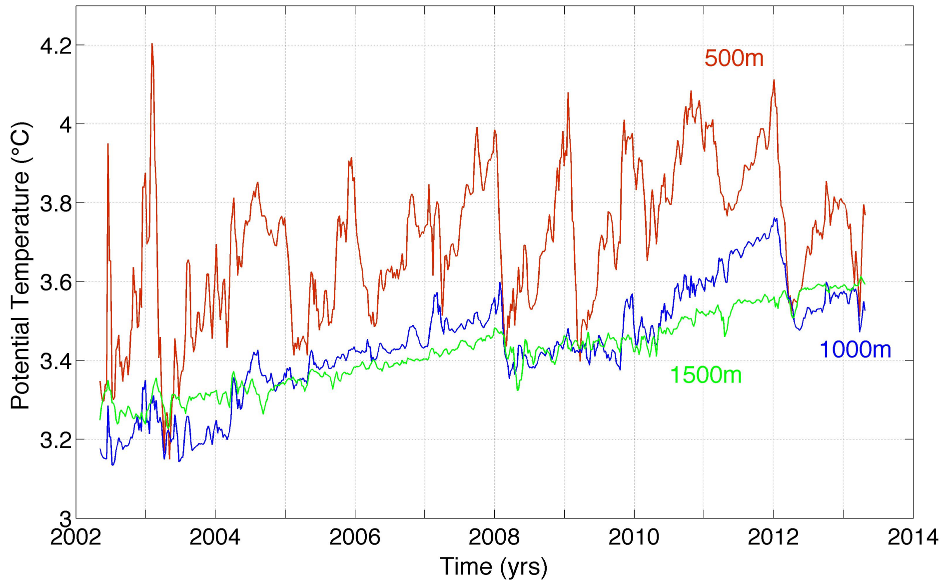

Figure 2.7: The potential temperature at three depths of 500m, 1000m and 1500m, respectively, in the central Labrador Sea.

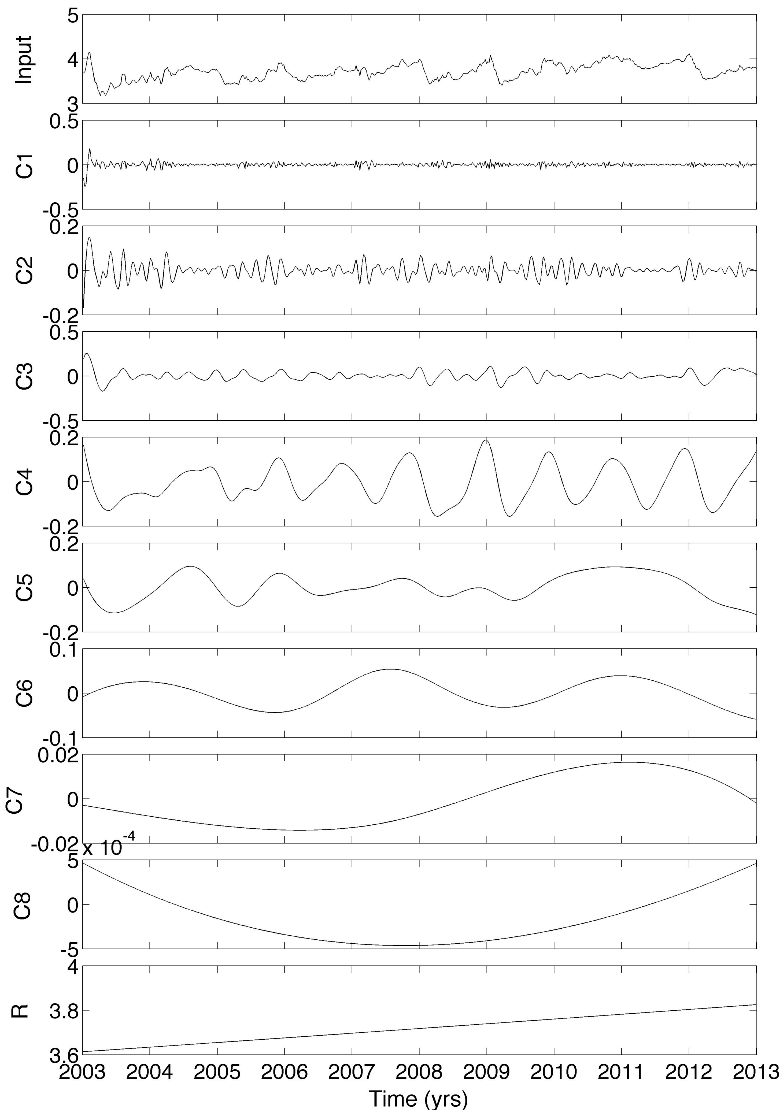

Figure 2.8: Progression of the EEMD results based on the potential temperature at the 500m depth averaged in the central Labrador Sea. Units are degree Celsius.

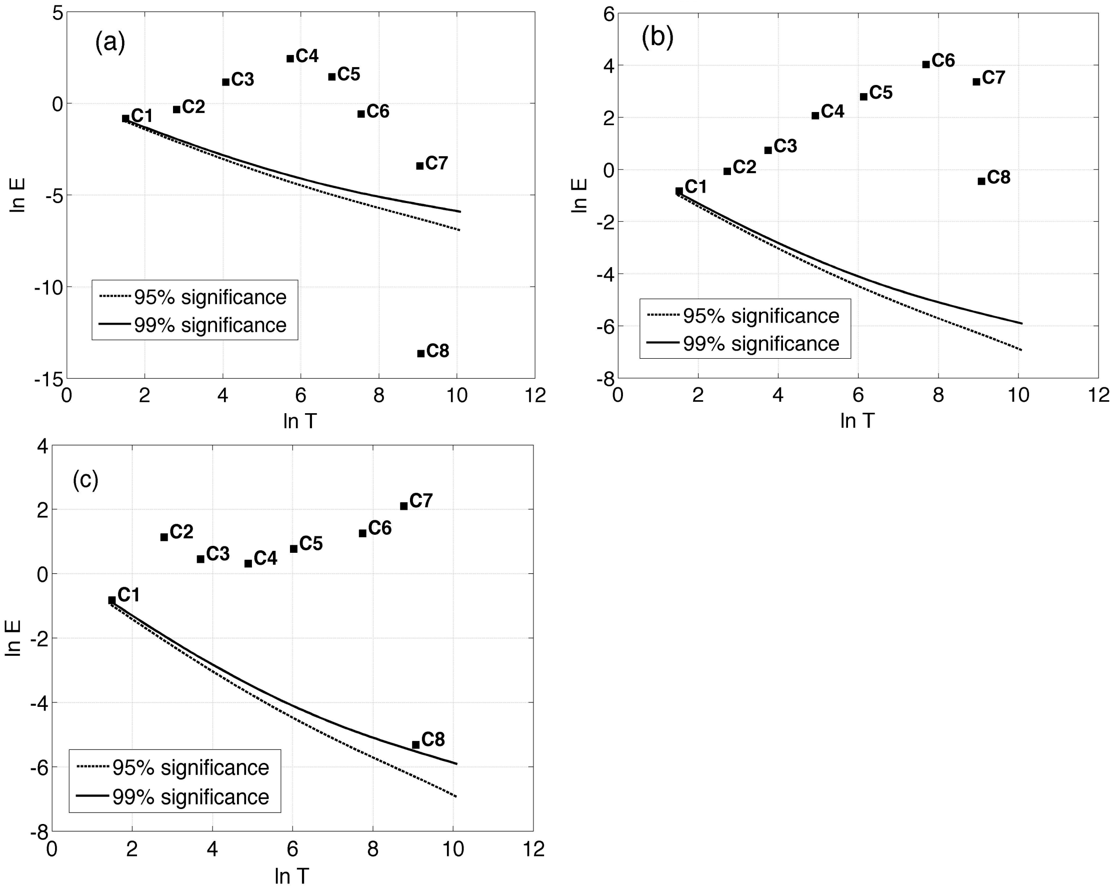

Figure 2.9: IMF significance test results for temperature variations at the 500m (a), 1000m (b), and 1500m (c) depths, respectively. The dashed and solid lines represent the 1th and the 5th percentiles determined from the probability distribution of the energy density of the white noise. The black dots correspond to the pairs of averaged mean normalized energy density (y-axis) and averaged mean period (x-axis) of the IMFs.

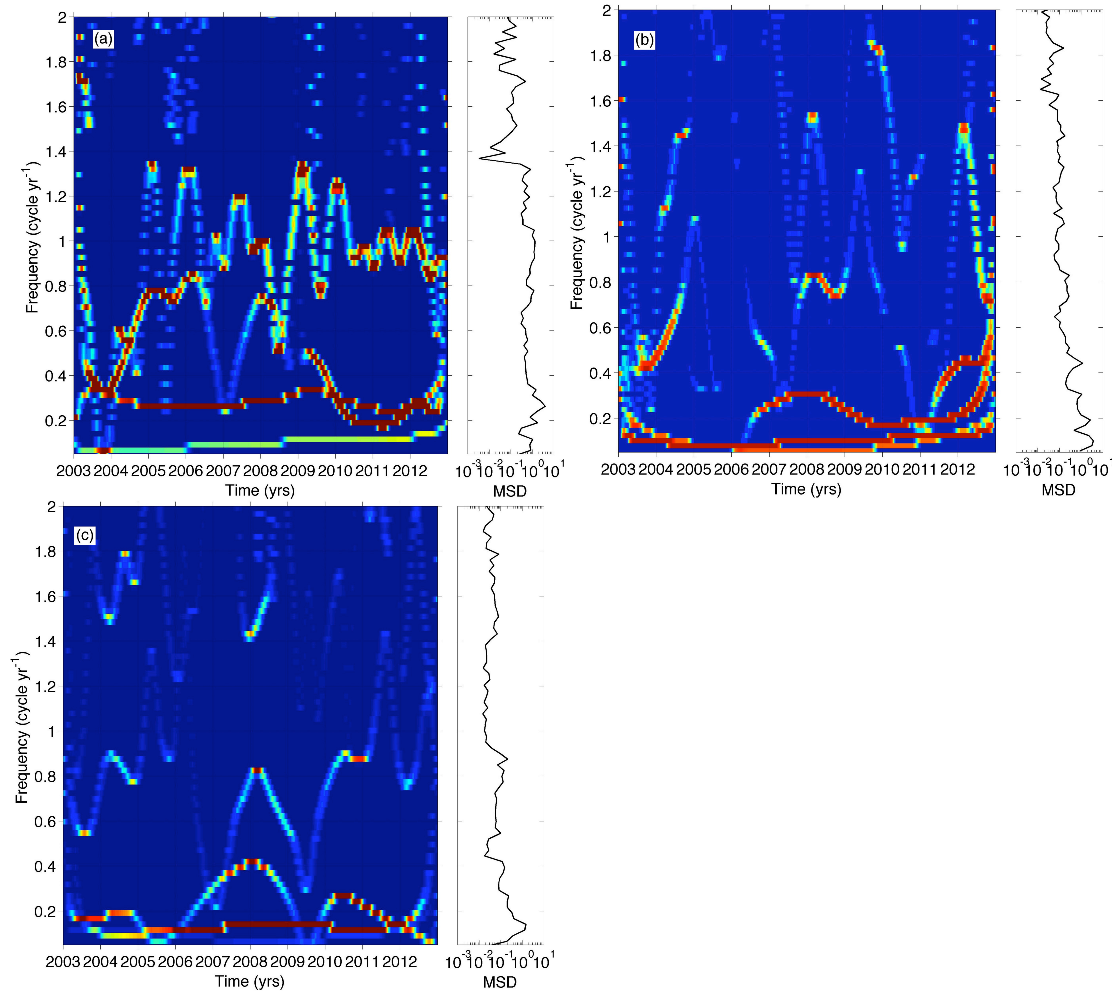

Figure 2.10: The Hilbert spectrum (left) and the marginal spectral density (right) for the IMFs obtained from temperature variations at the 500m (a), 1000m (b), and 1500m (c) depths respectively.

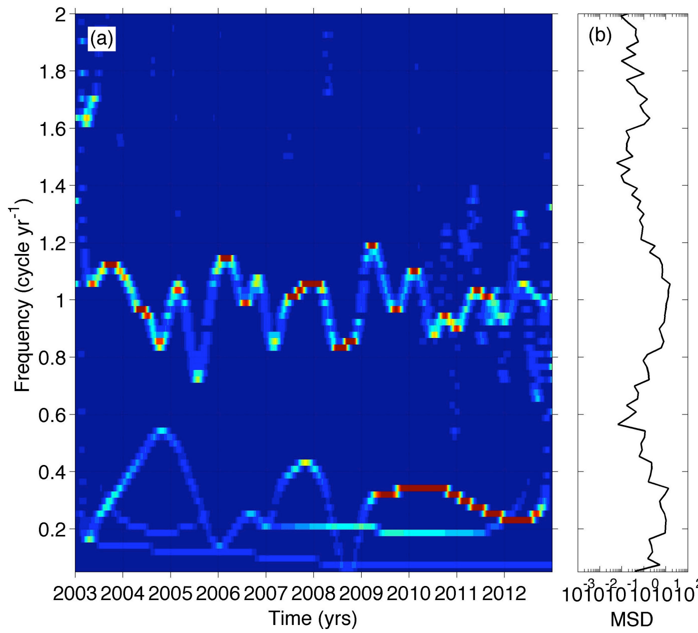

Figure 2.11: The Hilbert spectrum (a) and the marginal spectral density (b) of the IMF components from the EEMD of the heat content in the central Labrador Sea.

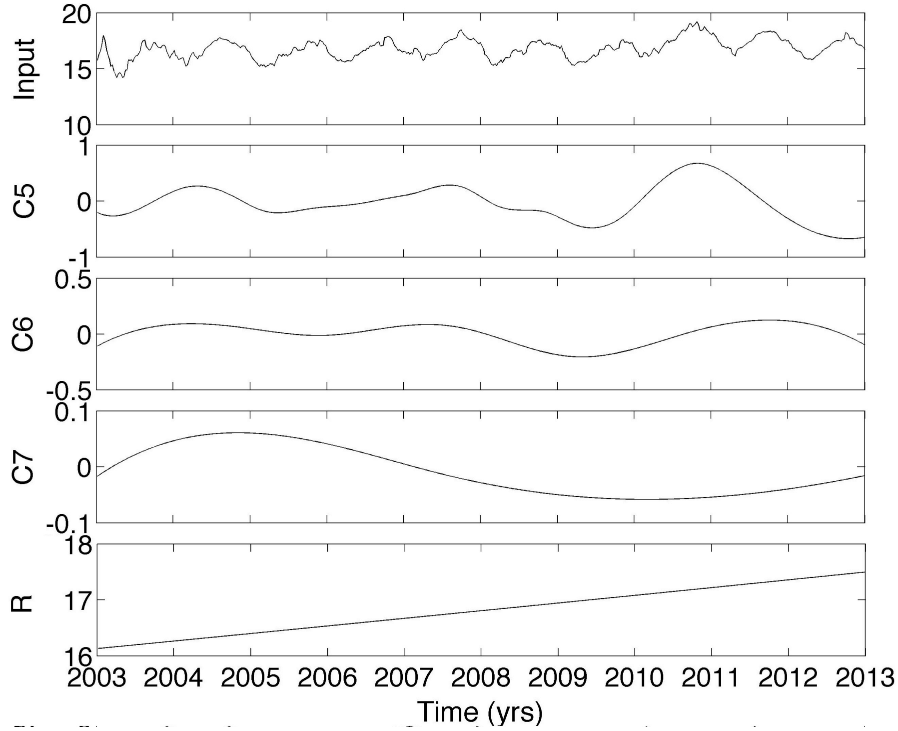

Figure 2.12: The IMF components (C5, C6, C7, all are significant at 99% confidence level) and the residual (R) used to reconstruct the low frequency heat content changes in the Labrador Sea interior. The original time-series (Input) is also shown for references. Units are $\mathrm{GJ\ m^{-2}}$.

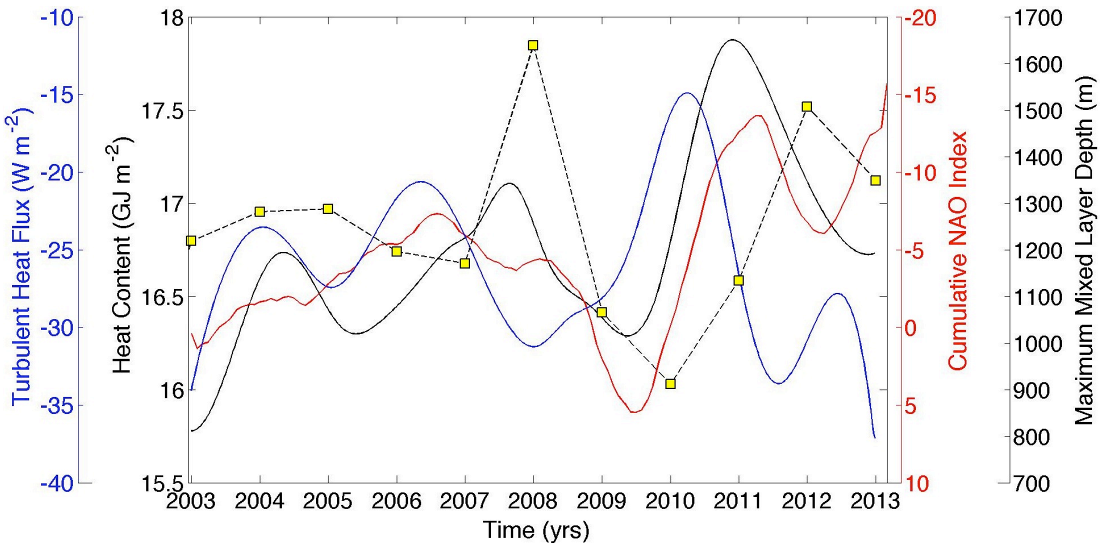

Figure 2.13: Time-series of the reconstructed low frequency heat content (black solid line) from the significant IMFs with periods > 1 year and the non-linear trend, the cumulative NAO index (red solid line; y-axis inverted), low frequency variations in the turbulent heat flux averaged over the Labrador Sea (blue solid line), and wintertime maximum MLD (yellow squares). Note that a 12-month running smoothing was applied to the cumulative NAO index.

Chapter 3

A DIPOLE PATTERN OF THE SEA SURFACE HEIGHT ANOMALY IN THE NORTH ATLANTIC: 1990S – 2000S

3.1 Abstract

Despite a long-term trend of sea level rise continuing into the 2000s in the subpolar North Atlantic, variations in the sea surface height have behaved differently in both spatial and temporal domains. A dipole pattern, centered between the Northern Atlantic subpolar region and the region near the Gulf Stream, was observed in the linear trends of the sea surface height anomaly (SSHA). By applying the Ensemble Empirical Mode Decomposition (EEMD), we found that this dipole pattern is mainly associated with the interannual to decadal SSHA oscillations of the two regions, which are 180° out of phase with each other over the time span of this study. The low-frequency variations of the SSHA in the subpolar region are strongly inversely correlated with the cumulative North Atlantic Oscillation (NAO) index ($r = -0.84$), in contrast with the Gulf Stream region, which is positively correlated ($r = 0.22$). Both correlations are statistically significant. This therefore reveals an asymmetric response of the regional SSHA to the cumulative NAO-forcing, in which the subpolar variability leads that of the Gulf Stream region by 29 months. Moreover, there is a remarkable reversal of the SSHA trends from the 1990s to the 2000s, which is unexpected given a

weak and fluctuating NAO behavior since mid-1990s. Such SSHA variations in the 2000s might be related to the lagged variations of the Atlantic meridional overturning circulation (AMOC).

3.2 Introduction

Sea surface heights have been measured by the repeat coverage of altimeters since 1992, providing one of the most important oceanic signals related to the climate change. The sea surface height anomaly (SSHA) is often interpreted as either the variations of upper ocean heat storage based on a simple linear relationship (e.g., Chambers et al., 1997) or the changes in the oceanic circulation given that the dynamic sea level variations balance geostrophic velocity anomalies (e.g., Häkkinen and Rhines, 2004; Böning et al., 2006). Therefore, advanced temporal and spatial resolution of the SSHA has great potential to serve as indicators of large-scale oceanic processes, which in the North Atlantic have a wide range of dominant frequencies.

Previous studies have investigated the sea level variability in the North Atlantic from either observations or numerical simulations. Esselborn and Eden (2001) found that a sign change of SSHA dipole pattern, centered in the subpolar and subtropical North Atlantic, follows a drop in the North Atlantic Oscillation (NAO) index between 1995 and 1996. They attributed the interannual sea level variability to a fast response of large-scale circulation to changes in the wind stress curl. Häkkinen and Rhines (2004) presented a similar pattern in the leading Empirical Orthogonal Function (EOF) of SSHA with a continual rise in the subpolar region in the 1990s, suggesting weakening subpolar gyre (SPG) circulation due to a decline of deep convection in the Labrador Sea whose variability is at interannual to decadal time scales (e.g., Yashayaev, 2007). A recent study by Zhang (2008) showed that the dipole pattern in the leading SSHA mode is likely to be a distinctive 'fingerprint' of the Atlantic meridional overturning circulation (AMOC) variations and is a part of multi-decadal variability. Lorbacher et al. (2010) argued that there is a wind-driven interannual SSHA variability presented by a dipole pattern as well as a gradual SSHA increase in the entire North Atlantic ocean associated with multi-decadal decline of the AMOC. These two patterns differ significantly because of different mechanisms, in which the basin wide SSHA change is not useful as a 'fingerprint' of longer-term AMOC changes and could be masked by the faster wind-driven variability. Given an essential role of the subpolar gyre variability in the climate change, it is of interests to study the relative importance of SSHA variability, especially at low frequency, in the subpolar North Atlantic and their possible causes.

Our objectives in this study are to examine the characteristic pattern of sea level variations based on altimeter observations in the mid- to high-latitudes of the North Atlantic and to analyze the SSHA variability at different time scales by the newly proposed noise-assisted data analysis method, the ensemble empirical mode decomposition (EEMD). The present study will shed light on nonstationary climate processes probably related to recent rapid changes (i.e., reginoal warming) in the northern North Atlantic in terms of regional sea level variations.

3.3 Data and Method

The multi-mission satellite altimeter datasets are processed by the Ssalto/Duacs and distributed by CLS/AVISO. Combining data from different missions significantly improves the estimation of mesoscale signals (Le Traon et al., 1999). Monthly gridded maps at $1/3^{\circ}$ spatial resolution were used in this study.

The EEMD is used to separate different modes of the sea level variations in the mid- to high-latitude North Atlantic based on their characteristic frequencies. Extensive details of the EEMD method are described in Appendix A.

3.4 Sea Surface Height Anomaly

Figure 3.1 shows the SSHA trends in the study domain from November 1992 to January 2011. No spatially uniform rise of sea level was found. Instead, the SSHA trends appear to vary considerably by location. There is an overall sea level rise in the subpolar region from 50°N to 65°N latitudes, whereas in the region near the Gulf Stream, the sea level follows an overall decreasing trend. This pattern resembles the distinct dipole pattern of the sea level variations in the regions north and south of 50°N latitude, which has been seen in earlier studies (e.g., Esselborn and Eden, 2001; Häkkinen and Rhines, 2004; Hátún et al., 2005; Lorbacher et al., 2010). Sea level is manifestly rising in the southwestern Labrador Basin and the central Irminger Basin with a maximum magnitude of approximately 8 mm yr^{-1}. Increased sea level reflects accumulation of water mass in the interior of the subpolar gyre accompanied by an anomalous anti-cyclonic circulation, which may be due to the decline of the deep ocean convections in the subpolar North Atlantic (Häkkinen and Rhines, 2004; Böning et al., 2006; Bersch et al., 2007). In comparison, an overall sea level decrease dominates the region near the Gulf Stream path and the North Atlantic Current path that extends northeastward through the gap between the Mid-Atlantic Ridge and the Reykjanes Ridge. The minimum sea level decrease is approximately $-10\ \mathrm{mm\ yr^{-1}}$, spreading along $40°\mathrm{N}$ latitude over the main eastward path of the Gulf Stream.

In order to evaluate the temporal evolution of the dipole pattern, we applied EEMD to the spatially averaged SSHA time series in regions covering the subpolar gyre and the Gulf Stream path, respectively. For simplicity, we arbitrarily divided these two regions by latitude of $50°\mathrm{N}$ and labeled them with 'North' and 'South' (see blue boxes in Figure 3.1). The results of EEMD are presented in Figure 3.2, which includes the full decomposition to illustrate the high to low frequency progression with which EEMD extracts independent signal components (C1 to C6) and the residual long-term trend (Residual). The significance test was performed to the IMFs, and the results are displayed in Figure 3.3. Except C6, all other IMFs are significant at 99% confidence level. The significant IMFs are assigned a physical meaning based on the interpretation of their mean period. The first component (C1) corresponds to signals at intra-seasonal time scale. C2 has the largest amplitudes with clear seasonality for both regions, which is associated with the solar irradiance variation in this region. At interannual to decadal time scales (C3, C4 and C5), the most prominent feature of the SSHA oscillations between the 'North' and 'South' is their coherent appearance of nearly opposite changes throughout the time span of this study. The majority of differences between the two regions' SSHA signals was manifested in the time period from 1993 to 2002, and diminished later, especially from 2002 to 2008 (see C3 and C4, Figure 2.2). The long-term trends (Residual) also behave differently for 'North' and 'South' regions. The overall sea level gradually increased in the 'North' region whereas only small increase of the SSHA was in the 'South' region from the 1990s to early 2000s. Specifically, the sea level rise in the 'North' region was 3.6 mm yr^{-1}, while in the 'South' region it was 0.8 mm yr^{-1}. Given a globally mean sea level rise rate at 3.2 ± 0.6 mm yr^{-1} (AVISO, http://www.aviso.oceanobs.com/en/news/ocean-indicators/mean-sea-level/), the 'North' region embraces the largest local sea level rise signal. Moreover, the reduction of the SSHA variations was also seen in the residuals. The rate of sea level rise in the 'North' in the period of 2002 – 2011 was approximately half of that in 1993 – 2001, while there was almost indistinguishable sea level change in the 'South' region from 2002 to 2011.

3.5 Geographic Differences in the SSHA

The difference in the SSHA variability between the 'North' and 'South' regions was also investigated. We combined the statistically significant, low frequency modes with the long-term trend (C3, C4, C5 and Residual) in order to quantitatively compare patterns of interannual and longer variability with each other and with the dominant climatic indices in the North Atlantic. Unless otherwise noted, the SSHA variations discussed hereinafter represent the low frequency changes.

While the sea level variation in the 'North' region is concomitant with the intensity of the cyclonic circulation, the SSHA variations in the 'South' region, especially at low frequency, are associated with the changes in the thermohaline properties, which reflect predominantly overturning changes (Häkkinen, 2001; Volkov and van Aken, 2003). The opposite SSHA changes in the two regions showed in Figure 3.2 may suggest some lagged communications between corresponding oceanic processes. The 'North' and 'South' sea level variations in Figure 3.4 have a maximum correlation of 0.44 with a time lag of 29 months in which the 'North' variations lead.

In the North Atlantic, the NAO is the leading mode of large-scale atmospheric variability whose 'positive' phase is associated with enhanced cold and dry westerlies across the mid-latitudes of the North Atlantic onto Europe, with anomalous southerly flow over the eastern U.S. and anomalous northerly flow across the Canadian Arctic and the Mediterranean (Hurrell, 1995). Because that the ocean signal reflects a time integration of the atmospheric forcing, for example, through mixed layer 'memory' and Rossby wave propagation (Curry and McCartney, 2001), we used the cumulative NAO index instead by integrating monthly NAO index over time starting from November 1992 (http://www.cgd.ucar.edu/cas/jhurrell/indices.html). The cumulative NAO index highlights any persistent situations and shifts in the normal NAO index (Figure 3.4, black solid and dotted lines), which may more accurately represent the cumulative effects of oceanic signal variations in response to the atmospheric forcing.

The SSHA variability in the 'North' region is strongly correlated with the cumulative NAO Index ($r = -0.84$). The correlation coefficient is, however, only 0.22 between the 'South' region SSHA and the cumulative NAO index. In comparison, the 'North' and 'South' SSHA are weakly correlated with the normal monthly NAO index with coefficients of -0.32 and 0.33 respectively.

The low frequency components and the long-term trend of the SSHA in the 'North' region, therefore, more effectively respond to the NAO than the 'South' region. A period of persistent positive NAO corresponds to decreased sea level in the 'North' region and to increased sea level in the 'South' region (e.g., 1992 – 1995, Figure 3.4). Due to relatively weak correlation, however, nearly no change was found in the 'South' SSHA in the period of 2002 to 2008, despite the generally increasing sea level in the 'North' region associated with an overall decreasing of the cumulative NAO index. The NAO-forcing, thereby, have more contributions to changes in the low-frequency oscillations of the 'North' SSHA. It is also noted of different contributions from the SSHA trends (Residual) in the two regions. If the long-term trend of the SSHA was taken out of consideration, the correlation coefficient between the 'North' SSHA and the cumulative NAO index became -0.59. This suggests the importance of the SSHA trend in the total variance and reflects a time-integrated response of the 'North' region SSHA to the NAO-forcing. In the 'South' region, the correlation coefficient increased to 0.43 after the long-term SSHA trend was removed. Therefore, the low-frequency oscillations of the 'South' region SSHA have stronger correlations to the cumulative NAO index than its long-term trend.

It is also of interests to examine whether the western and the eastern subpolar North Atlantic SSHA variations respond to the NAO-forcing differently since changes in the two regions may bear different mechanisms (e.g., Herbaut and Houssais, 2009). To do this, we divided the 'North' region into west and east sub-regions by 33°W (namely 'NW' and 'NE' for simplicity). Only statistically significant low-frequency components of SSHA were considered (C3, C4 and C5). The SSHA variations have strong correlation to the cumulative NAO index with correlation coefficients of -0.62 for the 'NW' region and -0.60 for the 'NE' respectively. In comparison, the SSHA variations have weaker correlations to the normal monthly NAO index; the highest correlation coefficients are -0.45 at 12-month lag for 'NW' and -0.52 at 8-month lags for 'NE'. This implies that (1) the low-frequency SSHA oscillations in the entire subpolar gyre are strongly concomitant with the accumulated changes in the NAO, and (2), however, in terms of interannual NAO changes, the eastern subpolar gyre responds faster than does the western subpolar gyre.

We considered the NAO index because of its dominating role in representing the atmospheric variability especially at mid- to high-latitudes in the North Atlantic (e.g., Hurrell, 1995; Marshall et al., 2001). The Eastern Atlantic Pattern (EAP) and the Atlantic Oscillation (AO) as well as the first two Principle Components (PCs) of the wind stress curl (data from NCEP) were also tested for comparison (Table 3.1). The results showed that the NAO and the AO have relatively strong correlation with the SSHA variations in both 'North' and 'South' regions. Given that the NAO is more like a regional expression of the AO (e.g., Thompson and Wallace, 1998; Wallace et al., 2000), it will not be improper to emphasize the impacts of the NAO forcing instead of the AO given that the area of interests covers only mid- to high-latitudes of the North Atlantic and not the Arctic.

3.6 Dipole Pattern

Recalling that the sea level variations are not homogenous over time (there are reduced SSHA amplitudes in the 2000s as seen in C3, C4 and C5 components as well as in Residual), we examined changes in the two time periods respectively. The time separation also takes into account the shifts in the winter (Dec – Mar) NAO behavior from years with positive index to years with weak and fluctuating index. The linear SSHA trends were computed for the period of 1992 to 2001 and 2002 to 2011, respectively. Figure 3.5a shows a similar dipole pattern of the SSHA trend as shown in Figure 3.1 with a positive center in the subpolar region, especially in the Irminger and the Iceland Basins, and a negative center in the region near the Gulf Stream, especially between 35°N to 50°N latitudes. In the 1990s, sea level rise manifested itself in the entire subpolar region (approximately 15 mm yr^{-1} maximum in the Irminger Basin), which indicates a rebound of the sea level from the early 1990s to the early 2000s. Meanwhile, the region of the Gulf Stream path experienced decreasing sea level at a minimum rate of approximately -30 mm yr^{-1}. Both rates are 2 to 3 times greater than the overall trends in corresponding areas. A reversal of the SSHA trends appeared in the 2000s with exception in the Labrador Basin. For example, decreasing sea level in the Irminger Sea was at approximately -3 mm yr^{-1}, compensating for the increased sea level in the previous 9 years.

It was noted that the winter of 2009/2010 has a negative NAO index (DJFM averaged of -4.64) after two successive winters of positive NAO index (2.79 and 2.10 respectively) and a winter of mild NAO index (-0.41). This, to some extent, resembled a drop of the NAO index of the 1995/1996. Following Esselborn and Eden (2001), we made a SSHA composite for December 2008 to May 2009 minus December 2009 to May 2010 (not shown here). A northern increasing and southern decreasing sea level was clearly divided by 50°N in the study area, which is similar to that of 1995/1996 (see Figure 2a in Esselborn and Eden (2001)). This confirms that the interannual change of SSHA follows the NAO index when it changed sign (e.g., Volkov and van Aken, 2003). However, the dipole SSHA from 2002 to 2008 has the similar reversal pattern in Figure 3.5b, which is opposite to changes in 2009 – 2010. Hence, the reversal of SSHA dipole pattern is not sensitive to changes in the NAO index in the 2000s.

3.7 Conclusions and Discussion

The linear trends of the SSHA show a dipole pattern between the subpolar North Atlantic and the region near the Gulf Stream path. Given recent rapid changes in the northern North Atlantic since the 1990s (e.g., Sarafanov et al., 2008; Reverdin, 2010; Häkkinen et al., 2011; Robson et al., 2012), the present study focused more on nonstationary processes in the North Atlantic by decomposing the spatially averaged

SSHA of the two regions based on the EEMD method. We found that this dipole pattern is associated with the low-frequency SSHA oscillations (at interannual to decadal time scales) that are nearly 180° out of phase with each other, and with the different long-term SSHA trends that have variable rate of increase during the study period. The low-frequency SSHA variability in the subpolar region has stronger correlation with the cumulative NAO index ($r = -0.84$ compared to $r = 0.22$ for the Gulf Stream region). This characterizes the cumulative effects of the NAO-forcing on the oceanic signals, particularly on the variability of the subpolar gyre.

Note that the dipole pattern shown in the present paper is similar to the previously identified AMOC fingerprint in the leading Empirical Orthogonal Function (EOF) of the SSHA (Zhang, 2008). Actually, both these two dipole patterns are representative of low frequency sea level variability. The EOF analysis decomposes data set into spatially orthogonal patterns that account for different percentage of the total variances along with the associated Principle Components (PCs) in which the leading mode explains the most variance. However, the spatial orthogonality constraints can cause the EOFs to have structures over the most of the domain and thus to be sensitive to choice of spatial domain. The leading values of EOFs, thereby, do not reflect the local behavior of the data (Hurrell et al., 2003; Hannachi et al., 2007). In contrast, the construction of dipole pattern with specified frequency bands based on the EEMD results gives well-defined prior information. This, in turn, would underscore the use of EEMD as an efficient filter yielding meaningful characteristics modes of variability at different timescales.

A remarkable reversal of the dipole pattern in the SSHA trends was found from the 1990s to the 2000s. Such a reversal, especially in the eastern subpolar gyre, is unexpected given recent low NAO-forcing (e.g., Herbaut and Housssais, 2009; Lorbacher et al., 2010). Variability of the subpolar gyre in the 2000s, thus, might reflect more contributions from the oceanic internal processes, for example, through lagged AMOC dynamics (e.g., Lohmann et al., 2009a, 2009b; Robson et al., 2012). Furthermore, the SSHA variations in the subpolar region were found to lead the variations in Gulf Stream region of 29 months, suggesting delayed responses in the Gulf Stream to the cumulative NAO-forcing. This time lag is consistent with findings by Zhang (2010) that demonstrated a 2 years lag of the AMOC variations at 50°N to the Labrador Sea mixed layer depth variations based on numerical simulation. This may indicate the linkage between the deep convection in the Labrador Sea, the SPG intensity and the subtropical intensity (associated with the Gulf Stream path shifts), a scenario, which has also been suggested by others (e.g., Bersch et al., 2007; Rhein et al., 2011), can be detected from the sea level variations. The Labrador Sea is an exception that has continuously increasing sea level over the past two decades yet with variable rates with time, which may be related to the localized variability of the deep ocean convection (Bersch et al., 2007).

It is worth noting that exclusion of the SSHA trend in the subpolar region weakened the correlation to the cumulative NAO index ($r = -0.59$), while it enhanced the correlation in the Gulf Stream region ($r = 0.43$). The long-term trend of the subpolar region SSHA correlates more strongly to the NAO than that of the Gulf

Stream region, which may explain why there was a significant sea level rise in the 'North' region (3.6 mm yr^{-1}) rather than in the 'South' (0.8 mm yr^{-1}). We examined the spectral power of different time scales after applying Fourier Transform to the decomposed components and found that the 'North' trend accounts for 47.8% of the total variances (energy) while the 'South' trend only explains 3.14% of the total variances. Because of the limited time span of the available SSHA data, we could not resolve multi-decadal oscillations here. However, a covarying dipole pattern was shown by Zhang (2008) between the surface sea level and the subsurface temperature variations, suggesting a part of multi-decadal variability associated with the AMOC. As longer time series of the SSHA become available in the future, further investigations will be needed to provide observational evidence to numerical simulations.

Since our tests were all based on domain averaged SSHA, it is of interests then to examine that how the results are sensitive to the choice of the domains of the 'North' and the 'South'. We examined the SSHA variations in a new 'South' region by shifting the northern boundary of the 'South' region from 50ºN to 42ºN (its western and eastern boundaries are kept the same), which now more concentrates on the sea level variations at the subtropics. There is a decreasing trend of new 'South' region SSHA especially in the 2000s (Figure 3.6, red line). The SSHA variations of the 'North' region lead that of the new 'South' region by 66 months with a significant correlation of -0.37. Longer time lead may be accounted by the propagation of the

AMOC variations from the high latitude to the subtropics, which follows the interior pathway with the advection speed and takes about 6 years (e.g., Curry et al., 1998; Zhang, 2010). Therefore, the low-frequency SSHA variability in the Gulf Stream region as illustrated in the manuscript (~50ºN) and here (~42ºN) are consistent in terms of the AMOC variations between different latitudes

Cautions should be taken here since that this asymmetrical relationship might be influenced by the choice of 'North' and 'South' domains and be probably due to different underlying mechanisms that determine how oceanic signals respond to the NAO-forcing. This study indicates the potential of using the altimeter observations to detect the AMOC variations associated with low-frequency variability in the North Atlantic ocean. Future work is needed to investigate with more details in the North Atlantic, especially in the subpolar region.

Table 3.1: The correlation coefficients between low-frequency SSHA in 'North' and 'South' with different indices.

	EAP	NAO	AO	WSC PC1 (24.8%)	WSC PC2 (10.4%)
'North'	0.26	-0.32	-0.28	-0.21	-0.19
'South'	0.08	0.33	0.24	0.21	-0.02

*Note: EAP, AO and NAO are all monthly index. WSC PC1 and WSC PC2 are the first two leading principle components of the wind stress curl over the North Atlantic (65°W – 15°E, 25°N – 70°N) covering the area larger than the study domain, which explain 24.8% and 10.4% of the total variances respectively.

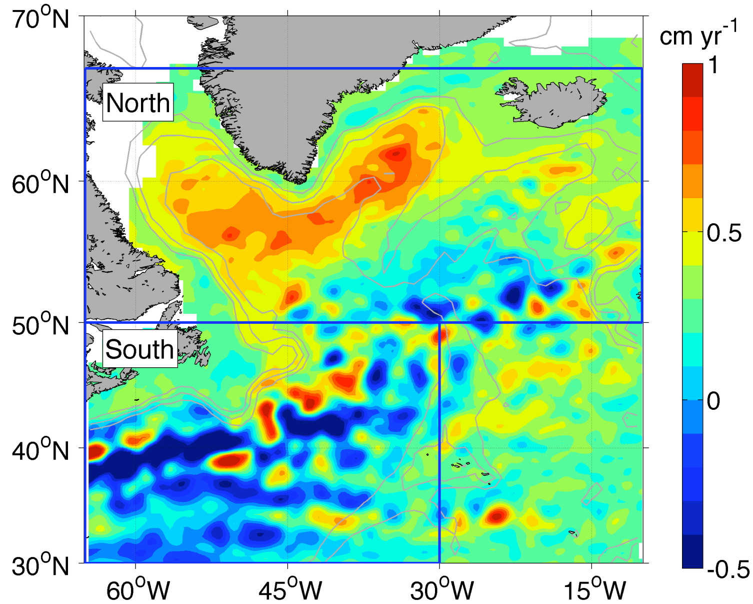

Figure 3.1: Dipole pattern in the overall trend of the sea surface height anomaly of the northern North Atlantic from November 1992 to January 2011. Two blue boxes (labeled as 'North' and 'South') are the domains for averaging, corresponding to the subpolar region and the Gulf Stream region, respectively. 1000m-, 2000m- and 3000m-isobaths are shown in solid grey lines.

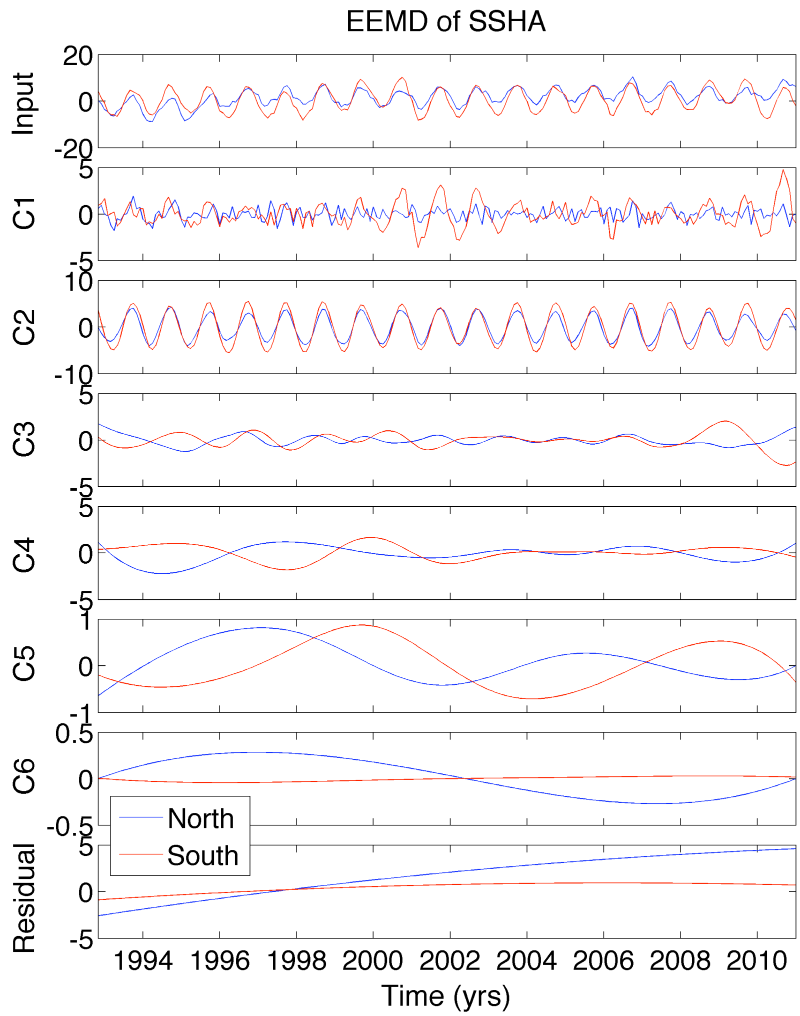

Figure 3.2: The intrinsic mode functions and the residuals decomposed from the spatially averaged sea surface height anomaly over regions 'North' (blue line) and 'South' (red line). Units are cm. The domain for averaging is shown in Figure 3.1.

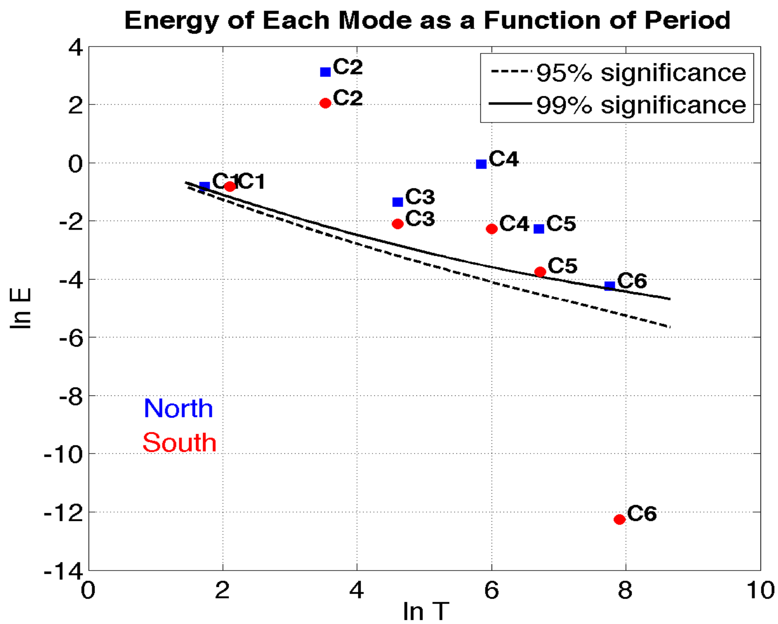

Figure 3.3: Significance test of the Intrinsic Mode Functions (IMFs) for the areas of 'North' and 'South' SSHA shown in Figure 3.1, respectively. 95% and 99% significant level were also displayed.

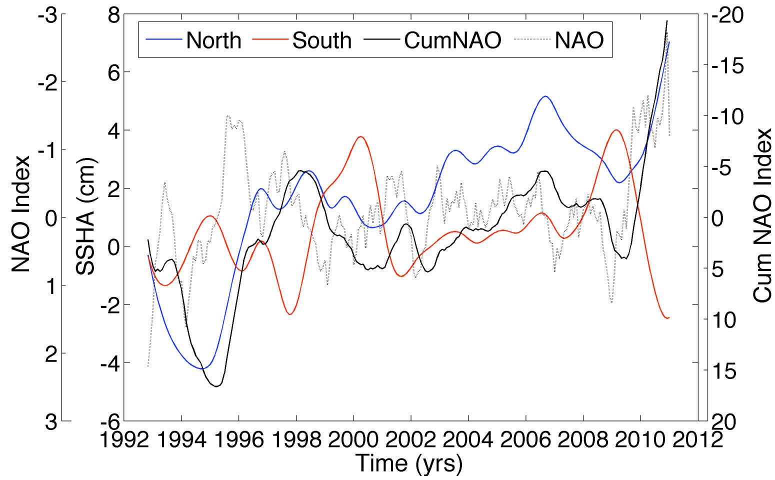

Figure 3.4: Low frequency SSHA oscillations and the long-term trends of the 'North' and 'South' regions, respectively (blue and red lines). The normal monthly NAO index (black dotted line) and the cumulative NAO index (black solid line) are also shown with reversed y-axis as references. A 9-month running smoothing was applied to both NAO indices.

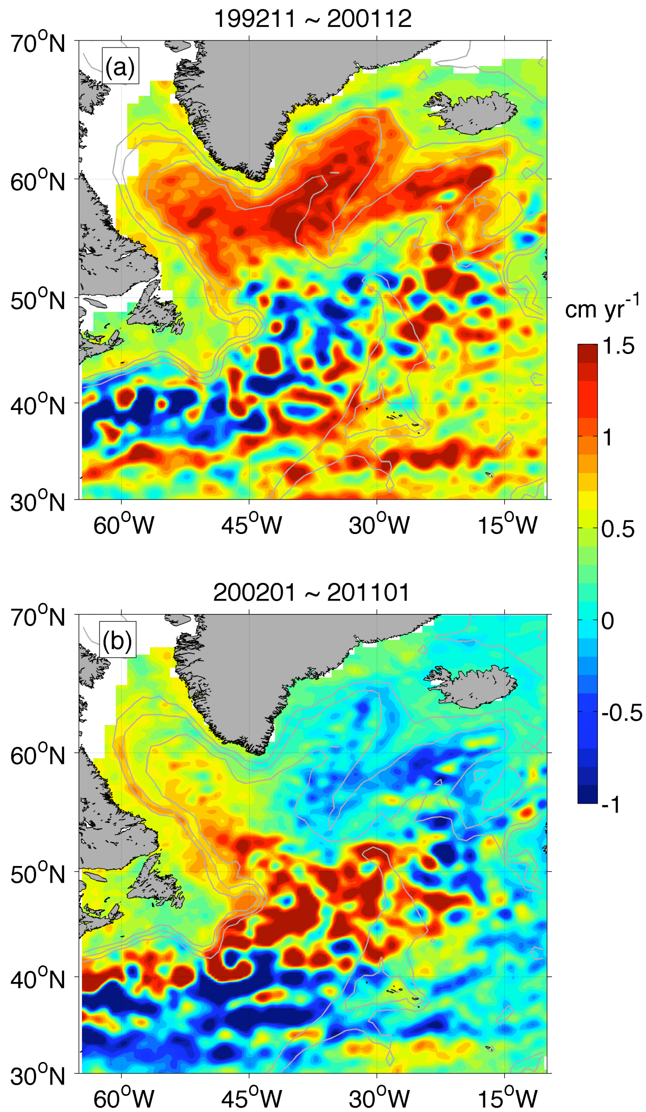

Figure 3.5: Trends of the SSHA in the study domain for periods of (a) November 1992 to December 2001 and (b) January 2002 to January 2011, respectively. 1000m-, 2000m- and 3000m-isobaths are shown in solid grey lines.

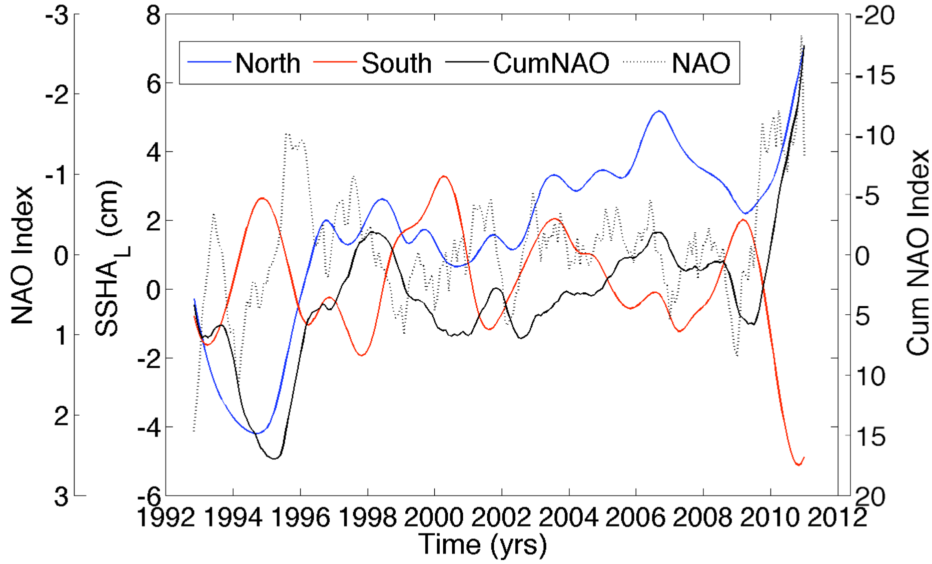

Figure 3.6: Same as Figure 3.4 but with different division of 'South' region.

Chapter 4

CHARACTERISTIC FEATURES OF THE SEA SURFACE HEIGHT ANOMALY IN THE NORTH ATLANTIC FROM ALTIMETER OBSERVATIONS

4.1 Abstract

The variability of the sea surface height anomaly (SSHA) in the mid- to high-latitude North Atlantic for the period of 1993 – 2010 was investigated using the Ensemble Empirical Mode Decomposition to identify the dominant timescales. Sea level variations in the North Atlantic subpolar gyre (SPG) are dominated by the annual cycle and the long-term increasing trend. In comparison, the SSHA along the Gulf Stream (GS) is dominated by variability at intra-seasonal and annual timescales. Moreover, the sea level rise in the SPG developed at a reduced rate in the 2000s compared to rates in the 1990s, which was accompanied by an increase in spectral energy starting from around 2002 after a period of energy loss in the system. These changes in both apparent trend and low-frequency SSHA oscillations reveal the importance of low-frequency variability in the SPG. To identify the possible contributing factors for these changes, the heat content balance (equivalent variations in the sea level) in the subpolar region was examined. The results indicate that horizontal circulations may primarily contribute to the interannual to decadal variations, while the

air-sea heat flux is not negligible at annual timescale. Furthermore, the low-frequency variability in the SPG might be related to the propagation of Atlantic meridional overturning circulation (AMOC) variations from the deep-water formation region to mid-latitudes in the North Atlantic.

4.2 Introduction

Vigorous large-scale oceanic circulations and intense air-sea interactions in the mid- to high-latitude North Atlantic make this region an important component in global climatic studies. Here, tropical warm and saline seawaters, transported northward by the Gulf Stream (GS) and the North Atlantic Current (NAC), meet the cold and fresh Arctic waters that transported southward by the Greenland and the Labrador Currents. The strong boundary currents consist of the cyclonic North Atlantic subpolar gyre (SPG), whose variability, in both intensity and shape, is critical in the redistribution of heat and salt in the North Atlantic (Hátún et al., 2005; Sarafanov, 2009; Häkkinen et al., 2011). The SPG is also known as the formation region of the intermediate water mass due to intense air-sea interaction, especially during severe winters (Dickson et al., 1996; The Lab Sea Group, 1998). Warm and saline waters become dense after releasing heat to the atmosphere and thus sink at certain locations in the SPG, generating an equatorward return flow at depth. This return flow coupled with surface northward western boundary currents together form the lower and the upper limbs of the Atlantic meridional overturning circulation (AMOC), which may have significant impacts on abrupt climate changes (Clark et al., 2002; McManus et al., 2004; Lynch-Stieglitz et al., 2007; Lynch-Stieglitz et al., 2011).

One of the most challenging aspects in studying the variability of the North Atlantic is the involvement of physical processes acting over a wide range of temporal and spatial scales, from the short timescale local tip jets events (e.g., Våge et al., 2008) to eddy activities with strong seasonality and interannuality (e.g., Lilly et al., 2003; Volkov, 2005) to variations in horizontal gyre circulations at intra-seasonal to interannual timescales whose spatial scales could have an impact on climate change. The subpolar region is particularly climate-relevant as variability in the SPG intensity in past decades has been linked to variations in both the deep-water formation rates in the Labrador Sea and the AMOC (Böning et al., 2006; Bersch et al., 2007; Rhein et al., 2011). The observed spin-up (Belkin, 2004) and the subsequent spin-down of the SPG (Häkkinen and Rhines, 2004) and the recent weakening of the AMOC (Latif et al., 2006) have revealed the dramatic variability of the North Atlantic at interannual to decadal timescales. Moreover, the apparent warming of subsurface ocean waters in the subpolar has been suggested to be a major contributor for the accelerated glacier melting (Bindschadler, 2006; Holland et al., 2008), implying a potential relationship between the SPG intensity that determines the amount of heat transported along Greenland coast and the melting ice mass along the margin of the SPG. It is, however, still not well understood whether the ongoing warming is part of low-frequency variations or a long-term trend. Therefore, distinguishing the relative importance of different modes of variability and possible related causes has become of great necessity and has increasingly captured the interest and attention of both scientists and policymakers.

Sea surface heights, which have been measured by the repeat coverage of altimeters, provide one of the most important oceanic signals related to the climate variability at both global and regional scales. The sea level responds to high-frequency wind forcing, for example, during storms and hurricanes, and has been used for eddy studies (e.g., Volkov, 2005; Chelton et al., 2011). In addition, the sea surface height anomaly (SSHA) can be interpreted as either the variations of upper ocean water properties due to changes of temperature and salinity in the water columns or the changes in the oceanic circulation given that the dynamic sea level variations balance geostrophic velocity anomalies (e.g., Häkkinen and Rhines, 2004; Böning et al., 2006). Therefore, the sea level is a good indicator for large-scale oceanic variability particularly at annual and longer timescales. Since the launch of TOPEX/Poseidon and ERS-1/2 in the early 1990s, followed by Jason-1 and Jason-2, the precision of an individual sea surface height measurement based on these missions has now reached the 1-2 cm level (e.g., Beckley et al., 2010). This continuous sampling of sea level with increasing accuracy using altimetry measurements provides a powerful tool to study the variability of the sea level in the context of climate variability and climate change.

Sea level variations in the North Atlantic have been investigated in previous studies for certain timescales. Ferry et al. (2000) attributed the seasonality of the SSHA in the North Atlantic to the steric changes of heating by examing in situ data and a numerical simulation. At interannual timescales, the SSHA changes were found to coincide with the shifts in the North Atlantic Oscillation (NAO) index (Häkkinen, 2001; Esselborn and Eden, 2001; Volkov and van Aken, 2003). Based on numerical simulations, Häkkinen (1999, 2001) concluded that the low frequency SSHA variability along the GS and in the SPG is related to the meridional overturning process. Zhang (2008) further suggested that the SSHA pattern could be used as a 'fingerprint' of the AMOC variations at mid- to high- latitudes using a 1000-year model simulation. Li et al. (2012), based on altimeter observations alone, indicated that the low frequency SSHA variability in the North Atlantic responds to the cumulative NAO-forcing and its distinct reduction of variance between the 1990s and 2000s might relate to the propagation of AMOC variations. However, the use of SSHA to represent the AMOC change should be cautious given the existence of a high-frequency wind-driven response as suggested by Lorbacher et al. (2010), based on a sequence of global ocean-ice model experiments. The authors also pointed out that a careful interpretation of the SSHA patterns is needed since its causes depend on the timescales of interest. In the present paper, we primarily analyzed 18-year records of the SSHA (1993 – 2010) using the merged products of multiple altimetry missions that were or currently are on operation. We explored the characteristic features of the SSHA patterns in the North Atlantic at various timescales and then investigated the possible causes. This analysis helps to advance our understanding of the North Atlantic variability, especially in the SPG, in terms of the SSHA variations. The Hilbert-Huang Transform (HHT) was applied to examine different modes of variability as well as the long-term trends in the

SSHA. Based on the separation of sea level modes, we intended to find the dominant timescales of variability and factors that may be responsible for each mode of variability.

Contents are organized such that Section 4.3 offers a brief description on the data and methods used. In Section 4.4, the altimeter data and its decomposed components at various timescales are analyzed. Spatial and temporal differences of the SSHA variability are discussed with more emphasis on the SPG. The possible causes of the SSHA variability at corresponding timescales are explored in Section 4.5 by primarily investigating the upper layer heat content anomaly. The conclusions appear in Section 4.6.

4.3 Data and Method

Weekly and monthly altimeter products with 1/3 degree spatial resolution were produced by Ssalto/Duacs and distributed by Archiving, Validation and Interpretation of Satellite Oceanographic data (AVISO), with support from the Centre National d'Etudes Spatiales (CNES). The delayed time (DT) products combine data from different missions, significantly improving the estimation of mesoscale features (Le Traon and Dibardoure, 1999).

Quality controlled subsurface ocean temperature and salinity data was obtained from the Ensemble3 (EN3) dataset (Ingleby and Huddleston, 2007). This dataset combines data from the World Ocean Database 2005 (WOD05), the Global Temperature and Salinity Profile Project (GTSPP), Argo and the Arctic Synoptic

Basin-wide Oceanography (ASBO) project. The quality control procedure includes the use of altimeter data. Objectively analyzed gridded data with monthly interval at 1 by 1 degree resolution were used.

Monthly surface flux data are provided by the National Center for Environmental Prediction (NCEP) Reanalysis datasets from Physical Sciences Division (PSD) (Kalnay et al., 1996). Net heat flux is obtained by summing up the sensible and latent heat fluxes and the shortwave and longwave radiations with positive values denoting heat gain by the ocean.

The Ensemble Empirical Mode Decomposition (EEMD) was used to separate different modes of SSHA variations at each location. Hilbert transform was then applied to estimate the amplitude and frequency of the obtained components as a function of time, by which localization of events in time-frequency space can be realized. Extensive details about the HHT and the significance test can be found in Appendix A. For more details on the applications of the HHT to geophysical research, please refer to Huang and Wu (2008).

4.4 SSHA in the North Atlantic

4.4.1 Dipole Pattern

We investigated the characteristic patterns of the SSHA over the mid- to high latitudes of North Atlantic using multi-satellite altimeter measurements from 1993 – 2010. The SSHA evolution in the North Atlantic reveal a positive sea level trend centered over the SPG (Figure 4.1a), which corresponds to a scenario of weakening SPG surface circulation after mid-1990s that has been seen in previous studies (Verbrugge and Reverdin, 2003; Häkkinen and Rhines, 2004; Böning et al., 2006; Li et al., 2012). Such sea level changes could also indicate shifts in the SPG shape as suggested by Hátún et al. (2005). The SSHA trends in the other regions, especially in the GS region (weakly negative trend), may not represent true long-term changes given their small coefficients of determination (Figure 4.1b). Hence, the SSHA changes in the SPG could be characterized by a linear trend while they may fluctuate without a simple trend in the GS region. The formal signal could highlight the persistence of the sea level changes in the SPG since the 1990s.

Figure 4.2 indicates high standard deviation (STD) of the SSHA over the GS region and low STD over the SPG, which is consistent with the low and high determination coefficients, respectively, as shown in Figure 4.1. The GS, the NAC and the Azores Current embrace most of the SSHA variance, in which the highest STD values (>10 cm) are constrained by 1000-m isobath to the west and the east and by the Sub-Arctic Front (SAF) to the north. The SPG interior has more variability than its periphery, which reflects larger variations of the horizontal circulations. The contrast between the SPG and the GS region in the linear trend as well as in the STD suggests different dominant timescales of variability due to different physical processes. Given that the linear trend might be a part of long timescale variability, a more general conclusion could be made here: the SSHA variability in the SPG has very important low-frequency components compared to that in the GS. This is tested in following sections.

4.4.2 SSHA Variability

Volkov and van Aken (2003) examined the SSHA variability at annual timescales and interannual timescales in the North Atlantic. The authors used a harmonic shape with a frequency of 1 cycle yr^{-1} to determine the annual sea level cycle and applied a running mean with a window width equal to about 1 year to estimate the interannual signal. However, given that even mean sea level fluctuates from year to year, estimation of a signal with a fixed frequency window may remove physically meaningful non-stationary information carried by the signal. A sine function, therefore, may not be suitable to analyze the SSHA variability, especially when the study area has undergone a clear non-stationary warming process. Volkov and van Aken (2003) also noted the difficulties in estimating the characteristic period of the interannual change or in obtaining meaningful long-term trend with only 8 years of measurements.

In order to differentiate the SSHA signals with limited frequency bands and take into account the non-linear and non-stationary nature of the process, we decomposed the monthly SSHA time-series into components with variable periods (the IMFs and residual) by using the EEMD method. The decomposition of SSHA was applied spatially over the study domain. Figure 4.3 shows the temporal averages of the IMFs at high to low frequency (C1 to C6) and of the residual (R), respectively. Given that the SSHA was obtained referencing to the 7-year mean sea level from 1993 to

1999 (AVISO procedure), the time-averaged SSHA over the entire period of this study (1993 – 2010) represents the sea level changes relative to the reference period. Therefore, Figure 4.3 reflects the 1993 – 2010 average relative to the 1993 – 1999 average using monthly mean data. It is worth mentioning that the residual (or the long-term trend) differs from a linear trend because it can still have time-dependent fluctuations yet at a very low frequency. Significance testing was performed and only those values significant at the 95% significance level were kept. C1 represents the intra-seasonal sea level variation, which may be associated with mesoscale eddy activity (e.g., Volkov and van Aken 2003). C2 and C3 have periods around 1 year, representing annual or quasi-annual cycle. C4 – C6 correspond to interannual variations. It is notable that the residual and the original SSHA data have the same order of amplitude, which is greater than that of the other components. This again suggests the importance of the long-term SSHA variability in the North Atlantic, whose actual period may not be well resolved because of the limited time span of data used. Moreover, the SSHA variations are found to mainly localize in the SPG and the GS regions while the variations in the regions beyond are generally negligible but with increasing trends. The increases and decreases of sea level in the SPG and the GS respectively as shown in Figure 4.3a and Figure 4.3h occurred mainly in the 2000s. For the other components, however, the sea level in the SPG changed slightly (Figure 4.3b, 4.3c, 4.3d) or even decreased somehow at longer timescales (Figure 4.3e, 4.3f) in the 2000s. Caution should be taken in the GS region, because in this region only the intra-seasonal and annual signals (C1 and C2) are statistically significant. Both of these two modes showed increased sea level in this region, which are in contrast to the decreasing trend (Figure 4.3h).

After the decomposition of the sea level variability, we examined the contribution from each component to the total variance, showing the percentage of the variance explained by sea level variability over certain timescales (Figure 4.4). Sea level variations in the SPG are mostly explained by the long-term trend (R, about 50%, Figure 4.4g), confirming a persistent change in the SPG sea level from the 1990s to the 2000s. The second largest percentage of total sea level variance in the SPG is accounted by the annual oscillation (C2, about 30%, Figure 4.4b). In contrast, the total variance of the sea level in the GS region is dominated by the intra-seasonal (C1, about 40%) and the annual signals (C2, about 30%), while less than 20% is explained by the residual. The intra-seasonal SSHA signals may relate to direct wind forcing and current meandering and resultant persisting eddy generation. The annual signal could be due to annual changes such as solar radiation and wind pattern change etc. It was also noted that in the regions beyond the SPG and the GS, small SSHA variations with amplitude of ± 1 mm are dominated by the annual signal.

4.4.3 Characteristic Variations in the Subpolar Gyre

We focused on the SPG given its crucial role in linking the upper and the lower limbs of the AMOC (Bersch et al., 2007; Rhein et al., 2011) and its undergoing changes in terms of both its intensity and its shape (Hátún et al., 2005; Sarafanov et al., 2008; Sarafanov, 2009). Weekly SSHA was spatially averaged over the SPG domain

$(65°W - 20°W, 52°N - 66°N)$ for analysis. The EEMD results are presented in Figure 4.5, which includes the full decomposition to illustrate the high to low frequency progression. In total eight IMFs and a residual were obtained due to the improved temporal resolution of the data set. All IMF components are statistically significant at 99% confidence level. C1, C2 and C3 are the intra-seasonal signals with periods ranging from weeks to months. They correspond to fast sea level variations that might relate to regional events such as storm surge occurrences. Given that the contributions from the intra-seasonal signals are generally small in comparison to the total SSHA variances (Figure 4.4), we did not perform further interpretation on this timescale. C4 has the largest amplitude of variations with clear seasonality, which is associated with the solar radiation in this region. At interannual to decadal timescales (C5, C6, C7 and C8), signals have irregular cycles in which a depressed sea level was observed in the 2000s. The long-term trend (R) shows an overall sea level rise at the rate of approximately $4\ \mathrm{mm\ yr^{-1}}$, suggesting a regional exaggeration of the sea level rise in the SPG (a global mean rate is $3.2 \pm 0.6\ \mathrm{mm\ yr^{-1}}$ reported by AVISO, http://www.aviso.oceanobs.com/en/news/ocean-indicators/mean-sea-level/). However, there is variable rate of the sea level rise in the long-term trend and a reduction of the rates was observed after around 2002.

Hilbert transforms were then performed on all IMFs in order to examine not only the contribution from each mode to the total SSHA variations but also how this contribution changes with time. The resultant Hilbert amplitude spectrum provides a unique amplitude-frequency-time plot in which the amplitude is a function of both frequency and time. The MSD and IE were computed and displayed along for illustration. Figure 4.6 shows the results after applying Hilbert transform to all IMFs (C1 – C8). The amplitudes with frequency higher than 2 cycle yr^{-1} are not displayed. A maximum in the Hilbert spectrum was found at the frequency of 1 cycle yr^{-1}, corresponding to the annual signal dominating over the time span of this study. This annual signal is also reflected in a rather broad peak in the MSD given small fluctuations still exist in the annual signal. Another persistent maximum appeared at very low frequencies around approximately 0.1 cycle yr^{-1}. This maximum yields a relatively sharp peak in the MSD, indicating its periodic nature. Besides the dominant annual signal, the appearance of signals within a small band of low frequencies may be of more interests given their potential connection to long timescale processes in the North Atlantic. There are also some local maxima appeared at the interannual timescales, revealing more complex and non-periodic phenomena associated with sea level variations in the SPG. Furthermore, the IE plot shows a decreasing spectrum density for the period from the 1990s to the early 2000s but is followed by a period of increasing energy. While the decrease may be related to reduction in kinetic energy due to weakening of the SPG surface circulation since the 1990s (Häkkinen and Rhines, 2004), the following regain of energy might be a result of a major ‘shift in the system’ that occurred in the beginning of the 2000s (Sarafanov et al., 2012). The latter may relate to the changes in the production of the intermediate layer water mass in the

Labrador Sea (van Aken et al., 2011) as well as to the changes in the SPG intensity indicated by the first principal component of the sea surface heights (Häkkinen and Rhines, 2009).

Given the importance of low-frequency SSHA variations, we then isolated the signals at longer than annual timescales (C5, C6, C7 and C8) and applied the Hilbert transform to them. Figure 4.7 shows the Hilbert spectrum of the selected low-frequency components. After removing the intra-seasonal and annual signals, the progression of IE becomes smoother with a reversal around the early 2000s (Figure 4.7a). This suggests that such a reversal is mainly influenced by the low-frequency signals and the high-frequency signals only produce fluctuations along this trend. Therefore, the importance of the low-frequency signals and their contributions to the total SSHA variability should be especially considered in an analysis of ongoing processes in the North Atlantic from the 1990s to the 2000s. Maximum amplitudes appear in the frequency range of 0.05 - 0.1 cycle yr^{-1}, corresponding to signals with periods between 10 and 20 years (Figure 4.7b and 4.7c). Furthermore, there are several local maxima of amplitude existing in $0.1-1$ cycle yr^{-1} frequency range, suggesting of more complex interannual components of sea level variations in the SPG. However, these maxima were generally shifted towards a smaller frequency bands between 0.1 and 0.2 cycle yr^{-1} (periods of 5 – 10 years) in the late 2000s. Considering the limited time span of the SSHA, the very low frequency component decomposed from the SSHA may be plausible and, therefore, should be interpreted with caution. Moreover, sudden drops of the IE in 1995-1996 and 2009-2010 (Figure 4.7a) were found to be concomitant with drops in the wintertime NAO index, which indicates the close relationship between the SSHA and the sign changes of the NAO index that has been previously observed (Esselborn and Eden, 2001; Volkov and van Aken, 2003).

4.5 Possible Causes of the Variability in the SPG

The total SSHA can be split in two components including contributions from steric effects and variations in bottom pressure, respectively (Gill and Niiler, 1973). We first tested the steric effects in the subpolar region. To make the steric height anomalies (η'_{st}) comparable to the SSHA, we derived η'_{st} relative to the mean compatible with the mean used to derive the SSHA (both reference periods are 1993-1999). The results are shown in Figure 4.8. We regarded both the SSHA and η'_{st} as a composition of two parts: a mixture of modes of variability and a linear trend. The former can be obtained by detrending the data sets. Then, we were able to compare the variance of the steric height anomalies and the SSHA, thus showing the percentage of the total SSHA variance explained by each of the steric components. Regardless of long-term trends, η'_{st}, as a sum of the thermosteric height anomaly (η'_t) and the halosteric height anomaly (η'_s), explains 60% of the total variance in the SSHA. In comparison, η'_t explains 63% of the SSHA variance, while η'_s explains 5% of the total variance. Removing high-frequency variations in the time-series, after applying a 3-month smoothing, barely changes the results. Moreover, if the trends were added back, the variance explained by η_t' increases to 73%, but the determination coefficient for η_s' becomes negative. This is due to the opposite long-term trends between η_t' and η_s' as shown in Figure 4.8 in which the trend of η_t' largely represents the SSHA trend. Therefore, most of the SSHA variability in the SPG at annual and longer timescales is dominated by the steric effects, and especially by the thermosteric effect due to either heating or advection of heat. In addition, at low frequency ($< 1 \text{ cycle yr}^{-1}$), the thermosteric and halosteric height variations are effectively canceling each other. The contribution from salinity is, therefore, not trivial at these timescales. The results showed a consistent scenario as has been suggested by others (Antonov et al., 2002; Volkov and van Aken, 2003; Ivchenko et al., 2008; Cazenave and Llovel, 2010; Stammer et al., 2013). The limited period of the study may not allow for resolution of variability at timescales longer than decadal. However, the leading mode of altimeter SSHA data is known to covary with the subsurface temperature anomalies in the North Atlantic, which is likely a part of multidecadal timescales linked to the AMOC strength (Zhang, 2008; Mahajan et al., 2011).

Direct measurements of the bottom pressure anomalies are very scarce and the data is usually from numerical modeling. The bottom pressure anomalies have amplitudes of less than 1 cm over most parts of the deep ocean and of several centimeters over shallow, boundary regions at high latitudes and short timescales (Ponte, 1999; Ferry et al., 2000; Vinogradova et al., 2007; Bingham and Hughes, 2008). Quinn and Ponte (2012) demonstrated coherence between ocean bottom pressure and sea level anomalies at mid- and high latitudes at periods less than 100 days based on observations from GRACE and altimetry. On longer timescales, the sea level and bottom pressure variability are essentially different with the former prevailing (Vinogradova et al., 2007; Ivchenko et al., 2008; Stammer et al., 2013). Jayne et al. (2003) found that combining altimetry observations with satellite measurements of the time-varying bottom pressure improves the ocean heat storage estimates well on timescales of the annual cycle and shorter. However, in the SPG, inclusion of bottom pressure anomalies contributed to a reduction in RMS error about 0.05 GJ m^{-2} at semiannual, annual cycles and in the linear trends (see Figure 4, Figure 5 and Figure 6 in Jayne et al., 2003). Piecuch et al. (2013) demonstrated that considerable sea level variances could be explained by bottom pressure variances at interannual scales in several regions by using the newly updated GRACE data along with altimetry. Nevertheless, their results identified the northeastern corner of the North Atlantic as the region that bottom pressure is important at interannual scales (see Figure 5 in Piecuch et al., 2013).

We are then concerned with the sea level variations induced by changes in heat exchange between ocean and atmosphere and by advective processes, i.e., changes at annual and longer timescales. Recall that the SSHA variability in the SPG is dominated by annual cycles and the long-term increasing trend, which can explain 50% and 30% of the total SSHA variance, respectively. At these dominant timescales, the SSHA and heat content anomaly estimated from the temperature are strongly correlated with correlation coefficients of 0.89 for the annual cycles and 0.97 for the long-term trends.

We obtained the total heat content anomaly, ΔH_T, from the SSHA by using a linear relationship, $\Delta H_T = \frac{\rho C_P}{\alpha} \Delta\eta$, after Chambers et al. (1997), where ρ is the seawater density, C_P is the heat capacity of the seawater, α is the thermal expansion coefficient, $\Delta\eta$ is the SSHA. The use of a linear relationship to derive changes in the heat content from the SSHA has its advantages for using continuous and consistent satellite measurements with high accuracy and high resolution to infer changes in ocean heat content and taking into account changes take place through the whole water columns without the need of a known depth to perform the temperature integration. The specific heat and density vary by less than 1% over most of the ocean, and so assuming that they are constant introduces little relative error (Chambers et al., 1997). However, the thermal expansion coefficient varies with time and locations especially at high latitudes, which may cause large error in the heat content anomaly estimation. For example, the α in the SPG varies between months with a maximum difference of 4.96×10^{-5} °C^{-1}, which yields an error in the ΔH_T of 0.3 GJ m^{-2} (assume a value of $\rho = 1027$ kg m^{-3}, $C_P = 4000$ J Kg^{-1} °C^{-1} and $\alpha = 2 \times 10^{-4}$ °C^{-1}). This is even greater than the heat content caused solely by surface heating. Therefore, monthly values of α were determined for each grid using WOA2009 temperature and salinity data (http://www.nodc.noaa.gov/OC5/WOA09/pr_woa09.html; interpolated to the same resolution as the altimeter data). The total heat content anomaly in the upper oceans is balanced by air-sea heat flux, ΔH_V, horizontal heat transport, ΔH_H, and diffusion (Kelly, 2004; Kelly and Dong, 2004). Diffusion is found to be relatively small and thus heat transport variations, ΔH_H, can be inferred as a residual between heat content changes and air-sea fluxes (Kelly, 2004). The surface heating term, ΔH_V, can be calculated based on the NCEP heat flux reanalysis data and was tested in this paper. We converted the surface heat flux into changes in the upper ocean heat content by multiplying monthly surface net heat flux by the seconds of a month.

Figure 4.9 illustrates the progression of signals with increasing periods that are decomposed from the spatially averaged ΔH_V and ΔH_T respectively. All the IMFs, except C3 – C6 in the ΔH_V time-series, are statistically significant at the 99% confidence level. Totally, ΔH_V accounts for about 1/5 of ΔH_T amplitudes. This ratio becomes approximately 1/4 ~ 1/2 for the signals that have periods of less than 1 year (C1) and approximately 1 year (C2), suggesting that ΔH_V is more significant to ΔH_T at intra-seasonal and annual timescales. In contrast, at longer than annual scales (C3 – C6), the IMFs of ΔH_V are neither statistically significant nor are their amplitudes comparable to that of corresponding ΔH_T signals, making their contributions to the total heat budget in the SPG negligible. To conclude, the contributions from air-sea heat fluxes are important in analyzing the intra-seasonal and annual regional SSHA variations in the SPG. In comparison, gyre scale circulations, which contribute to the heat budget of the upper oceans in an advective fashion, play a dominant role in setting SSHA variations in the SPG at interannual and longer timescales. Besides the different amplitudes, Figure 4.9, for the first time, shows different time lags between ΔH_V and ΔH_T at annual and interannual timescales. ΔH_V leads ΔH_T at both frequencies given known oceanic response to the overlying atmospheric forcing in the SPG. The time lead is 2 to 3 months at annual timescales (C2 in Figure 4.9) and increases to about 2 years at inter-annual timescales (C4 and C5 in Figure 4.9). The former is related to the time used to heat up the upper oceans from surface and the latter involves heat transport through the internal adjustments of the ocean.

Figure 4.9 also presents heat content anomalies estimated from the temperature for comparison (only C6 in this time-series is not significant). Heat content anomalies in the SPG estimated from the temperature and the SSHA agree well with each other in terms of both amplitude and phase. The strongest correlations for these two time-series exist in the long-term trends (correlation coefficient r = 0.96), the annual cycles (r = 0.84) and the decadal cycles (r = 0.76). Therefore, great care should be taken in the estimation of heat content anomalies by altimetry alone when considering interannual scales. Moreover, Figure 4.9 shows that the discrepancies between the two heat content anomalies have reduced from the 1990s to the 2000s at the decadal timescale (C5) and in the residuals (R), which may relate to the concomitant warming observed in the northern North Atlantic (e.g., Häkkinen and Rhines, 2009; Häkkinen et al., 2011).

We then examined the relationship between the SSHA variability in the SPG and possible underlying processes at longer than annual timescales. These low-frequency changes are typically attributed to the variability in the deep ocean convection (DOC) processes in the Labrador Sea (Häkkinen and Rhines, 2004; Bersch et al., 2007; Rhine et al., 2011) and large-scale AMOC variations (Zhang, 2008; Lohmann et al., 2009a, 2009b; Robson et al., 2012; Li et al., 2012). The DOC is a direct form of heat exchange between atmosphere and the intermediate- to deep-ocean. A large amount of heat is released to the atmosphere during strong DOC years from the ocean, resulting in a reduction of heat content in the upper to intermediate water column. The associated interannual trends reflect the atmospheric winter conditions persisting for more than a year (Lazier et al., 2002). Therefore, we chose the depth-integrated heat content of the central Labrador as a DOC index for the analysis of the interannual and longer timescales variability. The heat content is almost steadily increasing since mid-1990s. This is closely associated to the interannual changes of the DOC: after a period of enhanced deep convection with production of large volume of the classic Labrador Sea Water (CLSW) in the early 1990s, there were some years of ventilation of the CLSW and formation of the upper Labrador Sea Water (ULSW) due to reduced DOC intensity and activity in the 2000s (Kieke et al., 2007; Rhein et al., 2011). The SPG index is defined as the SSHA of the central Labrador Sea (see Häkkinen and Rhines, 2004; Böning et al., 2006). The AMOC transport index used here is the meridional transport at $26.5°\mathrm{N}$ (Cunningham et al., 2007) from the RAPID-WATCH MOC monitoring project (www.noc.soton.ac.uk/rapidmoc). We considered the NAO forcing as a possible driving force in the low-frequency changes in the North Atlantic (e.g., Hurrell, 1995; Marshall et al., 2001). Since the ocean signal reflects a time integration of the atmospheric forcing, for example, through mixed layer 'memory' and Rossby wave propagation (Curry and McCartney, 2001), the cumulative NAO index (CumNAO) was adopted instead, following Li et al. (2012), by integrating monthly NAO index over time (https://climatedataguide.ucar.edu/climate-data/hurrell-north-atlantic-oscillation-nao-index-station-based), which may more accurately represent the cumulative effects of oceanic signal variations. Since the NAO index includes positive or negative phases over time, this time-integral could also provide a clear view of any accumulations as well as any shifts in time. A period of persistent positive NAO index becomes an increasing slope in the CumNAO index, vice versa. The CumNAO can, therefore, highlight the shifts in the atmospheric conditions compared to the normal NAO index. For instance, a sign change of the NAO index that happened between 1995 and 1996 corresponds to a peak in the CumNAO. In addition, using different time origin of integration does not change the shape of the cumulative NAO index, which instead introduces a shift in magnitude for every point.

Figure 4.10 shows the close relationship between DOC, the SPG, the AMOC variability and the cumulative NAO forcing especially at interannual to decadal timescales. The CumNAO index matches with the DOC and the SPG indices well and leads the AMOC variability with some time lags. A persistent high NAO index in the early 1990s lead to consecutive winters of strong DOC events accompanied by a reduction of heat content and an enhancement of the SPG circulation. After mid-1990s, a steady warming of the central Labrador Sea was observed with the exception of the periods of 1999 to 2003 and 2008 to 2010 – two periods of observed large production of CLSW (Yashayaev, 2007; Våge et al., 2009; Yashayaev and Loder, 2009). The AMOC variability follows the changes in DOC and the SPG with a time lag of approximately 1 to 2 years, which agrees with previous findings based on numerical simulations (Zhang, 2008; Zhang, 2010). Therefore, at interannual to decadal timescales, the SSHA variations in the North Atlantic closely represent the AMOC variability driven by the NAO forcing.

4.6 Conclusions and Discussion

This study has presented an analysis of 18-year SSHA records in the mid- to high-latitude North Atlantic that examined the characteristic features of sea level variations. A dipole pattern, centered between the SPG and the GS path, appears in both the linear trends and the STD of the SSHA, indicating different modes of variability in the two regions. A simple increase in the SSHA could represent most changes in the SPG throughout the entire time span of the study. This increase corresponds to a continuous weakening of surface circulation. In contrast, the linear trend along the GS path is not representative of the overall sea level changes that are instead associated with greater variance. The separation of the SSHA time-series into components with various timescales and the long-term trend showed more details about the contrast between the SPG and the GS regions. It is worth mentioning, however, the long-term trends may have contribution from aliasing due to the limited length of data record. The SSHA variability along the GS is dominated by intra-seasonal to annual fluctuations, which together could account for 70% of the total sea level variance. These intense, high frequency variations in the SSHA time-series would effectively mask the low-frequency signals of greater interests (e.g., Lorbacher et al., 2012). In the SPG, the long-term trend accounts for 50% of the total variance and the annual signal for 30% of the total variance. The long-term trend might also be a part of longer timescale variability that cannot be resolved in the limited altimeter record length of 18 years. Therefore, the dominance of the long-term trend in the SPG sea level changes may indicate the critical role of low-frequency processes in the North Atlantic. Furthermore, by applying the Hilbert transform to the IMF components of the SPG sea level, signals at decadal and longer timescales were observed with maximum spectral amplitude in addition to the well-known strong annual cycles, confirming the important role of the low-frequency components in the SPG variability. In the regions beyond the SPG and the GS, the SSHA varies smaller and is dominated by annual variations with an overall increasing trend.

Although the long-term trends have similar pattern of the linear trends, the EEMD derived trends contain more time-dependent information. This observation was not possible using most traditional time-series analysis methods that assume stationary changes. In the SPG, a sea level rise rate reduction was found around the early 2000s, which is concomitant with the reduced amplitudes in the low-frequency signals. Spectral analysis indicated coinciding changes in the energy with the amplitude changes, which increases after the early 2000s following a period of energy removal from the system since the early 1990s. Such reversal of energy loss was influenced by the low-frequency SSHA signals (removal of the high frequency signals did not change the result). The timing of such changes may correspond to a 'shift in the system' around 2002, which was also found in the observations of the LSW formation and the first principal component of the altimetry-derived sea level in the northern North Atlantic (Sarafanov et al., 2012 and references therein). These changes in the SSHA from the 1990s to the 2000s might suggest a new cycle of SPG intensification as observed in part of its boundary currents from repeat hydrographic sections in the early 2000s (Han et al., 2010; Daniault et al., 2011). Actually, deep-water transport strengthened in opposition to its surface layer counterpart in the 1990s (Dengler et al., 2006; Sarafanov et al., 2010). Moreover, after years of weak or absent DOC activities, the Labrador Sea experienced a strong DOC event in the winter of 2007/2008 even without a clear phase of preconditioning (Våge et al., 2009). Rapid development of convection under intensified atmospheric forcing greatly deepened the mixed layer to more than 1600m , disrupting steady warming of the intermediate depth waters since 1994 (Yashayaev and Loder, 2009). All of these recent observations cast questions about the future of the SPG under a warming scenario and its relationship to both external atmospheric forcing as well as internal oceanic dynamics. This requires a future investigation on understanding the low-frequency variability in the subpolar North Atlantic.

This study also showed that, among factors responsible for the SPG sea level variability, advection is important at interannual to decadal timescales while the air-sea heat flux is not negligible at annual timescale. The result is in line with previous studies on the interannual sea level anomaly in the North Atlantic (Reverdin et al., 1999; Hakkinen, 2001; Esselborn and Eden, 2001; Verbrugge and Reverdin, 2003; Volkov and van Aken, 2003). Moreover, it has been suggested that air-sea heat flux explains most of the sea level variance at annual scales in the northeastern North Atlantic (Ferry et al., 2000; Volkov and van Aken, 2003). This, therefore, suggests different underlying mechanisms accounted for the SSHA in the western and eastern subpolar North Atlantic (Herbaut and Houssais, 2009; Li et al., 2012). Such importance has been studied in the GS given that advection plays a more determinant role in regulating the heat content than air-sea fluxes on interannual-to-decadal timescales (Dong and Kelly, 2004; Kelly and Dong, 2004). Based on results from numerical simulations, Häkkinen (1999, 2001) attributed the low-frequency sea level changes predominately to overturning changes. The close relationship among DOC, the SPG and the AMOC especially at interannual timescale was also presented here by comparing adequate indices of each process. Matches between these crucial physical processes, as well as their relationship to the cumulative NAO forcing, may explain changes in the advection and thus account for low-frequency variability in the SSHA in the North Atlantic. Since the AMOC index used here is available for a very limited time period, we tested the role of the AMOC in another way to see how low-frequency SSHA variability relates to AMOC variations. Li et al. (2012) suggested the potential of using low-frequency SSHA to represent changes in AMOC variations between different latitudes based on analysis of two regional SSHA covering the SPG and the GS respectively.

Here, we extended their works by dividing the study domain into three adjacent regions in order to examine the meridional propagation of SSHA variations (Figure 4.11). For consistency, we considered only significant low-frequency components (period > 1 year) in these three regions (namely Region 1, Region 2 and Region 3). Unless otherwise noted, SSHA variations discussed hereinafter represent the low-frequency changes. The propagation of SSHA variations from high to mid-latitude was observed with certain time lags between two adjacent regions. SSHA variations of Region 2 lag Region 1 by about 2 years with a significant correlation of 0.52. Towards the south, there is a 5-year lead between SSHA variations in Region 2 and Region 3 with a significant correlation of -0.36. The propagation velocity is estimated by V = L/T, where L is the meridional distance between 50°N and 30°N (about 2297km) and T is 5 years, which gives a propagation velocity of approximately 1.46 cm s^{-1}. This finding is consistent with modeled climatological mean meridional velocity of 1.5 cm s^{-1} speed at which AMOC variations at high latitude propagate to mid-latitude (Curry et al., 1998; Zhang, 2010) following interior pathways observed recently (Bower et al., 2009). Therefore, it confirms that the low-frequency SSHA variations in the SPG and along the GS are mostly related to AMOC variations, which might be a part of multi-decadal variability as suggested in numerical models (Zhang, 2008; Mahajan et al., 2011).

It is worth mentioning that across most of the SPG, surface heat flux is positively correlated with the heat content, which indicates that surface flux introduces variations to the heat content (and thus the sea level anomaly) in the upper oceans. In contrast, the situation in the GS is different and has opposite values of ΔH_V and ΔH_T (not shown here). This is consistent with negative correlation between heat content and surface heat flux found in the western boundary currents, which suggests the dominance of oceanic feedback over atmospheric forcing (Dong and Kelly, 2004; Kelly and Dong, 2004). The warming of the eastern North Atlantic subsurface waters has been observed due to northward invasion of waters of subtropical origin along the eastern boundary in the 2000s (Sarafanov et al., 2008; Häkkinen et al., 2011). The warming of the Irminger Sea might be related to the contraction of the SPG and the westward retreat of the SAF, which needs further investigation and is beyond the topic of this present work.

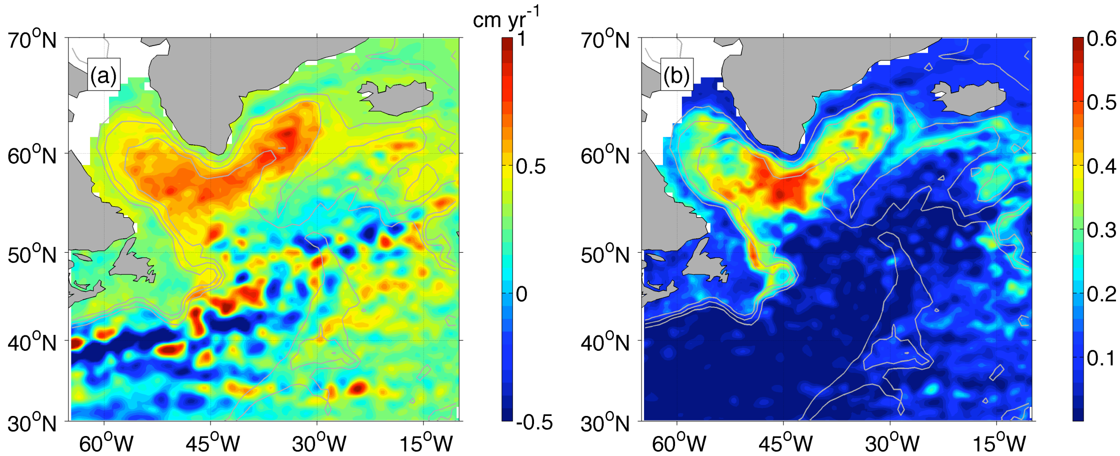

Figure 4.1: (a) The linear trend of the sea surface height anomaly in the study domain, and (b) the coefficient of determination which is a measure of the goodness of linear fit. The 1000m-, 2000m- and 3000m-isobaths are shown in solid grey lines.

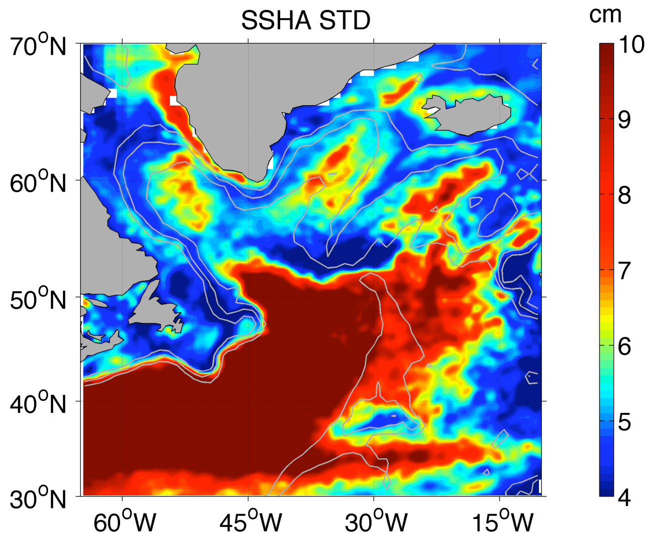

Figure 4.2: The standard deviation of the sea surface height anomaly.

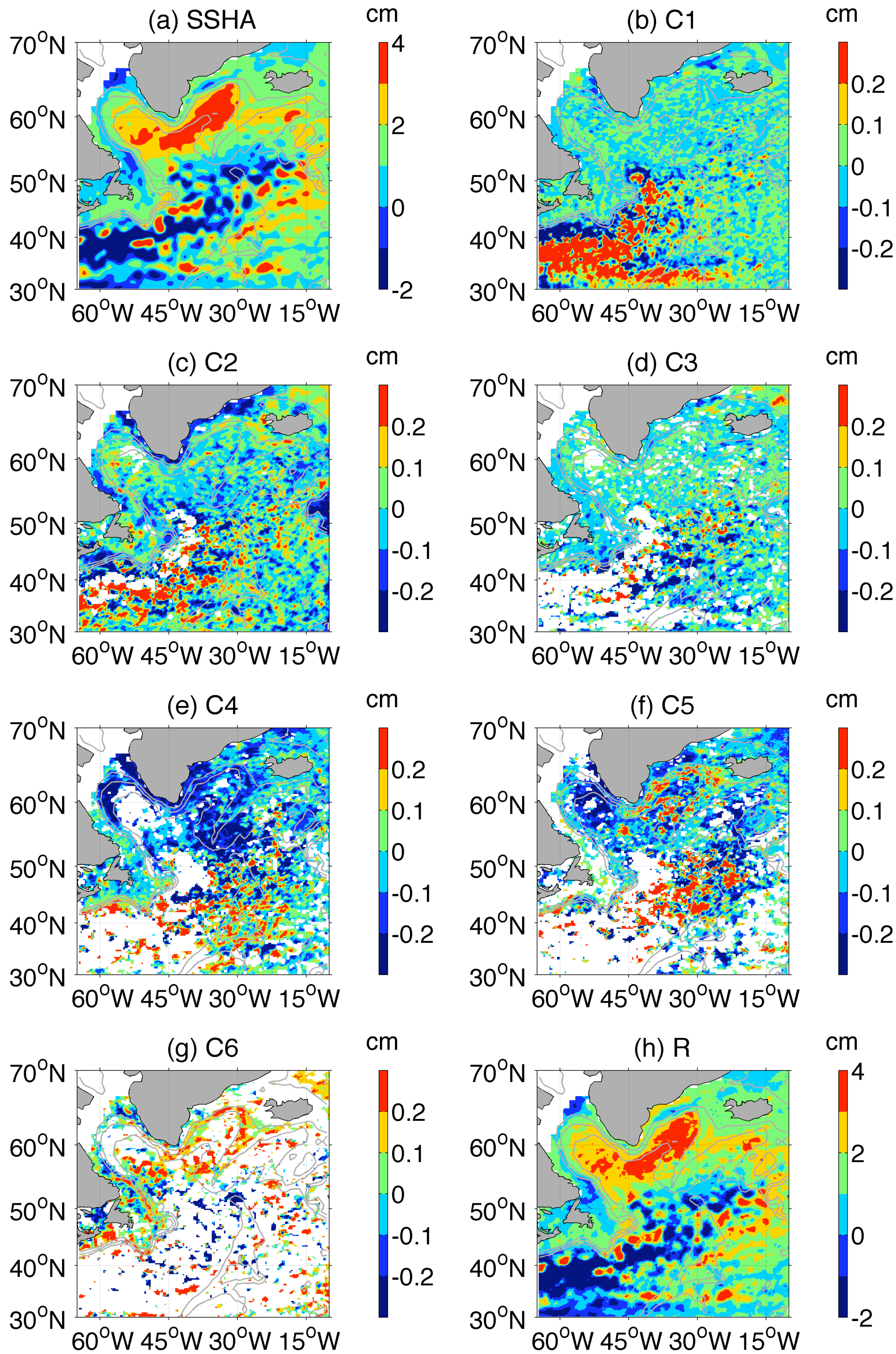

Figure 4.3: The temporal averages over the period of 1993 – 2010 of (a) original SSHA, (b) – (g) the IMFs at increasing timescales and (h) the residual (long-term trend).

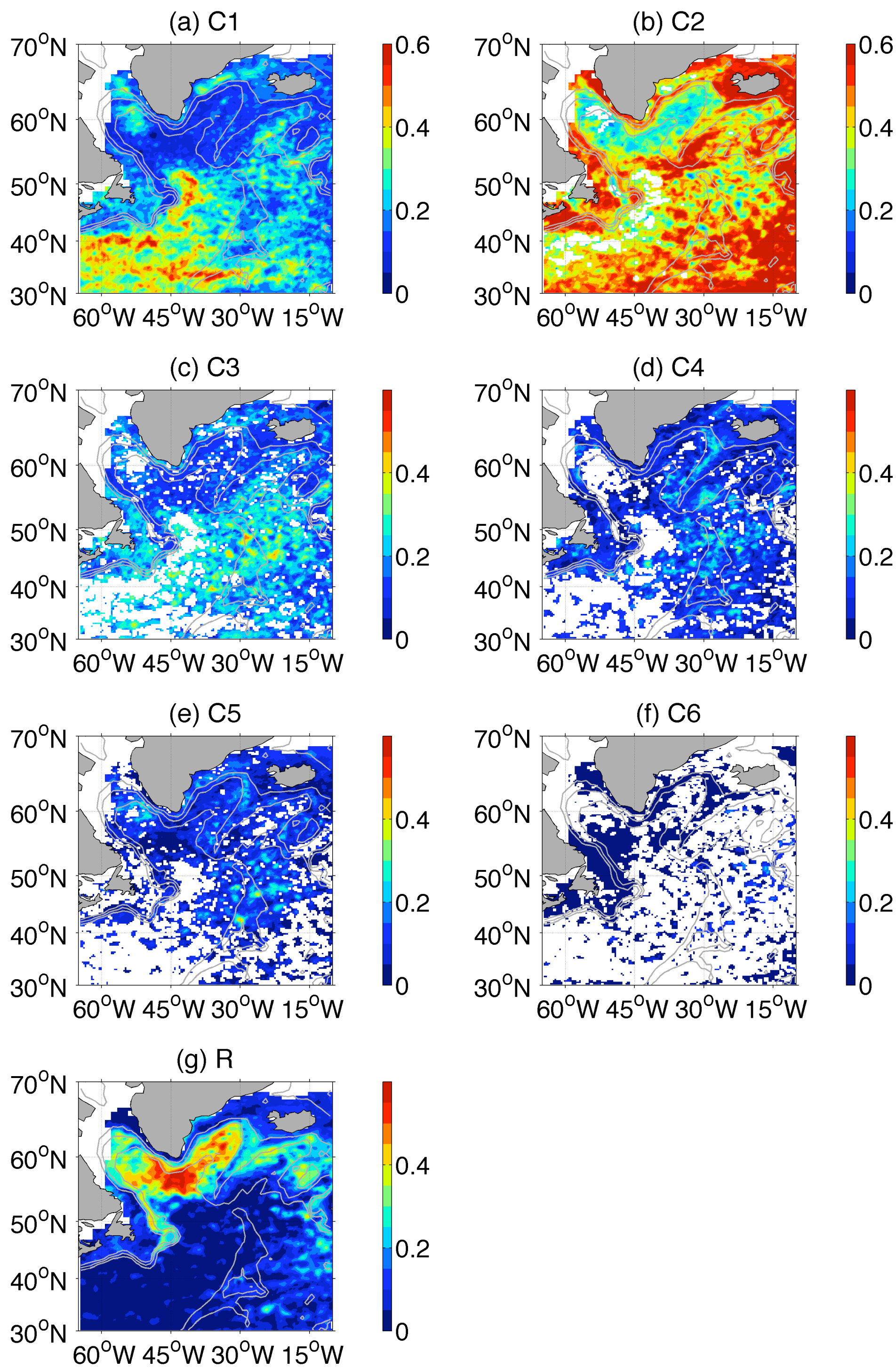

Figure 4.4: The variations explained by the signals over different timescales corresponding to components in Figure 4.3b – 4.3h.

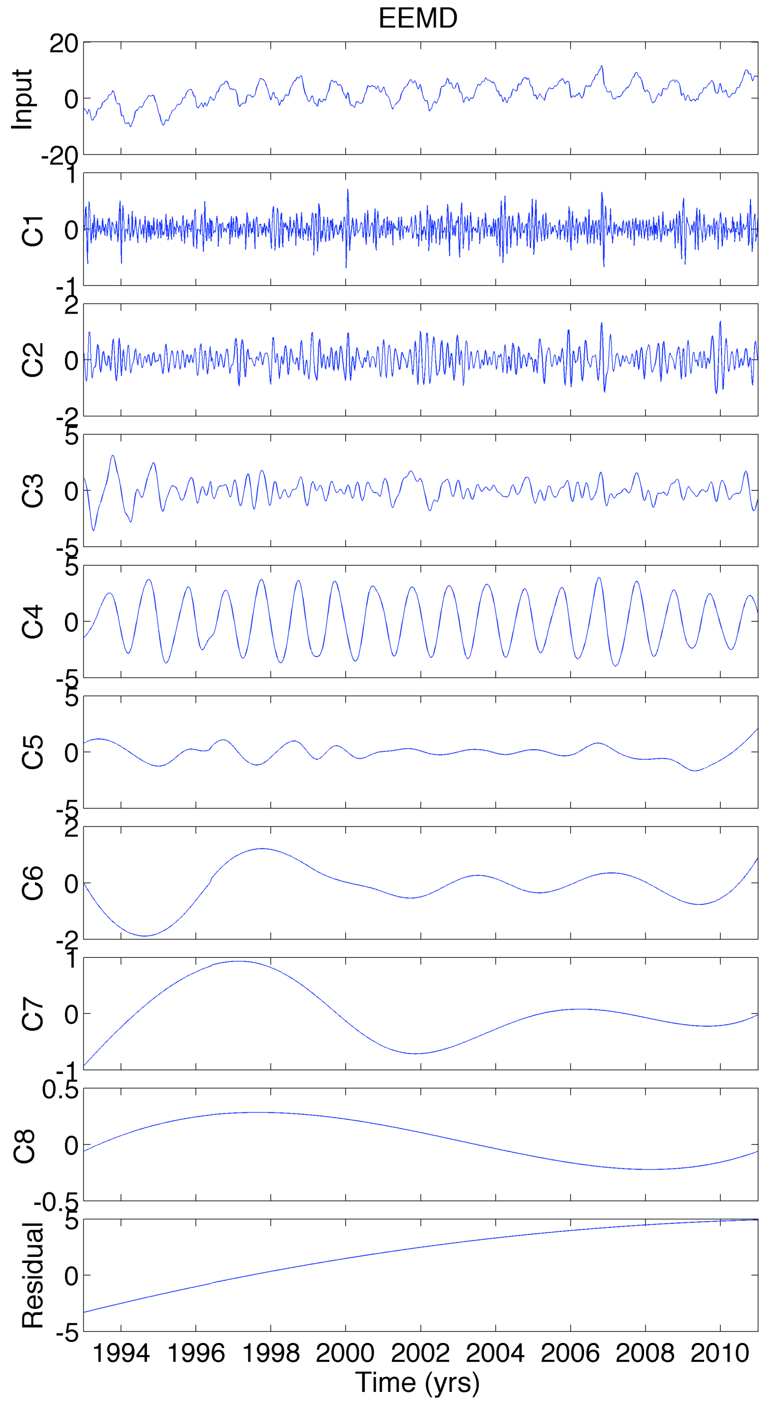

Figure 4.5: The IMFs and the residual decomposed from the spatially averaged sea surface height anomaly over the subpolar gyre. Units are cm.

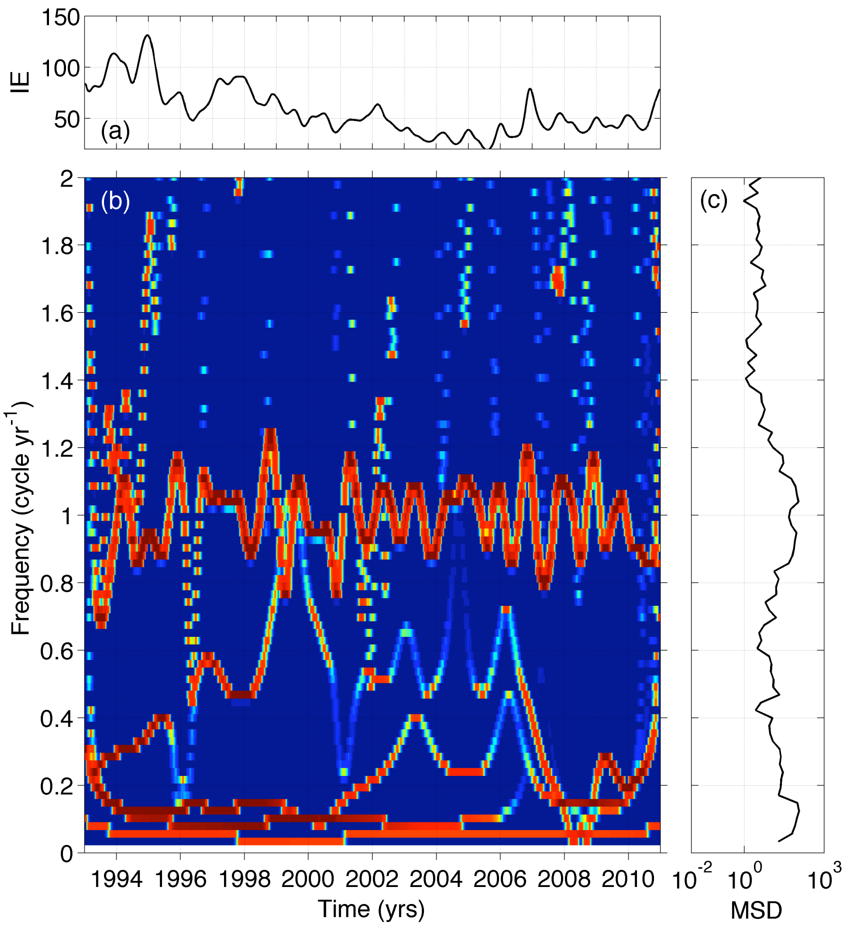

Figure 4.6: The Hilbert transform of the IMFs (C1 – C8). (a) The instantaneous energy density level (IE) in cm^2, (b) the Hilbert spectrum and (c) marginal spectral density (MSD) of each frequency in cm.

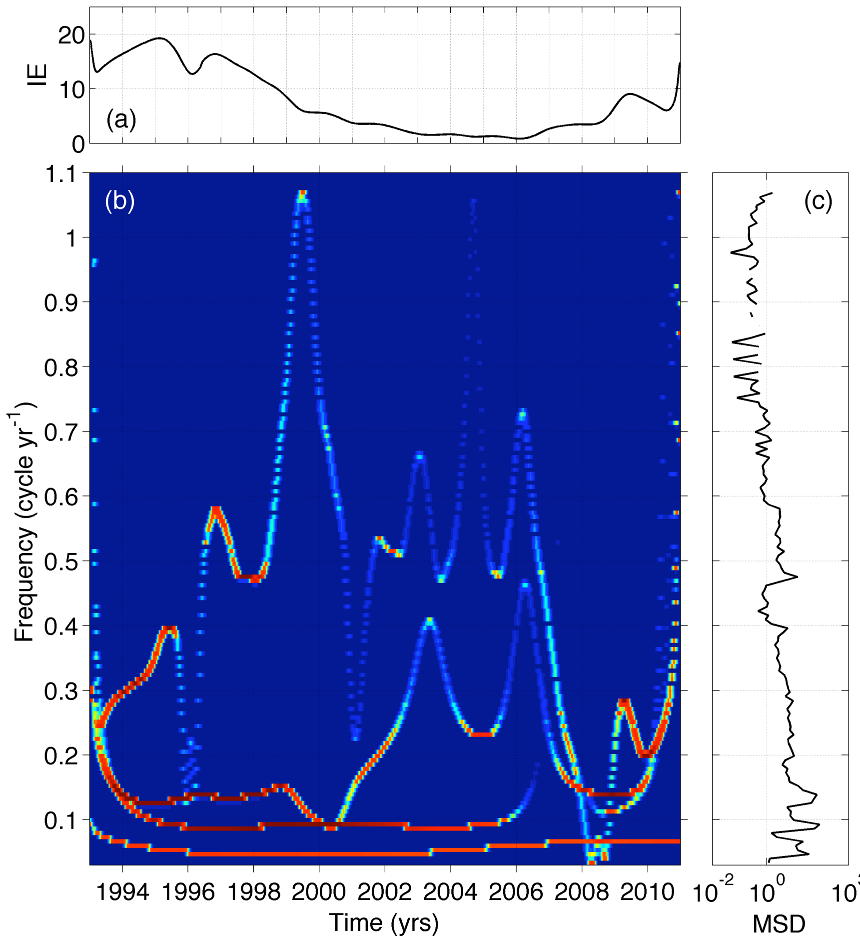

Figure 4.7: Similar to Figure 4.6, but only applying the Hilbert transform to the selected IMFs (C5 – C8). (a) The instantaneous energy density level (IE) in cm^2, (b) the Hilbert spectrum and (c) marginal spectral density (MSD) of each frequency in cm.

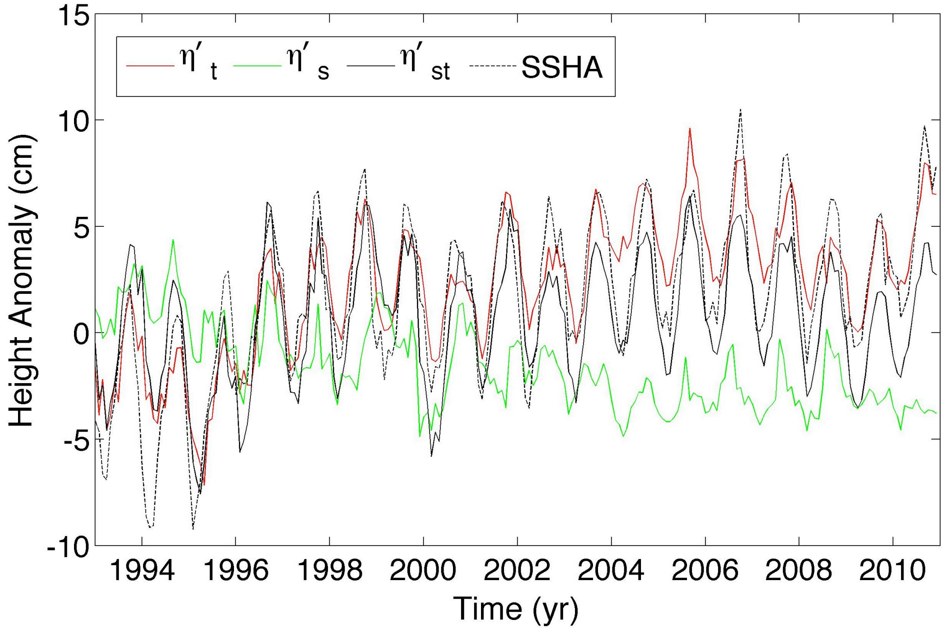

Figure 4.8: The altimeter SSHA and steric height anomaly calculated from temperature and salinity observations in the SPG.

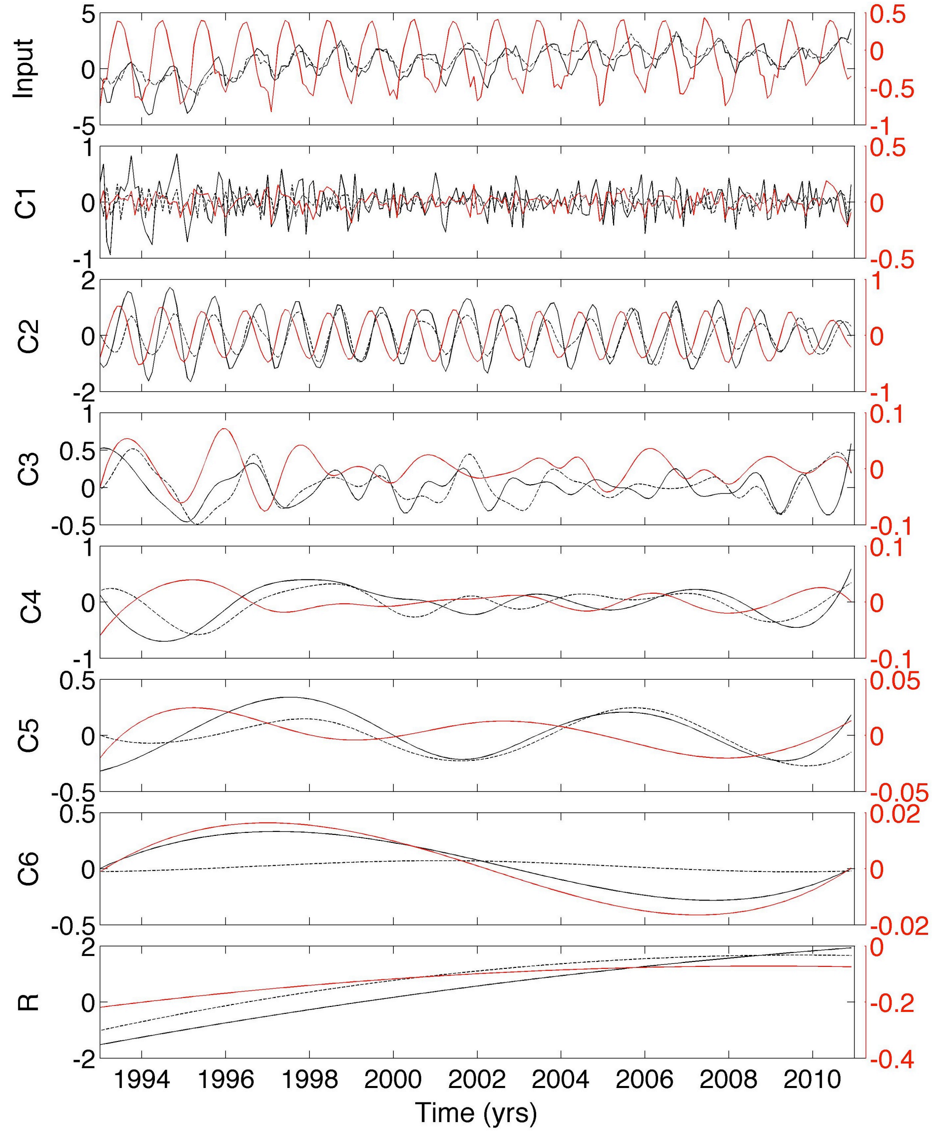

Figure 4.9: The IMFs and the residuals decomposed from the heat content anomalies estimated from surface heat flux (red line; right y-axis) and the SSHA (solid black line; left y-axis). The depth-integrated heat content anomaly (dashed black line; left y-axis) is also shown for comparison. Units are GJ m^{-2}.

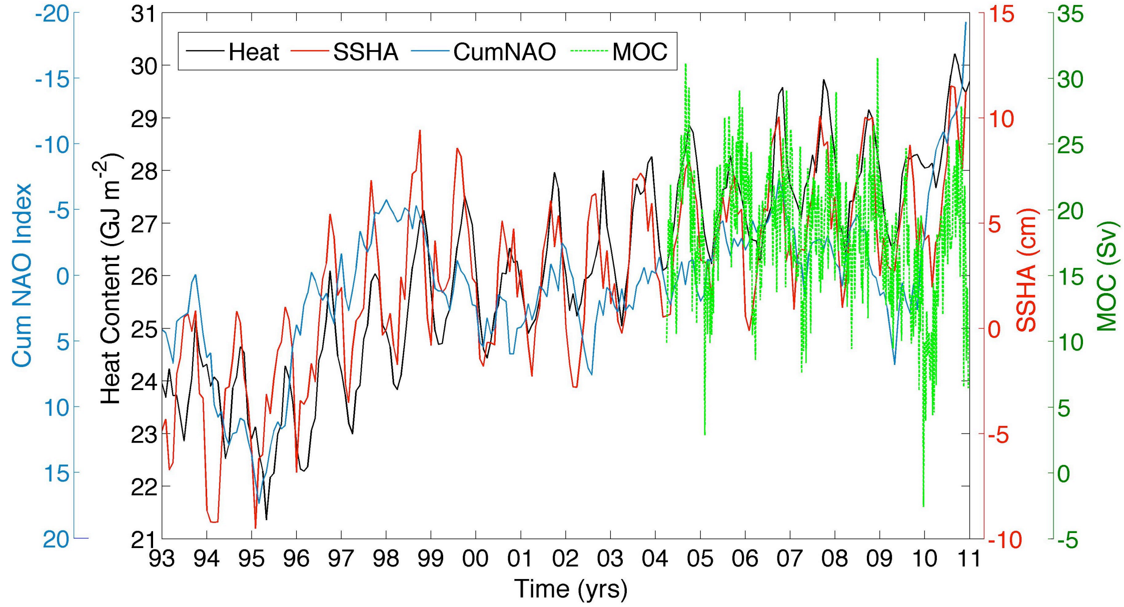

Figure 4.10: Close relationships among the heat content of the central Labrador Sea (black solid line), the sea surface height anomaly of the central Labrador Sea (red solid line), the meridional overturning circulation transport at 26.5°N (green dash line) and the cumulative NAO index (blue line). The central Labrador Sea is defined by a box between 58°W – 48°W and 56°N – 61°N . Unit and range of each index is labeled with y-axis of same color. Note that the y-axis of the CumNAO Index is reversed.

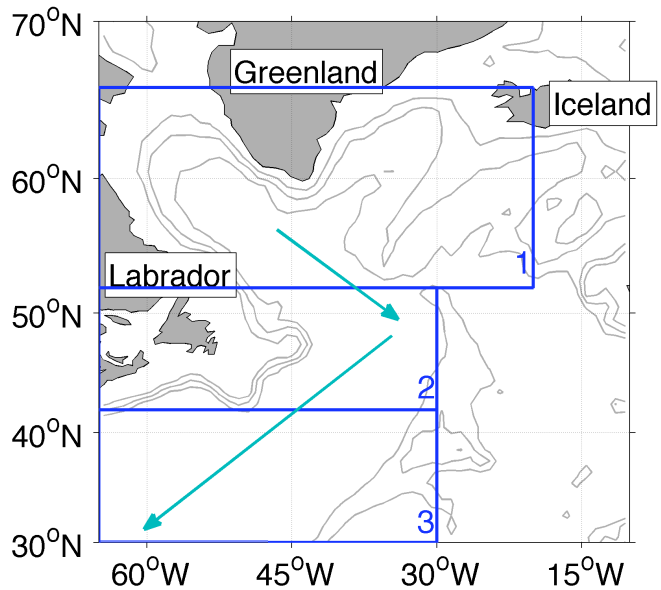

Figure 4.11: Domains of area 1, 2 and 3 used to spatially average the SSHA and examine the lagged correlation between each other. Arrows indicate possible propagation pathway of the AMOC variations. The 1000m-, 2000m- and 3000m-isobaths are shown in solid grey lines.

Chapter 5

CONCLUSIONS AND DISCUSSION

Characteristic features and their associated timescales in relation to AMOC variations in the mid- to high-latitude North Atlantic have been investigated, with a special emphasis on the deep convective activity at high latitudes and latitudinal coherence of the AMOC in terms of several key oceanic variables, such as water temperature, ocean heat content, and SSHA. Some of the main results are: (i) at annual timescales, atmospheric forcing over the Labrador Sea is essential to initiating the deep convective process and to deepening the mixing of the water columns. Therefore, it allows for the direct observation of characteristic surface features that are associated with enhanced deep convection, such as sea ice extent, land and sea surface temperature, and sea level anomaly (and derived eddy kinetic energy anomalies); (ii) at interannual timescales, deep convection is strongly influenced by the existing preconditions of the water column due to the ocean's residual 'memory' of previous winters and changes in the boundary currents and the boundary current eddies; (iii) consistent altimeter observations with advanced temporal and spatial coverage are important to providing a synoptic view of the coherent changes in the SPG and the mid-latitudes pertaining to propagation of the AMOC variations in the North Atlantic; (iv) the cumulative NAO forcing drives low-frequency oceanic changes at high latitudes (i.e., changes in heat content and sea level anomaly) which then propagate to the mid- and low latitudes at an advective speed.

5.1 External and Internal Forcing

The response of the Labrador Sea involves a fundamental fluid dynamical process: buoyancy-driven convection on a rapidly rotating planet. Sources of buoyancy anomalies in the Labrador Sea interior are from heat and freshwater exchange with both the overlying air and the boundary currents. Based on atmospheric data collected from ships at typical upper-ocean conditions, previous study found that the direct effect of heat fluxes on the ocean buoyancy is about five times the salinity effects (The Lab Sea Group, 1998). Therefore, wintertime heat flux primarily contributes to the development and strength of deep convection by balancing the contributions from the vertical and horizontal fluxes. During a winter with intensified atmospheric forcing, heat loss from the sea surface can exceed the horizontal heat gain from warm boundary currents. The mixed layer becomes denser and colder and convection deepens gradually (Figure 2.5). During a mild winter, when the heat loss is less than the horizontal flux, a shallow mixed layer develops and undergoes a rather constant warming and salinification. This is consistent with the results in Chapter 2, where we found that temperature and heat content variations in the upper layers are directly related to the variability of deep convection. Furthermore, the intensity of atmospheric forcing varies most notably during a winter, which directly determines the amount of heat loss and how long it takes for the mixed layer to deepen. For example, a suddenly enhanced heat loss of -600 W m^{-2} in the late January of 2008 induced a drop of approximately 500 m in the mixed layer depth over a period of less than 10 days. However, although atmospheric forcing has relatively significant contributions at the monthly and annual timescales, at the interannual timescales, there is no one-to-one correspondence between the NAO index and deep convection activity at the interannual timescales. Conditions such as wind direction play a role in favoring or suppressing the surface heat loss (e.g., Våge et al., 2009). This explains why there was an enhanced deep convection in the winter of 2008 other than the winter of 2007, both of which had a positive NAO index greater than 2. Instead, low-frequency variations in heat content and sea level anomaly respond to the atmospheric forcing in a cumulative way as suggested by their strong correlation to the cumulative NAO index. This is consistent with previous studies showing that intense weakening of surface circulation and warming in the subpolar region in the mid-1990s reflects a lagged response to a period of positive NAO during the early 1990s (Lohmann et al., 2009a; Robson et al., 2012). The cumulative response, again, reflects the role of the ocean's 'memory'. Limited accessible heat reservoir available for cooling can reduce cross-surface temperature gradients and weaken the surface heat flux during cold winters and, therefore, depresses the convective activity (Zhu and Demirov, 2011; Gelderloos et al., 2012). Low-frequency variability in the heat content and sea level anomaly can be primarily attributed to oceanic changes (i.e., advections and convections). In the meantime, air-sea heat flux can explain most of the heat content's variance in the subpolar region at the monthly and annual timescales as shown in Chapter 4. Therefore, analysis of the relative contributions from atmospheric forcing and internal oceanic adjustment, for example on ocean heat content, depends on the timescales of interest. High latitude heat content variations are thus is in need of further investigation based on data from observations of extreme events and from numerical models.

5.2 Meridional Coherence of the Overturning Variations

The latitudinal dependence and propagation of the AMOC variations has been the subject of many, mostly model-based studies over the years (Bingham et al., 2007; Köhl and Stammer, 2008; Zhang, 2010). The AMOC variations at high latitudes respond to NAO-forced deep-water formation anomaly with a lag of two to three years. The southward deep transport anomaly triggered by ocean convection in the Labrador Sea propagates to low latitudes and follows either advective speed or boundary waves speed, depending on the model resolution (Getzlaff et al., 2005; Zhang, 2010). However, no direct estimates of the coherent variations across different latitudes were obtained observationally until the AMOC estimates recently became available at $26.5°N$ from the implementation of the pioneering RAPID program (Cunningham et al., 2007), and at $41°N$ based on a combination of Argo and altimetry data (Willis, 2010). The derived meridional covariability at the interannual variability may contain high uncertainty because of 1) the limited length of data records – RAPID-based and ARGO-based AMOC estimates are less than a decade in length, 2) inconsistencies in the AMOC estimates – there are fundamental differences of how the AMOC is calculated at these two latitudes (Mielke et al., 2013). Alternatively, studies have proposed sea surface height anomaly (SSHA) and upper ocean heat content as the 'fingerprints' of the AMOC variations from model simulations, which have great implications for climate predictability and predictions (Zhang, 2008; Msadek et al., 2010). As was shown in Chapter 3 and Chapter 4, in fact, the low frequency SSHA signals in the mid-latitude North Atlantic lagged those at the high latitudes. There is a time lag of 2 years from the deep water formation region (near $65°N$) to about $50°N$, and a 5 year lag between $50°N$ and $30°N$. Components with frequencies smaller than 1 cycle yr^{-1} decomposed using the EEMD are used to reconstruct low frequency SSHA variations for different regions in the North Atlantic. With known frequency information and flexibility of domain choices, the results provide a better understanding of spatial coherence of the SSHA variability at the interannual and decadal timescales.

The mechanism that links atmospheric forcing and the low-frequency SSHA variations in relation to the propagation of AMOC variations is still not understood. For example, while North Atlantic SSHA changes coincide with shifts in the NAO (Esselborn and Eden, 2001; Häkkinen, 2001; Volkov and van Aken, 2003), the low-frequency SSHA, in relation to the propagation of AMOC variations, is mostly correlated to the cumulative NAO index as shown in Chapter 3 and Chapter 4. The cumulative response may imply low-frequency rectification in ocean circulations, and associated heat transport, under the impact of atmospheric forcing, which can be observed by the SSHA changes. Furthermore, the use of SSHA to represent changes in the AMOC should be with caution, given the existence of a high-frequency wind-driven response as was suggested by Lorbacher et al. (2010) based on a sequence of global ocean-ice model experiments. Therefore, a careful interpretation of the SSHA patterns is needed since its causes depend on the timescales of interest. Future work requires a focus on exploring the relationship between low frequency SSHA variations related to the AMOC and changes in regional atmospheric circulation (i.e., the displacements of the atmospheric centers of action). There might be an active AMOC in which the AMOC variability influences regional atmospheric circulation and thus atmospheric pressure patterns (i.e., changes in NAO, and more specifically, in pressure and position of the Icelandic Low) that drive the SSHA variability, allowing for improved projections of future sea level changes.

Although altimeteric SSHA is useful for monitoring the AMOC variations across different latitudes, current altimeter records are less than enough to resolve long-term variations such as the global 60-year oscillation cycle (Chambers et al., 2012). It actually becomes less robust when interpreting cycles with long periods that are comparable to the record length itself. Analysis of meridional coherences at the inter-decadal to multi-decadal timescales requires more data from consistent sources in the future.

5.3 Subpolar AMOC Variability

With a northward heat transport of up to 1.3 PW (Ganachaud and Wunsch, 2003; Johns et al., 2011), the AMOC is one of the prominent components of the Earth's climate system. The AMOC's strength and patterns influence on the heat content at the high latitudes. Recent studies based on both satellite and in-situ observations have indicated a warming trend during the recent decade in the northern North Atlantic (Sarafanov et al., 2007; Häkkinen et al., 2011; Robson et al., 2012; Häkkinen et al., 2013) caused by the weakening of the SPG in terms of both its intensity and shape (Hátún et al., 2005; Sarafanov, 2009; Häkkinen et al., 2013), which may have had significant interactions with freshwater influx due to melting ice sheets and glaciers at high latitudes in the 2000s. Actually, a dramatic increasing of the ice melt rates has been observed in the most recent decade in the Arctic (Stroeve et al., 2008; Kwok et al., 2009; Rignot et al., 2011) and Greenland (Chen et al., 2006; Bindschadler, 2006; Holland et al., 2008; Khan et al., 2010). This implies a potential relationship between the SPG intensity, which determines the amount of heat transported along the Greenland coast, and the melting ice mass along the margin of the SPG.

Freshwater anomalies causing deep convection to shut down occurred when the 'Great Salinity Anomaly' (GSA; Dickson et al., 1988), a low salinity signal, passed through the Labrador Sea in the late 1960s and early 1970s and restricted convection to the upper 300 m (Lazier, 1980). In the early 1980s, convection was also strongly reduced by a freshwater anomaly (Belkin et al., 1998). Freshwater perturbations at high latitudes during the deglacial climate led to the absence of deep-water formation in the Labrador Sea (Wood et al., 1999; Hillaire-Marcel et al., 2001) and caused the slow-down or even shutdown of the AMOC (Rind et al., 2001; Hall et al., 2006; Stouffer et al., 2006; Thornalley et al., 2010; Hawkins et al., 2011). The acceleration in the melting of ice sheets and glaciers in the Arctic and Greenland has drawn significant attention because of their impact on regional oceanic dynamics which are closely related to the future of the climate system.

There are two major impacts of the increased freshwater influx on the deep convective process: 1) increased freshwater could lead to extended sea ice cover during the intense winter conditions. The advance of the sea ice edge in winter is favorable for bringing the atmospheric forcing to its adjacent water column, and thus regulates the locations of deep-water formation (e.g., McGeehan and Maslowski, 2011); 2) accumulation of freshwater in the Labrador Sea increases ocean stratification and therefore inhibits the convection of the water columns, which in turn reduces the surface buoyancy flux to the atmosphere during mild winters (e.g., Gelderloos et al., 2012). Moreover, the feedback between freshwater anomalies due to glacial destabilization and oceanic circulation also requires further investigation especially under a warming scenario. For example, several studies have examined the role of subglacial water in triggering the acceleration of the melting of Greenland glaciers (e.g., Shepherd et al., 2009). The results suggest that this forcing is not sufficient to destabilize the glaciers and does not yield an increase in speed comparable in magnitude to observed values. Ocean warming has been hypothesized as an alternative cause of glacial destabilization (Bindschadler, 2006; Holland et al., 2008; Hanna et al., 2009; Christoersen et al., 2011). An increase in the temperature of the subsurface waters at the front of these glaciers would increase the subaqueous melt rates of their calving faces, cause retreat of the glacier fronts, and yield changes in the force balance that could trigger a speed-up. Therefore, it is of importance and necessity to understand the linkage between the variations in the strength and heat content of the horizontal circulation at the high latitudes and potential changes in glaciers adjacent to the boundary currents.

REFERENCES

Antonov, J. I., S. Levitus, and T. P. Boyer, 2002: Steric sea level variations during 1957–1994: Importance of salinity. *J. Geophys. Res.,* 107 (C12).

Bailey, D., P. Rhines, and S. Häkkinen, 2005: Formation and pathways of North Atlantic deep water in a coupled ice–ocean model of the Arctic–North Atlantic Oceans. *Clim. Dyn.,* 25, 497-516.

Beckley, B. D., N. P. Zelensky, S. A. Holmes, F. G. Lemoine, R. D. Ray, G. T. Mitchum, S. D. Desai, and S. T. Brown, 2010: Assessment of the Jason-2 extension to the TOPEX/Poseidon, Jason-1 sea-surface height time series for global mean sea level monitoring. *Mar. Geod.,* 33, 447-471.

Belkin, I. M., 2004: Propagation of the "Great Salinity Anomaly" of the 1990s around the northern North Atlantic. *Geophys. Res. Lett.,* 31, L08306.

Belkin, I. M., S. Levitus, J. Antonov, and S.-A. Malmberg, 1998: "Great Salinity Anomalies" in the North Atlantic. *Prog. Oceanogr.,* 41, 1-68.

Bentsen, M., H. Drange, T. Furevik, and T. Zhou, 2004: Simulated variability of the Atlantic meridional overturning circulation. *Clim. Dyn.,* 22, 701-720.

Bersch, M., 2002: North Atlantic Oscillation–induced changes of the upper layer circulation in the northern North Atlantic Ocean. *J. Geophys. Res.,* 107, 3156.

Bersch, M., I. Yashayaev, and K. Koltermann, 2007: Recent changes of the thermohaline circulation in the subpolar North Atlantic. *Ocean Dyn.,* 57, 223-235.

Biastoch, A., C. W. Böning, J. Getzlaff, J.-M. Molines, and G. Madec, 2008: Causes of interannual–decadal variability in the meridional overturning circulation of the midlatitude North Atlantic Ocean. *J. Climate*, 21, 6599–6615.

Bindschadler, R., 2006: Hitting the ice sheets where it hurts. *Science,* 311, 1720-1721.

Bingham, R. J., and C. W. Hughes, 2008: The relationship between sea-level and bottom pressure variability in an eddy permitting ocean model. *Geophys. Res. Lett.*, 35, L03602.

Bingham, R. J., C. W. Hughes, V. Roussenov, and R. G. Williams, 2007: Meridional coherence of the North Atlantic meridional overturning circulation. *Geophys. Res. Lett.,* 34, L23606,

Böning, C. W., M. Scheinert, J. Dengg, A. Biastoch, and A. Funk, 2006: Decadal variability of subpolar gyre transport and its reverberation in the North Atlantic overturning. *Geophys. Res. Lett.,* 33, L21S01.

Bower, A. S., M. S. Lozier, S. F. Gary, and C. W. Böning, 2009: Interior pathways of the North Atlantic meridional overturning circulation. *Nature*, 459, 243–248.

Cazenave A., and W. Llovel, 2010: Contemporary sea level rise. *Annu. Rev. Mar. Sci.*, 2, 145-173.

Chambers, D. P., B. D. Tapley, and R. H. Stewart, 1997: Long-period ocean heat storage rates and basin-scale heat fluxes from TOPEX. *J. Geophys. Res.,* 102, 10525-10533.

Chelton, D. B., M. G. Schlax, and R. M. Samelson, 2011: Global observations of nonlinear mesoscale eddies. *Prog. Oceanogr.*, 91, 167-216.

Chen, J. L., C. R. Wilson, and B. D. Tapley, 2006: Satellite gravity measurements confirm accelerated melting of Greenland ice sheet. *Science,* 313, 1958-1960.

Clarke, R. A., and J. Gascard, 1983: The formation of Labrador Sea Water. Part I: Large-scale processes. *J. Phys. Oceanogr., 13*, 1764-1778.

Clark, P. U., N. G. Pisias, T. F. Stocker, and A. J. Weaver, 2002: The role of the thermohaline circulation in abrupt climate change. *Nature,* 415, 863-869.

Cromwell, D., 2006: Temporal and spatial characteristics of sea surface height variability in the North Atlantic Ocean. *Ocean Sci.,* 2, 147-159.

Cunningham, S. A., T. O. Kanzow, D. Rayner, M. O. Baringer, W. E. Johns, J. Marotzke, H. R. Longworth, E. M. Grant, J. J.-M. Hirschi, L. M. Beal, C. S. Meinen, and H. L. Bryden, 2007: Temporal variability of the Atlantic meridional overturning circulation at 26.5°N. *Science*, 317, 935-938.

Cunningham, S. A., and R. Marsh, 2010: Observing and modeling changes in the Atlantic MOC. *Climate Change,* 1, 180-191.

Curry, R., B. Dickson, and I. Yashayaev, 2003: A change in the freshwater balance of the Atlantic Ocean over the past four decades. *Nature,* 426, 826-829.

Curry, R., and C. Mauritzen, 2005: Dilution of the northern North Atlantic Ocean in recent decades. *Science,* 308, 1772-1774.

Curry, R. G., and M. S. McCartney, 2001: Ocean gyre circulation changes associated with the North Atlantic Oscillation*. *J. Phys. Oceanogr.,* 31, 3374-3400.

Curry, R. G., M. S. McCartney, and T. M. Joyce, 1998: Oceanic transport of subpolar climate signals to mid-depth subtropical waters. *Nature,* 391, 575-577.

Daniault, N., H. Mercier, and P. Lherminier, 2011: The 1992–2009 transport variability of the East Greenland-Irminger Current at 60°N. *Geophys. Res. Lett.,* 38, L07601.

de Boyer Montégut, C., G. Madec, A. S. Fischer, A. Lazar, and D. Iudicone, 2004: Mixed layer depth over the global ocean: An examination of profile data and a profile-based climatology. *J. Geophys. Res.,* 109, C12003.

Dengler, M., J. Fischer, F. A. Schott, and R. Zantopp, 2006: Deep Labrador Current and its variability in 1996–2005. *Geophys. Res. Lett.,* 33, L21S06.

Dickson, R., J. Lazier, J. Meincke, P. Rhines, and J. Swift, 1996: Long-term coordinated changes in the convective activity of the North Atlantic. *Prog. Oceanogr.,* 38, 241-295.

Dickson, R., I., Yashayaev, J. Meincke, B. Turrell, S. Dye, and J. Holfort, 2002: Rapid freshening of the deep North Atlantic Ocean over the past four decades. *Nature,* 416: 832–837.

Dong, S., and K. A. Kelly, 2004: Heat budget in the Gulf Stream region: The importance of heat storage and advection. *J. Phys. Oceanogr.,* 34, 1214-1231.

Esselborn, S., and C. Eden, 2001: Sea surface height changes in the North Atlantic Ocean related to the North Atlantic Oscillation. *Geophys. Res. Lett.,* 28, 3473-3476.

Fairall, C.W., E. F. Bradley, J. E. Hare, A. A. Grachev, and J. B. Edson, 2003: Bulk parameterization of air-sea fluxes: updates and verification for the COARE algorithm. *J. Climate*, 16, 571-591.

Ferry, N., G. Reverdin, and A. Oschlies, 2000: Seasonal sea surface height variability in the North Atlantic Ocean. *J. Geophys. Res.,* 105, 6307-6326.

Ganachaud, A., and C. Wunsch, 2003: Large-scale ocean heat and freshwater transports during the World Ocean Circulation Experiment. *J. Climate*, 16, 696–705.

Ganopolski, A., and S. Rahmstorf, 2001: Rapid changes of glacial climate simulated in a coupled climate model. *Nature,* 409, 153-158.

Ganopolski, A., and A. Robinson, 2011: Palaeoclimate: The past is not the future. *Nature Geosci,* 4, 661-663.

Gardner, A. S., and Coauthors, 2011: Sharply increased mass loss from glaciers and ice caps in the Canadian Arctic Archipelago. *Nature,* 473, 357-360.

Gelderloos R., C. A. Katsman, and K. Våge, 2013: Detecting Labrador Sea Water formation from space, *J. Geophys. Res.-Oceans*, 118, 2074–2086

Gelderloos, R., F. Straneo, and C. Katsman, 2011: Accessing the roles of three eddy types in restratifying the Labrador Sea after deep convection. *J. Phys. Oceanogr.*, 41, 2102-2119.

Gelderloos, R., F. Straneo and C. Katsman, 2012: Mechanisms behind the temporary shutdown of deep convection in the Labrador Sea: Lessons from the Great Salinity Anomaly years 1968-1971. *J. Climate,* 25, 6743-6755.

Getzlaff, J., C. W. Böning, C. Eden, and A. Biastoch, 2005: Signal propagation related to the North Atlantic overturning. *Geophys. Res. Lett.,* 32, L09602

Christoersen, P. and coauthors, 2011: Warming of waters in an East Greenland fjord prior to glacier retreat: Mechanisms and connection to large-scale atmospheric conditions. *The Cryosphere Discuss.,* 5, 1335-1364.

Gulev, S. K., B. Barnier, H. Knochel, J. Molines, and M. Cottet, 2003: Water mass transformation in the North Atlantic and its impact on the meridional circulation: Insights from an ocean model forced by NCEP–NCAR reanalysis surface fluxes. *J. Climate,* 16, 3085-3110.

Gill, A. E., and P. Niiler, 1973: The theory of seasonal variability in the ocean. *Deep-Sea. Res.*, 20, 141–177.

Häkkinen, S., 1999: Variability of the simulated meridional heat transport in the North Atlantic for the period 1951–1993. *J. Geophys. Res.,* 104, 10991-11007.

Häkkinen, S., 2001: Variability in sea surface height: A qualitative measure for the meridional overturning in the North Atlantic. *J. Geophys. Res.,* 106, 13837-13848.

Häkkinen, S., and P. B. Rhines, 2004: Decline of subpolar North Atlantic circulation during the 1990s. *Science,* 304, 555-559.

Häkkinen, S., and P. B. Rhines, 2009: Shifting surface currents in the northern North Atlantic Ocean. *J. Geophys. Res.*, 114, C04005.

Häkkinen, S., P. B. Rhines, and D. L. Worthen, 2011: Warm and saline events embedded in the meridional circulation of the northern North Atlantic. *J. Geophys. Res.,* 116, C03006.

Häkkinen, S., P. B. Rhines, D. L. Worthen, 2013. Northern North Atlantic sea surface height and ocean heat content variability. *J. Geophys. Res.,*118, 3670-3678.

Hall, I. R., S. B. Moran, R. Zahn, P. C. Knutz, C. Shen, and R. L. Edwards, 2006: Accelerated drawdown of meridional overturning in the late-glacial Atlantic triggered by transient pre-H event freshwater perturbation. *Geophys. Res. Lett.,* 33, L16616.

Han, G., K. Ohashi, N. Chen, P. G. Myers, N. Nunes, and J. Fischer, 2010: Decline and partial rebound of the Labrador Current 1993–2004: Monitoring ocean currents from altimetric and conductivity-temperature-depth data. *J. Geophys. Res.,* 115, C12012.

Hanna, E., and coauthors, 2009: Hydrologic response of the Greenland ice sheet: the role of oceanographic warming. *Hydrol. Process,* 23, 7-30.

Hannachi, A., I. T. Jolliffe, and D. B. Stephenson, 2007: Empirical orthogonal functions and related techniques in atmospheric science: A review. *Int. J. Climatol.*, 27(9), 1119 – 1152.

Hátún, H., A. B. Sandø, H. Drange, B. Hansen, and H. Valdimarsson, 2005: Influence of the Atlantic subpolar gyre on the thermohaline circulation. *Science,* 309, 1841-1844.

Hawkins, E., R. S. Smith, L. C. Allison, J. M. Gregory, T. J. Woollings, H. Pohlmann, and B. de Cuevas, 2011: Bistability of the Atlantic overturning circulation in a global climate model and links to ocean freshwater transport. *Geophys. Res. Lett.,* 38, L10605.

Herbaut, C., and M. Houssais, 2009: Response of the eastern North Atlantic subpolar gyre to the North Atlantic Oscillation. *Geophys. Res. Lett.*, 36, L17607,

Herrmann, M., J. Bouffard, and K. Beranger, 2009: Monitoring open-ocean deep convection from space. *Geophys. Res. Lett., 36*, L03606.

Hillaire-Marcel, C., A. de Vernal, G. Bilodeau, and A. J. Weaver, 2001: Absence of deep-water formation in the Labrador Sea during the last interglacial period. *Nature,* 410, 1073-1077.

Holland, D. M., R. H. Thomas, B. de Young, M. H. Ribergaard, and B. Lyberth, 2008: Acceleration of Jakobshavn Isbrae triggered by warm subsurface ocean waters. *Nature Geosci,* 1, 659-664.

Holliday, N. P., and coauthors, 2008: Reversal of the 1960s to 1990s freshening trend in the northeast North Atlantic and Nordic Seas. *Geophys. Res. Lett.*, 35, L03614S.

Huang, N. E., and coauthors, 1998: The Empirical mode decomposition and the Hilbert spectrum for nonlinear and non-stationary time series analysis. *Proc. R. Soc. London A,* 454, 903-995.

Huang, N. E., and Z. Wu, 2008: A review on Hilbert-Huang Transform: Method and its applications to geophysical studies. *Rev. Geophys.,* 46, RG2006.

Hurrell, J. W., 1995: Decadal trends in the North Atlantic Oscillation: Regional temperatures and precipitation. *Science,* 269, 676-679.

Hurrell, J. W., Y. Kushnir, G. Ottersen, and M. Visbeck, 2003: An overview of the North Atlantic Oscillation, *Geophy. Monograph*, 134, doi: 10.1029/134GM01.

Ingleby, B., and M. Huddleston, 2007: Quality control of ocean temperature and salinity profiles — Historical and real-time data. *J. Mar. Syst.,* 65, 158-175.

Ivchenko, V. O., S. Danilov, D. Sidorenko, J. Schröter, M. Wenzel, and D. L. Aleynik, 2008: Steric height variability in the Northern Atlantic on seasonal and interannual scales. *J. Geophys. Res.*, 113, C11007.

Jayne, S. R., J. M. Wahr, and F. O. Bryan, 2003: Observing ocean heat content using satellite gravity and altimetry. *J. Geophys. Res.,* 108, 3031.

Johns, W. E., and Coauthors, 2011: Continuous, array-based estimates of Atlantic ocean heat transport at 26.5°N. *J. Climate*, 24, 2429–2449.

Kalnay, E., and Coauthors, 1996: The NCEP/NCAR 40-year reanalysis project. *Bull. Amer. Meteor. Soc.,* 77, 437-471.

Kelly, K. A., 2004: The relationship between oceanic heat transport and surface fluxes in the western North Pacific: 1970-2000. *J. Climate,* 17, 573-588.

Kelly, K. A., and S. Dong, 2004: The relationship of western boundary current heat transport and storage to midlatitude ocean-atmosphere interaction, *Earth's Climate: The Ocean-Atmosphere Interaction*, *Geophys. Monogr. Ser.*, vol. 147, C. Wang, S.-P. Xie, and J. A. Carton, Ed., AGU, 347–363, Washington, D. C., doi:10.1029/147GM19.

Khan, S. A., J. Wahr, M. Bevis, I. Velicogna, and E. Kendrick, 2010: Spread of ice mass loss into northwest Greenland observed by GRACE and GPS. *Geophys. Res. Lett.,* 37, L06501.

Kieke, D., M. Rhein, L. Stramma, W. M. Smethie, J. L. Bullister, and D. A. LeBel, 2007: Changes in the pool of Labrador Sea Water in the subpolar North Atlantic. *Geophys. Res. Lett.,* 34, L06605.

Köhl, A., and D. Stammer, 2008: Variability of the meridional overturning in the North Atlantic from the 50-year GECCO state estimation. *J. Phys. Oceanogr.*, 38, 1913–1930.

Kuhlbrodt, A. Griesel, M. Montoya, A. Levermann, M. Hofmann, and S. Rahmstorf, 2007: On the driving processes of the Atlantic meridional overturning circulation. *Rev. Geophys.,* 45, RG2001, doi:10.1029/2004RG000166.

Kwok, R., G. F. Cunningham, M. Wensnahan, I. Rigor, H. J. Zwally, and D. Yi, 2009: Thinning and volume loss of the Arctic Ocean sea ice cover: 2003–2008. *J. Geophys. Res.,* 114, C07005.

Kwok, R., L. Toudal Pedersen, P. Gudmandsen, and S. S. Pang, 2010: Large sea ice outflow into the Nares Strait in 2007. *Geophys. Res. Lett.,* 37, L03502.

Langehaug, H.R., I. Medhaug, T. Eldevik, and O. H. Otterå, 2011: Arctic/Atlantic exchanges via the subpolar gyre. *J. Climate,* 25, 2421-2439.

Latif, M., C. Böning, J. Willebrand, A. Biastoch, J. Dengg, N. Keenlyside, U. Schweckendiek, and G. Madec, 2006: Is the thermohaline circulation changing? *J. Climate,* 19, 4631-4637.

Lazier, J., 1980: Oceanographic conditions at Ocean Weather Ship Bravo, 1964–1974. *Atmosphere-Ocean,* 18, 227-238.

Lazier, J., R. Hendry, A. Clarke, I. Yashayaev, and P. Rhines, 2002: Convection and restratification in the Labrador Sea, 1990–2000. *Deep Sea Res. I,* 49, 1819-1835.

Le Traon, P. Y. T., and G. Dibarboure, 1999: Mesoscale mapping capabilities of multiple-satellite altimeter missions. *J. Atmos. Oceanic Technol.,* 16, 1208-1223.

Li, F., Y.-H. Jo, W. T. Liu, and X.-H. Yan, 2012: A dipole pattern of the sea surface height anomaly in the North Atlantic: 1990s–2000s. *Geophys. Res. Lett.,* 39, L15604.

Lilly, J. M., P. B. Rhines, F. Schott, K. Lavender, J. Lazier, U. Send, and E. D'Asaro, 2003: Observations of the Labrador Sea eddy field. *Prog. Oceanogr.,* 59, 75-176.

Lohmann, G., H. Haak, and J. Jungclaus, 2008: Estimating trends of Atlantic meridional overturning circulation from long-term hydrographic data and model simulations. *Ocean Dyn.,* 58, 127-138.

Lohmann, K., H. Drange, and M. Bentsen, 2009a: A possible mechanism for the strong weakening of the North Atlantic subpolar gyre in the mid-1990s. *Geophys. Res. Lett.,* 36, L15602.

Lohmann, K., H. Drange, and M. Bentsen, 2009b: Response of the North Atlantic subpolar gyre to persistent North Atlantic Oscillation like forcing. *Clim. Dyn.,* 32, 273-285.

Lorbacher, K., J. Dengg, C. W. Boning, and A. Biastoch, 2010: Regional patterns of sea level change related to interannual variability and multidecadal trends in the Atlantic meridional overturning circulation*. *J. Climate,* 23, 4243-4254.

Luo, H., A. Bracco, I. Yashayaev, and E. Di Lorenzo, 2012: The interannual variability of potential temperature in the central Labrador Sea. . *J. Geophys. Res.,* 117, C10016.

Lynch-Stieglitz, J., M. W. Schmidt, and W. B. Curry, 2011: Evidence from the Florida Straits for Younger Dryas ocean circulation changes. *Paleoceanogr.,* 26, PA1205.

Lynch-Stieglitz, J., and Coauthors, 2007: Atlantic meridional overturning circulation during the Glacial Maximum. *Science,* 316, 66-69.

Mahajan, S., R. Zhang, T. Delworth, S. Zhang, A. J. Rosati, and Y.-S. Chang, 2011: Predicting Atlantic meridional overturning (AMOC) variations using subsurface and surface fingerprints. *Deep-Sea Res. II*, 58, 1895-1903.

Marshall, J., and Coauthors, 2001: North Atlantic climate variability: Phenomena, impacts and mechanisms. *Int. J. Climatol.,* 21, 1863-1898.

Marshall, J., and F. Schott, 1999: Open-ocean convection: Observations, theory, and models. *Rev. Geophys.*, 37, 1-64.

McGeehand, T., and W. Maslowski, 2011: Impact of shelf-basin freshwater transport on deep convection in the western Labrador Sea. *J. Phys. Oceanogr.,* 41, 2187-2210.

McManus, J. F., R. Francois, J.-M. Gherardi, L. D. Keigwin, and S. Brown-Leger, 2004: Collapse and rapid resumption of Atlantic meridional circulation linked to deglacial climate changes. *Nature,* 428, 834-837.

Medhaug, I., H. R. Langehaug, T. Eldevik, T. Furevik, and M. Bentsen, 2012: Mechanisms for decadal scale variability in a simulated Atlantic meridional overturning circulation. *Climate Dyn.*, 39, 77-93.

Msadek, R., K. W. Dixon, T. L. Delworth, and W. Hurlin, 2010: Assessing the predictability of the Atlantic meridional overturning circulation and associated fingerprints. *Geophys. Res. Lett.,* 37, L19608.

Nielsen, J. H., 1928: The waters round Greenland. *Greenland*, published by The Commission for the Direction of the Geological Geographical Investigation in Greenland. Copenhagen and London, Vol. 1, 185-230.

Paluszkiewicz, T., R. W. Garwood, and D. W. Denbo, 1994: Deep convective plumes in the ocean. *Oceanogr.*, 7, 37-44.

Piecuch, C. G., K. J. Quinn, and R. M. Ponte, 2013: Satellite-derived interannual ocean bottom pressure variability and its relation to sea level. *Geophys. Res. Lett.,* doi: 10.1002/grl.50549.

Pickart, R., D. Torres, and R. A. Clarke, 2002: Hydrography of the Labrador Sea during active convection. *J. Phys. Oceanogr.,* 32: 428–457.

Ponte, R. M., 1999: A preliminary model study of the large-scale seasonal cycle in bottom pressure over the global ocean. *J. Geophys. Res.*, 104(C1), 1289–1300.

Quinn, K. J., and R. M. Ponte, 2012: High frequency barotropic ocean variability observed by GRACE and satellite altimetry. *Geophys. Res. Lett.*, 39, L07603.

Renfrew, Ian A., G. W. K. Moore, P. S. Guest, and K. Bumke, 2002: A comparison of surface layer and surface turbulent flux observations over the Labrador Sea with ECMWF analyses and NCEP reanalyses. *J. Phys. Oceanogr.*, 32, 383–400.

Reverdin, G., 2010: North Atlantic subpolar gyre surface variability (1895-2009). *J. Climate, 23*, 4571-4584.

Reverdin, G., N. Verbrugge, and H. Valdimarsson, 1999: Upper ocean variability between Iceland and Newfoundland, 1993–1998. *J. Geophys. Res.,* 104, 29599-29611.

Rhein, M., D. Kieke, S. Hüttl-Kabus, A. Roessler, C. Mertens, R. Meissner, B. Klein, C.W. Böning, and I. Yashayaev, 2011: Deep water formation, the subpolar gyre, and the meridional overturning circulation in the subpolar North Atlantic. *Deep Sea Res.II,* 58, 1819-1832.

Ribergaard, M. H., 2009: Oceanographic Investigations off West Greenland 2008. *NAFO Scientific Council Documents* 09/003. Danish Meteorological Institute, Copenhagen, Denmark.

Ribergaard, M. H., 2010: Oceanographic Investigations off West Greenland 2009. *NAFO Scientific Council Documents* 10/004, Danish Meteorological Institute, Copenhagen, Denmark.

Ribergaard, M.H., S.M. Olsen, and J. Mortensen, 2008: Oceanographic investigations off west Greenland 2007. *NAFO Scientific Council Documents* 07/003. Danish Meteorological Institute, Copenhagen, Denmark.

Rignot, E., I. Velicogna, M. R. van den Broeke, A. Monaghan, and J. Lenaerts, 2011: Acceleration of the contribution of the Greenland and Antarctic ice sheets to sea level rise. *Geophys. Res. Lett.,* 38, L05503.

Rind, D., P. deMenocal, G. Russell, S. Sheth, D. Collins, G. Schmidt, and J. Teller, 2001: Effects of glacial meltwater in the GISS coupled atmosphereocean model 1. North Atlantic Deep Water response. *J. Geophys. Res.,* 106, 27335-27353.

Robson, J., R. Sutton, K. Lohmann, D. Smith, and M. D. Palmer, 2012: Causes of the rapid warming of the North Atlantic Ocean in the mid-1990s. *J. Climate,* 25, 4116-4134.

Sarafanov, A., 2009: On the effect of the North Atlantic Oscillation on temperature and salinity of the subpolar North Atlantic intermediate and deep waters. *ICES J. Mar. Sci.,* 66, 1448-1454.

Sarafanov, A., A. Falina, P. Lherminier, H. Mercier, A. Sokov, and C. Gourcuff, 2010: Assessing decadal changes in the Deep Western Boundary Current absolute transport southeast of Cape Farewell, Greenland, from hydrography and altimetry. *J. Geophys. Res.,* 115, C11003.

Sarafanov, A., A. Falina, A. Sokov, and A. Demidov, 2008: Intense warming and salinification of intermediate waters of southern origin in the eastern subpolar North Atlantic in the 1990s to mid-2000s. *J. Geophys. Res.,* 113, C12022.

Sarafanov, A., and Coauthors, 2012: Mean full-depth summer circulation and transports at the northern periphery of the Atlantic Ocean in the 2000s. *J. Geophys. Res.,* 117, C01014.

Srokosz, M., M. Baringer, H. Bryden, S. Cunningham, T. Delworth, S. Lozier, J. Marotzke, and R. Sutton, 2012: Past, present, and future changes in the Atlantic meridional overturning circulation. *Bull. Amer. Meteor. Soc.*, 93, 1663–1676.

Shepherd, A., A. Hubbard, M. King, M. McMillan, and I. Joughin, 2009: Greenland ice sheet motion coupled with daily melting in late summer. *Geophys. Res. Lett.,* 36, L01501.

Smith, E. M., F. M. Soule, and O. Mossby, 1937: The Marion and General Green expeditions to Davis Strait and Labrador Sea. *Bull. U.S. Coast Guard, 19,* 259.

Stammer, D., A. Cazenave, R. M. Ponte, and M. E. Tamisiea, 2013: Causes for contemporary regional sea level changes. *Annu. Rev. Mar. Sci.*, 5, 21-46.

Stouffer, R. J., and Coauthors, 2006: Investigating the causes of the response of the thermohaline circulation to past and future climate changes. *J. Climate,* 19, 1365-1387.

Straneo, F., 2006: Heat and freshwater transport through the central Labrador Sea*. *J. Phys. Oceanogr.*, 36, 606–628.

Stammer, D., H. H. Hinrichsen, and R. H. Käse, 1991: Can meddies be detected by satellite altimetry? *J. Geophys. Res.*, 96, 7005–7014.

Stroeve, J. C., V. Kattsov, A. Barrett, M. Serreze, T. Pavlova, M. Holland, and W. N. Meier, 2012: Trends in Arctic sea ice extent from CMIP5, CMIP3 and observations. *Geophys. Res. Lett.*, 39, L16502.

Stroeve, J., M. Serreze, S. Drobot, S. Gearheard, M. Holland, J. Maslanik, W. Meier, and T. Scambos, 2008: Arctic sea ice extent plummets in 2007. *Eos Trans AGU,* 89, 13-14.

Talley, L., and M. McCartney, 1982: Distribution and circulation of Labrador Sea Water. *J. Phys. Oceanogr.,* 12: 1189–1205.

The Lab Sea Group, 1998; 1998: The Labrador Sea Deep Convection Experiment. *Bull. Amer. Meteor. Soc.,* 79, 2033-2058.

Thompson, D. W., and J. M. Wallace, 1998: The Arctic Oscillation signature in the wintertime geopotential height and temperature fields. *Geophys. Res. Lett.*, 25, 1297-1230.

Thornalley, D. J. R., I. N. McCave, and H. Elderfield, 2010: Freshwater input and abrupt deglacial climate change in the North Atlantic. *Paleoceanogr.,* **25**, PA1201.

Våge, K., R. S. Pickart, G. W. K. Moore, and M. H. Ribergaard, 2008: Winter mixed layer development in the central Irminger Sea: The effect of strong, intermittent wind events. *J. Phys. Oceanogr.,* 38, 541-565.

Våge, K., and Coauthors, 2009: Surprising return of deep convection to the subpolar North Atlantic Ocean in winter 2007-2008. *Nature Geosci.,* 2, 67-72.

van Aken, H. M., M. F. de Jong, and I. Yashayaev, 2011: Decadal and multi-decadal variability of Labrador Sea Water in the north-western North Atlantic Ocean derived from tracer distributions: Heat budget, ventilation, and advection. *Deep Sea Res. I,* 58, 505-523.

Vellinga, M., and R. Wood, 2002: Global climatic impacts of a collapse of the Atlantic thermohaline circulation. *Climatic Change,* 54, 251–267.

Verbrugge, N., and G. Reverdin, 2003: Contribution of horizontal advection to the interannual variability of sea surface temperature in the North Atlantic. *J. Phys. Oceanogr.,* 33, 964-978.

Vinogradova, N. T., R. M. Ponte, and D. Stammer, 2007: Relation between sea level and bottom pressure and the vertical dependence of oceanic variability. *Geophys. Res. Lett.*, 34, L03608.

Visbeck, M. H., J. W. Hurrell, L. Polvani, and H. M. Cullen, 2001: The North Atlantic Oscillation: Past, present, and future. *Proc. Natl. Acad. Sci.,* 98, 12876-12877.

Volkov, D. L., 2005: Interannual variability of the altimetry-derived eddy field and surface circulation in the extratropical North Atlantic Ocean in 1993–2001. *J. Phys. Oceanogr.*, 35, 405–426.

Volkov, D. L., and H. M. van Aken, 2003: Annual and interannual variability of sea level in the northern North Atlantic Ocean. *J. Geophys. Res.,* 108, 3204.

Wallace, J. M., 2000: North Atlantic Oscillation/Annular Mode: Two paradigms–one phenomenon. *Quart. J. Roy. Meteor. Soc.*, 126, 791–805.

Wood, R. A., A. B. Keen, J. F. B. Mitchell, and J. M. Gregory, 1999: Changing spatial structure of the thermohaline circulation in response to atmospheric CO2 forcing in a climate model. *Nature,* 399, 572-575.

Wu, Z., and N. E. Huang, 2004: A study of the characteristics of white noise using the empirical mode decomposition method. *Proc. R. Soc. London, Ser. A*, 460, 1597 – 1611.

Wu, Z., and N. E. Huang, 2005: Statistical significance test of intrinsic mode functions, in *Hilbert-Huang Transform and Its Applications*, edited by N. E. Huang and S. S. Shen, pp. 107 – 127, World Scientific Publishing, Singapore.

Wu, Z., and N. E. Huang, 2009: Ensemble empirical mode decomposition: A noise assisted data analysis method. *Adv. Adaptive Data Anal.,* 1, 1-41.

Wust, G., 1935: Schichtung und Zirkulation des Atlantischen Ozeans. Die Stratosphare. *Wiss. Ergebn. Dtsch. Atlant. Exped. 'Meteor', 6: 1st Part, 2*, 180.

Xu, X., H. E. Hurlburt, W. J. Schmitz, R. Zantopp, J. Fischer, and P. J. Hogan, 2013: On the currents and transports connected with the Atlantic meridional overturning circulation in the subpolar North Atlantic. *J. Geophys. Res.,* 118, 502-516.

Yan, X.-H., Y.-H. Jo, W.T. Liu, and M.-X. He, 2006: A new study of the Mediterranean outflow, air–Sea interactions, and meddies using multisensor data. *J. Phys. Oceanogr.*, 36, 691–710.

Yashayaev, I., 2007: Hydrographic changes in the Labrador Sea, 1960–2005. *Prog. Oceanogr.,* 73, 242-276.

Yashayaev, I., M. Bersch, and H. M. van Aken, 2007: Spreading of the Labrador Sea Water to the Irminger and Iceland basins. *Geophys. Res. Lett.,* 34, L10602.

Yashayaev, I., and J. W. Loder, 2009: Enhanced production of Labrador Sea Water in 2008. *Geophys. Res. Lett.,* 36, L01606.

Yeager, S. G., and M. Jochum, 2009: The connection between Labrador Sea buoyancy loss, deep western boundary current strength, and Gulf Stream path in an ocean circulation model, *Ocean Modell.*, 30, 207 – 224.

Yu, L., X. Jin, and R.A. Weller, 2008: Multidecade global flux datasets from the objectively analyzed air-sea fluxes (OAFlux) project: Latent and sensible heat fluxes, ocean evaporation, and related surface meteorological variables. Woods Hole Oceanographic Institution, OAFlux Project Technical Report. OA-2008-01, 64pp. Woods Hole. Massachusetts.

Zhang, R., 2008: Coherent surface-subsurface fingerprint of the Atlantic meridional overturning circulation. *Geophys. Res. Lett.,* 35, L20705.

Zhang, R., 2010: Latitudinal dependence of Atlantic meridional overturning circulation (AMOC) variations. *Geophys. Res. Lett.,* 37, L16703.

Zhu, J., and E. Demirov, 2011: On the mechanism of interannual variability of the Irminger Water in the Labrador Sea. *J. Geophys. Res.,* 116, C03014.

Appendix A

HILBERT-HUANG TRANSFORM

A.1 Empirical Mode Decomposition

The empirical mode decomposition (EMD) method identifies the intrinsic mode function (IMF) by a ‘sifting’ process, which decomposes a data set into components with varying timescales (Huang et al. 1998). The sifting starts with identifying all the extrema and then connecting all the local maxima (minima) by a cubic spline line to form the upper (lower) envelope. The mean of the upper and the lower envelopes is then subtracted from the data to obtain the first guess of the first IMF. The sifting process is performed repeatedly in order to refine the IMF by eliminating background waves on which the IMF is riding and making the wave profiles more symmetric. The first IMF, which has the finest scale or the shortest-period oscillation in the data, is then subtracted from the original data to yield a residue, which is then treated as the new data and subjected to the same sifting process to obtain an IMF of lower frequency. Each IMF must satisfy two conditions: 1) in the whole data set, the number of extrema and the number of zero crossings in each must either equal or differ at most by one, and 2) at any data point, the mean value of the envelope defined using the local maxima and the envelope defined using the local minima is zero. With these requirements, an IMF oscillates in a narrow frequency band, a reflection of quasi-periodicity and nonlinearity. The decomposition procedure uses intrinsic information derived from the data set itself instead of prescribing frequency bands or imposing any particular basis function such as wavelets. Therefore, it is adaptive and very efficient to non-linear and non-stationary processes. The decomposition process finally stops when the residual becomes a monotonic function or a function with only one extreme from which no more IMF can be extracted. The original data set, X(t), can be therefore expressed as

$$\mathrm{X}(t)=\sum_{\mathrm{j}=1}^{\mathrm{n}}\mathrm{C}_{\mathrm{j}}(t)+\mathrm{R}(t), \tag{A.1}$$

where $\mathrm{C}_{\mathrm{j}}(t)$ is the *j*th IMF, *n* is the total number of the IMFs and R(*t*) is the residual.

The method used in this study is the improved white noise-assisted decomposition method of ensemble empirical mode decomposition (EEMD), described in detail by Wu and Huang (2009). By eliminating the problem of mode mixing, the EEMD defines the 'true' IMF components as the mean of an ensemble of trials, each consisting of the signal plus a white noise of finite amplitude (Huang and Wu, 2008). However, there are still some unsettled problems associated with the EEMD (see Wu and Huang, 2009). The EEMD results might not satisfy the strict definition of IMF. Therefore, additional post-processing techniques were employed in order to guarantee that the extracted IMFs are 'true IMFs' (Wu and Huang, 2009). As the level of added noise is not of critical importance, as long as it is of finite amplitude while allowing for a fair ensemble of all the possibilities, EEMD can be used without any significant subjective intervention (Huang and Wu, 2008).

A.2 Statistical Significance Test

Wu and Huang (2005) studied the characteristics of IMFs from the uniformly distributed white noise, and gave the empirical relationship between the energy density and the mean period. This leads to the establishment of the energy distribution function for each IMF and the spread function of the energy distribution for various percentiles. Based on the characteristics of the white noise, the information content of IMF components from a noisy dataset derived from EMD can be objectively determined relative to the white noise statistics. Therefore, statistical significance of the IMFs is based on the distribution of energy as a function of mean period of the IMF relative to that of pure white noise. This method allows one to differentiate true signals from components of noise with any selected statistical significance level (95%, 99%) (Wu and Huang 2004, 2005; Huang and Wu 2008). Insignificant IMFs are interpreted as noise inherent to the original signal.

A.3 Hilbert-Huang Transforms

The Hilbert transform is applied to each IMF. An IMF component, C(t), and its Hilbert transform, F(t), then can well define a complex function, the analytical signal,

$$z(t) = \mathrm{C}(t) + i \cdot \mathrm{F}(t). \tag{A.2}$$

The instantaneous amplitude of $z(t)$ is

$$a(t) = \sqrt{[\mathrm{C}(t)]^2 + [\mathrm{F}(t)]^2}, \tag{A.3}$$

and the instantaneous phase of $z(t)$ is

$$\theta(t) = \arctan\left[\frac{\mathrm{F}(t)}{\mathrm{C}(t)}\right]. \tag{A.4}$$

Then, the instantaneous frequency is defined as

$$\omega(t) = \frac{1}{2\pi}\frac{d\theta(t)}{dt}. \tag{A.5}$$

The instantaneous amplitude and frequency are calculated for all IMF components. The residual (R) has been left out of Hilbert transform by purpose since the energy involved in the residual represents typically a mean offset that could be overpowering (Huang et al., 1998). After performing the Hilbert transform on each IMF component, the original data can be expressed, then, in the following form

$$\mathrm{X}(t) = \sum_{j=1}^{n} a_j(t)\exp\left[i\int \omega_j(t)\,dt\right]. \tag{A.6}$$

This enables us to represent the amplitude and the instantaneous frequency as functions of time in a three-dimensional plot, in which each point of amplitude corresponds a pair of $(t, \omega(t))$.

Resultant frequency-time distribution of the amplitude is designated as the Hilbert amplitude spectrum, $H(\omega,t)$, or simply Hilbert spectrum. Two useful parameters can be defined based on the Hilbert spectrum: the first is the marginal spectrum density (MSD),

$$\mathrm{MSD} = \int_0^T H(\omega,t)\,dt \quad , \tag{A.7}$$

and the second is the instantaneous energy density level (IE),

$$\mathrm{IE} = \int_\omega H^2(\omega,t)d\omega \tag{A.8}$$

The MSD is a function of frequency, offering a measure of total amplitude (or energy) contribution from each frequency value. It represents the cumulated amplitude over the entire data span in a probabilistic sense, which means a higher likelihood for an oscillation at a frequency have appeared locally in the whole time span of the data (Huang et al., 1998). The IE depends only on time and can be thus used to check the energy fluctuation.

Appendix B

CUMULATIVE NORTH ATLANTIC OSCILLATION INDEX

The construction of the cumulative NAO (cumNAO) index takes into account of a time integration of the atmospheric forcing. Its calculation follows

$$\text{cumNAO}_i = \sum_{k=1}^{i} \text{NAO}_k,\ 1 \le k \le i \le M, \tag{B.1}$$

where, NAO is the original monthly index; M is the total number of monthly NAO index and subscripts k and i are the initial and final month indices respectively. Hence, a period of persistent positive NAO index becomes an increasing slope in the cumNAO index, vice versa. The cumNAO can highlight the shifts in the atmospheric variability compared to the normal NAO index. For example, a period of high NAO index in early 1990s corresponds to an increase in the cumNAO; a sudden drop between 1995 and 1996 follows a peak in the cumNAO (Figure B.1). Moreover, using different time origin of integration does not change the shape of the cumulative NAO index, which instead introduces a shift in magnitude for every point (Figure B.2). Hence, the trend and variability of the index is not sensitive to its time origin of integration.

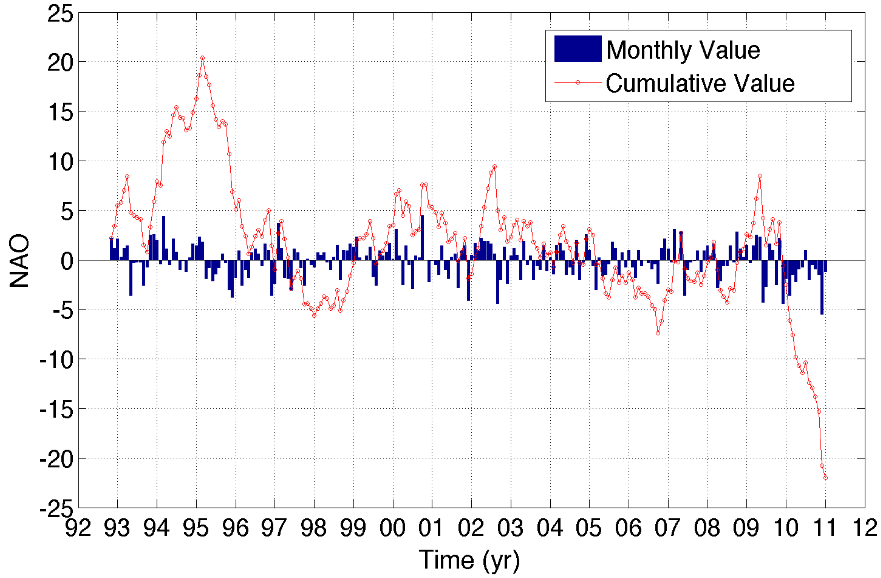

Figure B.1: Comparison of normal month NAO index (blue bar) and the cumulative NAO index (red line) calculated using Equation B.1.

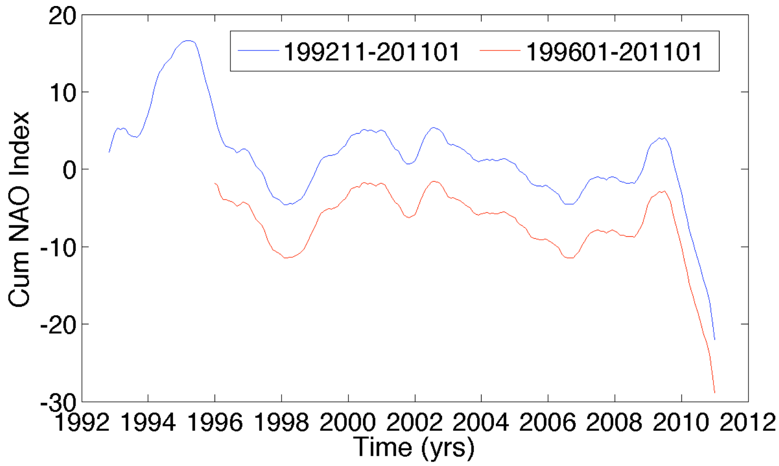

Figure B.2: The cumulative NAO index integrated from 1992 Nov (blue) and from 1996 Jan (red), respectively. A 9-month running smoothing was performed to both lines.

Appendix C

SURFACE CHARACTERISTIC FEATURES RELATED TO DEEP CONVECTION

The wintertime air-sea heat flux primarily contributes to the intensity of deep convection in the Labrador Sea since the associated temperature anomalies determine the surface layer density structure. Among the four components of the net heat flux, sensible heat flux contributes more than any single component in the Labrador Sea during the winters (e.g., Renfrew et al., 2002). Furthermore, according to the bulk formula, a major variation in the sensible heat flux is determined by temperature differences between the sea surface and the air. Abnormally cold air temperature, such as the one measured in the winter of 2008, should coincide with abnormally cold continental temperatures. Therefore, I examined surface temperature fields in the Labrador Sea and the surrounding continents (Figure C.1). Choice of the winters of 2007 and 2008 is to contrast surface conditions for a weak convective year against a strong convective year. The mixed layer depth (MLD) for the winter of 2007 was similar to the climatological value in Figure 1.2. During the winter of 2008, the MLD was observed as deep as 1600m (see Chapter 2 for details). It is noted that for the February of 2008, there was colder land surface temperature (LST) accompanied by strong westerlies. In contrast, the LST was relatively higher in February 2007, and southeasterlies prevailed over the central Labrador Sea. The sea surface temperatures (SST) for the two years are not discernable. Further, I computed the differences between the central Labrador Sea and its surrounding continents (Figure C.2). All of three land-sea temperature differences present consistent interannual variability. The land surface temperature is independent of internal variations in the ocean and the temperature difference has relation to the intensity of the convection (the winters of 2005 and 2008). It may, therefore, be used as a potential predictor of the deep convection intensity observed from satellites.

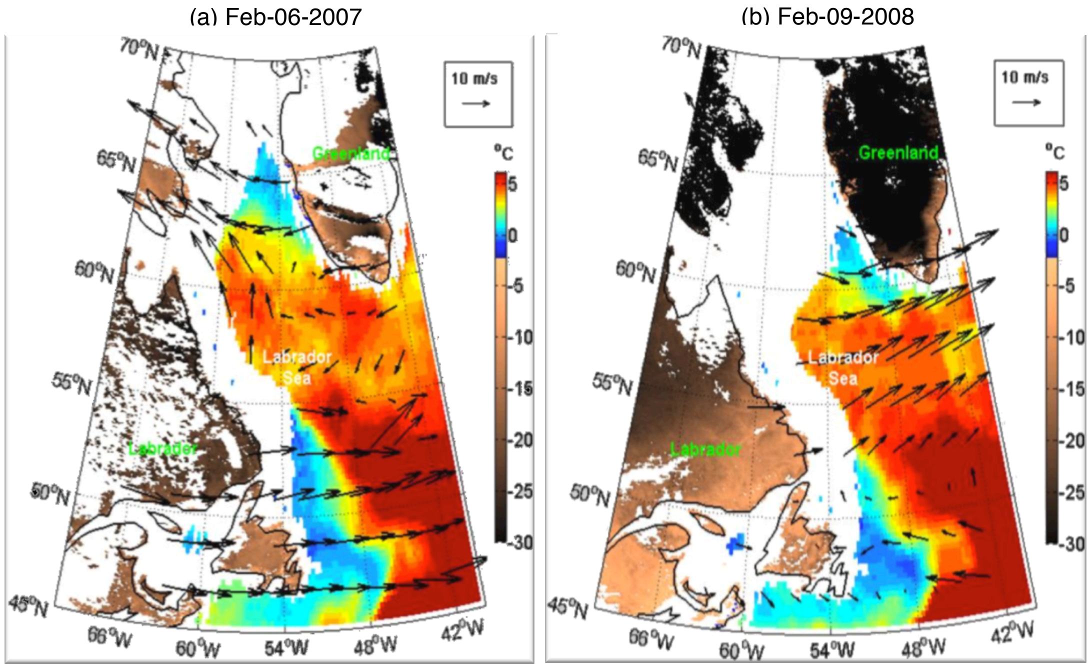

Figure C.1: Land and sea surface temperatures of (a) Feb 6, 2007 and (b) Feb 9, 2008. Wind vectors are also displayed. There was a weak convection during the winter of 2007 but a strong convection during the winter of 2008 (see Chapter 2 for more details). The land surface temperature (LST) is measured by the MODIS/Terra and provided by NASA Goddard Space Flight Center, http://modis-land.gsfc.nasa.gov/temp.html). The AMSR-E sea surface temperature (SST) and QuikSCAT sea winds are obtained from the Remote Sensing Systems (http://www.remss.com).

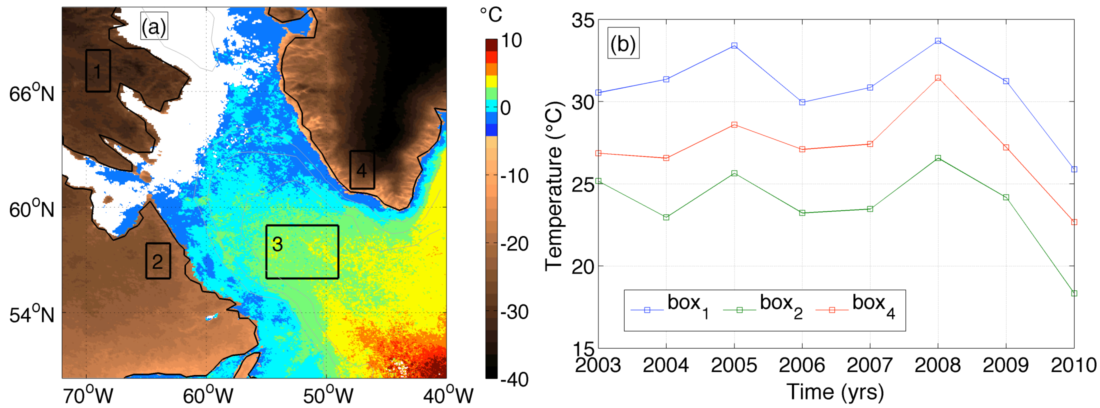

Figure C.2: (a) Land/sea surface temperature composite for the winter of 2008 over the study area. Black boxes indicate locations for temperature average. (b) Sea surface temperature (SST) over box 3 minus land surface temperature (LST) over box1, box2 and box4, respectively. SST data is fusion of microwave and infrared measurements obtained from the Remote Sensing Systems (http://www.remss.com).